UNCLASSIFIED

AD NUMBER
AD361774

CLASSIFICATION CHANGES
TO: **unclassified**
FROM: **secret**

LIMITATION CHANGES
TO: **Approved for public release, distribution unlimited**
FROM: **Distribution authorized to DoD only; Critical Technology; 15 MAR 1960. Other requests shall be referred to Defense Atomic Support Agency, Washington, DC 20301. Formerly Restricted Data.**

AUTHORITY
DNA-SSTL, via ltr dtd 14 Sep 1995; DNA-SSTL, ltr 14 Sep 1995

THIS PAGE IS UNCLASSIFIED

WT-1305

OPERATION REDWING — PROJECT 1.5

TRANSIENT DRAG LOADING of ACTUAL and IDEALIZED SHAPES from HIGH-YIELD DETONATIONS (U)

H.S. Burden
J.D. Day

Ballistic Research Laboratories
Aberdeen, Maryland

U. S. MILITARY
FROM DOC.

REPORT DIRECTLY
THROUGH Sponsoring
Agency to

Director
Defense Atomic Support Agency
Washington, D. C. 20301

DDC

3

#361774

DISCLAIMER NOTICE

THIS DOCUMENT IS BEST QUALITY AVAILABLE. THE COPY FURNISHED TO DTIC CONTAINED A SIGNIFICANT NUMBER OF PAGES WHICH DO NOT REPRODUCE LEGIBLY.

ABSTRACT

Part 1. Investigation of aerodynamic-drag characteristics by measurements on full-scale I beams (8WF67) and angle irons (8L56.9) were made at various pressure levels from Shot Cherokee. Drag and lift coefficients were obtained although the flow was not normal to the beams. Resolution of the flow was determined. Drag coefficients for the I beams varied from 2.44 to 2.82 which was somewhat higher than steady-state data, which is usually given at 2.03. The drag coefficient for the angle iron varied from 2.11 to 2.61, whereas the steady-state value was 1.83. The lift coefficient for the angle iron varied from 3.28 to 3.73, and the steady-state value was 2.07.

Part 2. A description of an experiment for determining drag coefficients for spherical shapes as a function of the dynamic pressure of the flow following blast wave fronts is given. Two sizes of spherical shell (3 and 10 inch diameter) were used in conjunction with three-dimensional, force-sensing mechanisms. The sensing mechanisms and calibration procedure are described. The objectives were not achieved because of a serious error in the position of the detonation and because of some dubious behavior by the gages. Speculative, rather than authoritative, values of peak drag coefficient are listed as deduced from the experiment. The results are briefly compared with those for gages used in a similar pressure range on Operation Teapot.

Part 3. Investigation of the response of drag-type targets and continuation of the statistical evaluation studies on military vehicles were made by the exposure of ¼-ton trucks (jeeps) on Shots Lacrosse, Zuni, and Yuma. Ground ranges were selected to give further data for predicting damage to vehicles under different blast conditions than those previously tested. Analysis of the data indicated an appreciable reduction in damage radii for non-precursor conditions below that for precursor conditions. There was further indication that displacement, like damage, resulting from exposure to a blast wave of classical shape was significantly reduced as compared to the displacement received from a nonclassical or precursor wave.

Part 4. Air Blast diffraction and drag loading measurements were made at a limited number of positions on a concrete cubicle during Shot Zuni. The target structure was 6 by 6 by 12 feet and located in a pressure region of 23 psi with a duration of approximately 3 to 5 seconds. The objective was achieved, in that successful records were obtained on representative locations on the various faces of the structure, but since the observed wave was non-ideal in character, it was not possible to correlate the actual loading with that predicted from a scaled shock tube model.

For comparison, the actual field records and predicted records are both presented in the body of the report. Although the free-stream record was only slightly rounded, the reflected pressure over the front of the structure remained high and did not decay as predicted.

Part 5. Electronic recording instrumentation was provided for provided for Project 1.3 on Shots Cherokee and Zuni and recording and structure instrumentation for structural response Project 3.1 on Shot Cherokee. A multi-channel magnetic tape recording system was utilized to record 100 data channels. The objective was not fully satisfield on Shot Cherokee because of the mis-orientation of ground zero, even though most of the instrumentation functioned satisfactorily. This mis-orientation adversely affected the data records obtained from the unidirectional electronic pitot-static q and other gages. The objective was satisfactorily met on Shot Zuni.

A description of the instrumentation and recording system are presented in the body of the report. A commentary on the records obtained is also given.

6

FOREWORD

This report presents the final results of one of the projects participating in the military-effect programs of Operation Redwing. Overall information about this and the other military-effect projects can be obtained from WT-1344, the "Summary Report of the Commander, Task Unit 3." This technical summary includes: (1) tables listing each detonation with its yield, type, environment, meteorological conditions, etc.; (2) maps showing shot locations; (3) discussions of results by programs; (4) summaries of objectives, procedures, results, etc., for all projects; and (5) a listing of project reports for the military-effect programs.

PREFACE

Since this project was one which consisted of several phases, although interrelated, it was considered too lengthy for the usual organization. Each phase was treated as being completely separate and the report is divided into parts with each part organized as a report in itself. Accordingly the body of the report was composed as follows:

Part 1   Structural Members;
Part 2   Spherical Gages;
Part 3   Military Vehicles;
Part 4   Cubicle Structure; and
Part 5   Electronic Instrumentation.

The authors would like to thank the many people who contributed to this report. Appreciation is expressed to Dr. E. E. Minor for his advice and guidance. The cooperation of all Task Group and Task Unit 3 personnel is gratefully acknowledged.

Special acknowledgement and appreciation is extended to: (1) J. J. Meszaros for his work as coordinator of the Ballistic Research Laboratories' projects; (2) Lt M. R. Johnston and Lt A. L. Holliday, for their excellent work in instrument design and development, the authors are especially grateful; (3) Martha S. Allison for her work in typing and assembling of the final report; and (4) Lt H. W. Wagenblast for his research in the shock tube on spherical gages.

The contributing authors are thanked for their cooperation and competent participation in the compiling of this report: Part 3, R. W. McNeil, R. C. Wise and N. H. Ethridge; Part 4, J. H. Keefer and C. N. Kingery; Part 5, E. G. Schwartz and G. L. Roark.

8

CONTENTS

SECRET

SECRET

9

TRANSIENT DRAG LOADING of ACTUAL and IDEALIZED SHAPES from HIGH-YIELD DETONATIONS

Part 1
STRUCTURAL MEMBERS

OBJECTIVE

The objective of this part of Project 1.5 was the investigation of the aerodynamic drag characteristics of full scale structural members when exposed to transient loading conditions resulting from a high yield nuclear device. Four wide-flange I beams (8WF67) and four angle irons (5 x 3 x 9) were exposed on Shot Cherokee in order to determine the blast loading and hence, their coefficients of drag and, in the case of the angle iron, coefficients of lift.

BACKGROUND AND THEORY

The drag forces acting on a body enveloped in a transient-flow field, such as those from a passage of a blast wave through a medium at rest, have been the subject of considerable interest in the past. A review of the problems arising from a study of drag in a transient (as opposed to a steady state) field has been made by the American Machine and Foundry Company (Reference 1). An important supplement was published by Sandia Corporation (Reference 2). A careful review of the available literature, in particular References 1 and 2, indicated that for blast-wave-produced transient-flow fields, the drag coefficients, C_d, obtained for $\tau > 10$ would be equivalent to the steady-state drag coefficients for like Reynolds numbers and media:

$$\tau = Ut/h \tag{1.1}$$

When: τ = Dimensionless quantity used for comparison of shock front travel over one obstacle to that of another.

U = Shock wave velocity.

t = Time.

h = Characteristic flow length dimension of the object.

It may be noted that for blast waves of interest, those for which $U = 2,000$ ft/sec and $h = 1$ foot, the time condition will require that for $t > 5$-msec, C_d will be that for a similar pseudo-steady-state condition.

Based on the above assumption, beam sensors for the test were designed for forces found by using steady-state drag coefficients (Reference 3) for dynamic pressures corresponding to those that were to be expected in the field. This basic assumption was confirmed, within experimental accuracy, by shock-tube experiments at BRL on small cantilevered beams mounted parallel to the wave front in the tube.

Response of simple uniform beams, subjected to various loading and end conditions, has been widely investigated (References 4 through 17). Factors brought out in such references suggested the advisability of a simply-supported beam set up for the field test to facilitate theoretical analysis and data reduction.

After deciding to use a simply-supported beam as the test instrument, the main problem was in choosing the correct combination of beam, supports, and mount. The beam was to be presented parallel to the shock front and was connected to its mount by a pair of supports. The supports were instrumented with strain gages. The basic theory of the measurements was that the reactions measured would be a good representation of the load if the period of vibration of the beam was much shorter than the durations of the significant details of the load. The design of the combination of beam, support, and mount was governed by this theory. The final test sections selected were 4WF67 for the wide-flanged beam and 8×56.9 for the angle iron.

A duplicate of the final mount design used in the field tests was emplaced in a firing area at Aberdeen Proving Ground and subjected to three high-explosive-produced blast waves. No drag data were obtainable since the blast waves produced were of short duration, but the test system bore up well and indicated reasonable response characteristics for the test mounting system, i.e., the fundamental period was short compared to the duration of the load.

For determining drag and lift coefficients, the following equations were used:

$$C_d = \frac{F_h \text{ or } v}{Q \, A} \tag{1.2}$$

Where   F   Net force on beam

A   Frontal area of beam

Q   Dynamic pressure (free stream)

Subscripts of F are h and v. F_h indicates the net force horizontal to the ground plane and is used to compute drag coefficients. F_v indicates the net force perpendicular to the ground plane and is used to compute lift coefficients. The angle irons were oriented so that negative lift would be experienced.

The significance of drag characteristics of structural members becomes evident when one considers the many structural complexes which are simply various configurations of structural members joined to form trusses and lattice-type networks. Although the drag characteristics will be altered when the members are joined, much will be gained by first examining simple structural beams.

OPERATIONS

Stations consisting of an I beam and an angle iron were placed on Sites Able, Man-Made Island 1, Man-Made Island 2, and Site Dog for exposure to Shot Cherokee (Table A.2).

A crew of four men installed the beams and made the necessary hookups to the recording equipment. A calibration crew followed, making final calculations of expected pressures and appropriate calibration values. Final checks were made just before shot day to insure proper operation of instruments.

Shields were installed over the sensing elements to protect them from adverse atmospheric and thermal exposures.

INSTRUMENTATION

Test Members. The test members were full scale structural members. There were two types used, wide-flange I beams and angle irons. Descriptions of these members can be found in Table 1. Sensor statistics are listed in Table 2.

Test Member Mounts. The mounts consisted of two vertical 12WF58 beams embedded in concrete and set on 10-foot centers for the I beam and on 6-foot centers for the angle iron; the centerline of each test member was 3 feet above ground. A horizontal section was welded to the vertical section and a gusset plate added at the joint for structural rigidity. A support knee brace was also used to provide additional strength. The web of the end portion of the horizontal section was removed and a butt plate welded against the cut section of the web for instrumenta-

12

SECRET

tion mounting. For the angle iron mount the top flange, as well as the web, was removed from the horizontal section. Where the depth of the coral and sand was insufficient to provide adequate mount-to-soil coupling, WF beams were driven into the coral and used as piling. Figure 1 shows typical structural member mounts.

Sensors. The total drag and lift forces exerted upon the structural members were measured by means of strain-sensing elements which were applied to the sensors. These sensors were

TABLE 1 TEST MEMBER STATISTICS

Test Member	Length	Depth	Type	Material
	ft. in.	in		
WF	10 8	8	8WF67	Steel
I	6 8	8	8I 6.9	Steel

attached, at each end of the test members, to the mount. Ball-and-socket joints at each end of the sensors were provided in order to give as closely as possible an approximation to the ideal pinned end for simply supported beams (Figure 2).

The total force felt by the beam was translated to the mount through the sensors. The gages used to instrument the sensors were Baldwin SR-4 strain gages, Type CB-11. These were 350-ohm bakelite gages. Two complete four-arm bridges were mounted on each sensor used with the I beam (Figure 3). In each bridge, two gages in opposite arms of the bridge and on opposite sides of the sensor were mounted with the sensing elements running parallel to the axial direction. The two remaining gages were mounted perpendicular to this direction on the remaining sides. With this symmetrical placement of the gages, when the sensor was loaded, the bridge had a bridge factor of approximately 2.6 (2.6 active arms). With these connections, any bending

TABLE 2 SENSOR STATISTICS

Station	Location	Effective Length	Width	Breadth	Material
		inches	inches	inches	
WF	Able	3	1.375	1.375	Dural
	Man-Made Island No. 1	3	0.650	0.650	Dural
	Man-Made Island No. 2	3	0.500	0.375	Dural
	Dog	3	0.500	0.130	Dural
I	Able	1	1.300	1.300	Dural
	Man-Made Island No. 1	1	0.620	0.620	Dural
	Man-Made Island No. 2	1	0.500	0.500	Dural
	Dog	1	0.500	0.120	Dural

moment canceled itself. By using the ball-and-socket joints on each end of the sensors, torsion was considered to be negligible.

Because of the short length of the sensors used on the angle-iron mounts, only 1 four-arm bridge could be mounted on each sensor (Figure 4). Exceptions were the sensors used on the angle iron at Station 153.04. Only two active gages were mounted, these on opposite sides and opposite arms. The bridge was completed with two dummy gages.

The material and dimension of the sensors were chosen to provide for: the maximum expected stresses transmitted by the test beams, sufficient unit strain for recording purposes, and a frequency roughly 10 times that of the beam fundamental frequency. Sensor statistics are given in Table 2.

13
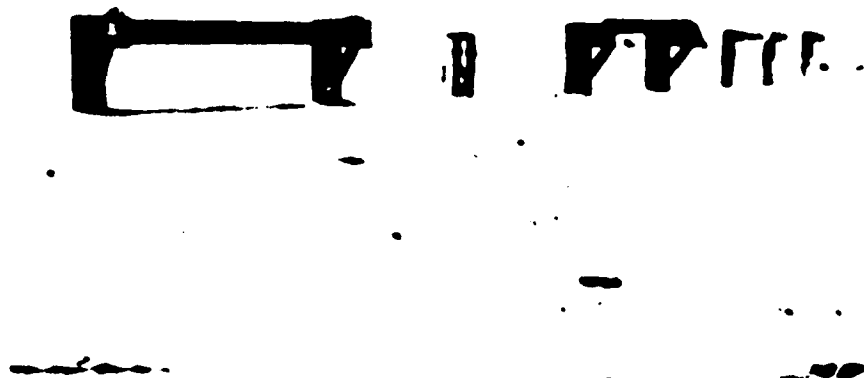
Figure 1 Typical structural member station.

Figure 2 Sensor assembly for structural members.

14

SECRET
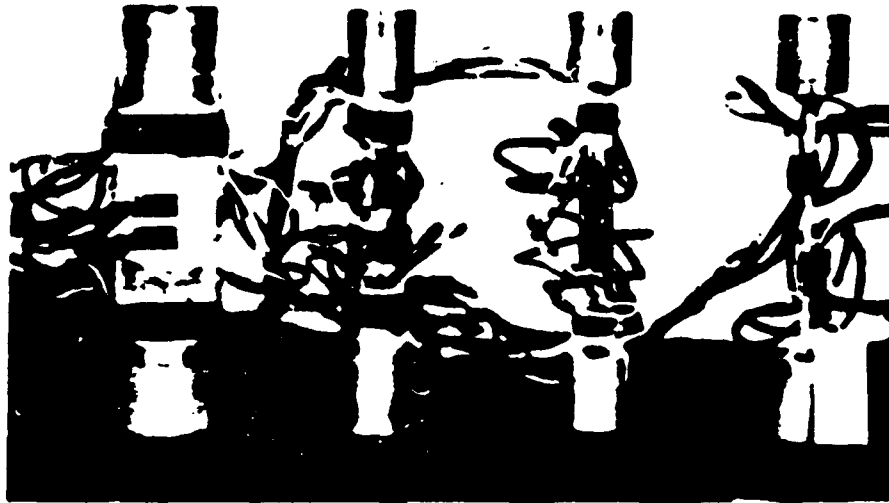
Figure 3 I-beam sensors, with strain gages attached.

Figure 4 Angle-iron sensors, with strain gages attached.

Calibration Procedure. The structural members after having been mounted and completely checked for circuit continuity, were calibrated in the following manner.

Knowing the intended location and the limits of the yield of the device, the maximum expected dynamic pressure and hence the force on each beam was computed. Calibration points were taken in 20-percent increments up to 100 percent of the expected force. For insurance against a higher yield, one final calibration point was taken a' 150 percent of the expected force.

Calibration of the I beam was a straight-forward procedure. A frame was placed over the test member and using the frame as a support, a hydraulic jack was inserted between frame and beam end. With a Dillon force gage indicating the actual force on the sensor, the jack was utilized to obtain the force necessary. This force was recorded as a signal output from the strain bridge mounted on the sensor.

In calibrating the angle iron, lift and drag were both considered. The same calibration procedure and equipment which were used on the I beam were used on the horizontal component of the angle iron. The same procedure but a different frame configuration was used to calibrate the vertical component of the angle iron.

Typical calibration curves for the I beam and angle iron are shown in Figures 5 and 6. This information is presented as a plot of recording galvanometer deflection versus applied load. The
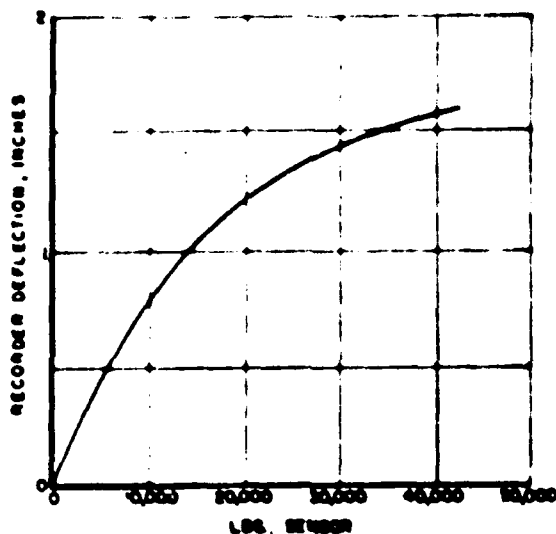
Figure 5 Typical calibration curve for the I beam.
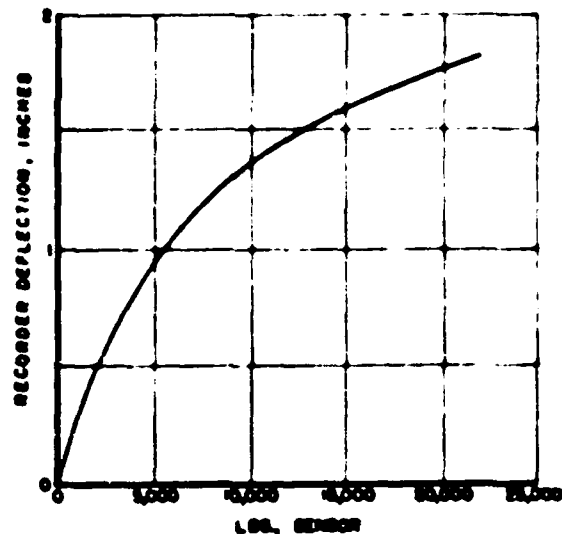
Figure 6 Typical calibration curve for the angle iron.

galvanometer is activated by the electrical signal from the strain gages, which is proportional to the applied load.

REQUIRED DATA

The primary data required were net force versus time recordings of each beam. Since a simply supported beam was desired, care was exercised to obtain such a support in the field. End plates were mounted over each end of the test members. This gave an approximation of a two-dimensional beam and, if the flow should yaw, no loading would be experienced on the ends of the members. With the I beams oriented normal to the flow, any forces perpendicular to the beams were considered to be negligible. The angle iron sensed the normal horizontal force and, in addition, the vertical force.

These forces were recorded by the BRL magnetic tape recorder described in References 18 and 19. The tape was then played back and the signal was printed on oscillographic paper in the form of a deflected trace (which represented force) versus time.

Since the beams were undamped, strong oscillations (superimposed on a mean deflection) were prevalent. Because of the similarity to situations existing with certain other gages used at BRL, data reduction was handled by the same means as used for these gages.

18

If the output of the oscillating gage is recorded linearly, an envelope of the oscillation can be constructed by joining each maximum peak with the succeeding one. Likewise, the minimum peaks can be joined. An average of this envelope will be the correct displacement or force. However, the recorder used was non-linear. This dictated a linearization of the trace before the envelope could be drawn.

The linearization and averaging were done simultaneously by the high-speed digital computer, the ORDVAC, at BRL. A complete and detailed treatment of this type reduction can be found in Appendix B, (Reference 2t .

The only data required from other projects were the basic blast measurements from Project 1.1.

RESULTS AND DISCUSSION

The deviation between actual ground zero and intended ground zero resulted in an unexpected flow direction and unexpected overpressures. However, all instrumentation functioned; though
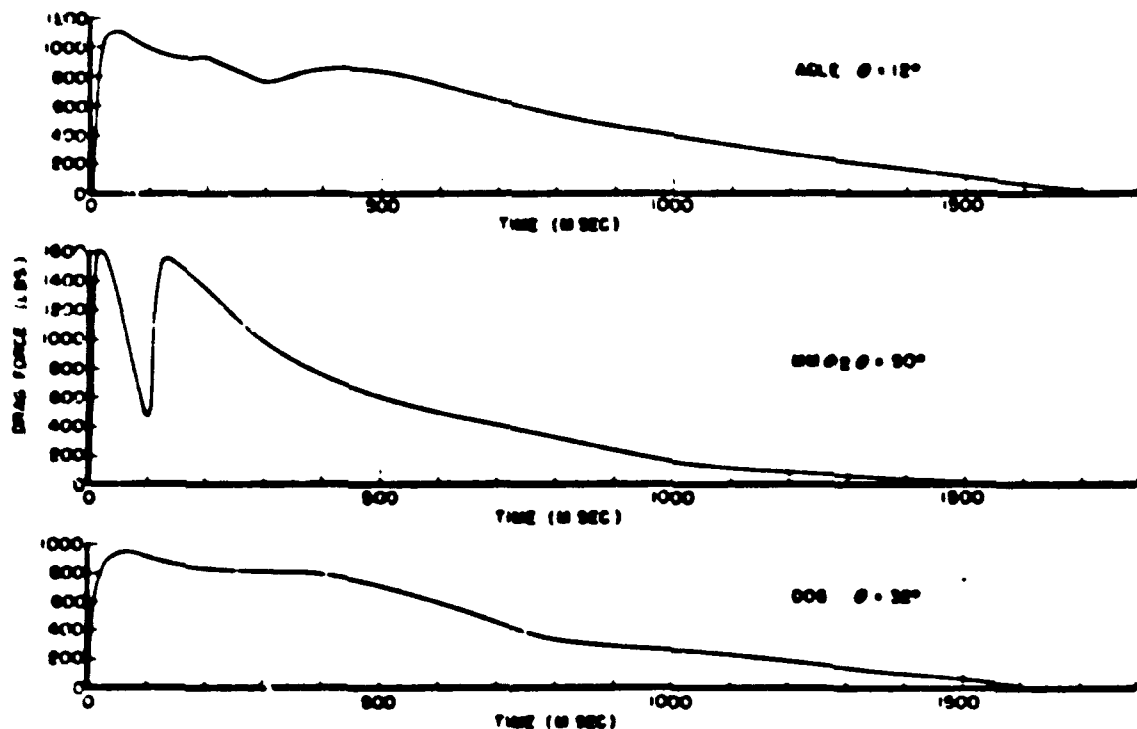
Figure 7 Drag force versus time for Sites Able, Man-Made Island 2, and Dog, net drag force sensed by I beam.

some of it not adequately. Since simple supports were used, if one support failed to give an adequate or reliable signal, the other support reading could be extended and used as a basis for a total reading. Furthermore, in the case of the I beam, there were two bridges per sensor which made it possible to assess the accuracy of the reading.

On Site Able, drag forces were obtained for the I beam and both drag and lift forces were obtained for the angle iron. On Man-Made Island 1, drag and lift were both obtained for the angle iron. The I beam instrumentation on Man-Made Island 1 did not function properly in that two channels had abnormal shifts and the other two channels were low amplitude with a high noise-to-signal ratio. On Man-Made Island 2, drag forces on both beams were obtained. On Site Dog, drag forces were obtained for the I beam only. The instrumentation on the angle iron at Site Dog, because it was not shielded in the correct direction for thermal radiation, failed to function properly. The signal drifted out of the calibrated range.

The measured peak drag and lift forces of each station are listed in Table 3. Figure 7 shows the drag force versus time recordings obtained from the I beam stations on Site Able, Man-

17

Made Island 2, and Site Dog. The recording from Man-Made Island 2 shows a pronounced effect of the reflected pressure from the Project 3.1 structure directly behind the test beams. The design of the angle-iron supports was such that once the beam was loaded, it did not show a typical recovery from the transient dynamic loading. Therefore, only peak force loadings were judged to be reliable, and no force-time histories were considered warranted.

The degree of reliability of the drag and lift coefficients obtained depended mainly on the correct resolution of the dynamic pressure experienced by the test members. Since an angle of deviation of flow occurred at each station, the full impact of the free stream pressure was not felt by the test members. Because the test members could only sense forces in the same direction as the sensors, only that part of the flow which was normal to the beams was considered.

Dynamic pressure (Q) was defined as:

$$Q = \tfrac{1}{2}\rho v^2 \qquad (1.3)$$

Where: Q = Measured free stream dynamic pressure

ρ   Density of air

v = Particle velocity behind the blast wave.

Q, being a pressure, is therefore a scalar and cannot be resolved into components, whereas particle velocity is a vector and can be resolved. The particle velocity normal to the beam is the product of particle velocity, and the cosine of the angle of yaw. Substituting this value in the above equation, the equation becomes:

$$Q' = \tfrac{1}{2}\rho(v\cos\theta)^2$$

$$Q' = (\tfrac{1}{2}\rho v^2)\cos^2\theta$$

or

$$Q' = Q\cos^2\theta \qquad (1.4)$$

Where: Q' = Corrected dynamic pressure.

Q = Measured free stream dynamic pressure.

θ = Angle of yaw.

This method was used in determining the drag and lift coefficient in Table 3. A sample calculation of a drag coefficient is as follows:

I beam   Yaw angle - 12 deg
Site Able   Frontal area - 1.152 square inches
                 Peak drag force - 1,100 pounds
                 Computed Q - 0.40 psi

$$C_d = \frac{F}{Q'A} \qquad \text{or} \qquad = \frac{F}{QA\cos^2\theta}$$

$$= \frac{1100}{0.4(1152)(0.978)^2}$$

$$C_d = 2.5$$

CONCLUSIONS

The instruments designed for measuring drag loading on structural members on Shot Cherokee, although primarily unidirectional, responded well. Three of the four I beam gages gave useable recordings. Considering the angle irons, three of the four gages gave useable drag data

19

SECRET

TABLE 3 FINAL DRAG DATA

Location	Distance from Actual Ground Zero ft	Angle of Inc. θ deg	Measured Overpressure psi	Positive Phase sec	Computed Dynamic Pressure psi	Corrected Dynamic Pressure q cos²θ psi	Peak Drag Forces			Coefficients		
							Angle Iron Vertical lb	Angle Iron Horizontal lb	I Beam lb	Drag I Beam	Drag Angle Iron	Lift Angle Iron
Able	20,711	12	41	6.13	0.40	0.38	360	500	1,100	2.52	2.11	4.25
Man-Made No. 1	19,340	38	87	4.06	1.71	0.89	940	740	—	—	2.40	2.73
Man-Made No. 2	20,682	30	72	4.24	1.19	0.49	—	800	1,600	2.62	61	—
Dog	20,456	32	45	4.65	0.47	0.34	—	—	900	2.46	—	—

* Dynamic Pressure computed using Rankine-Hugoniot relations.

TABLE 4 COMPARISON OF STEADY-STATE DRAG AND LIFT COEFFICIENTS WITH THOSE OBTAINED ON OPERATION REDWING

Structural Members	Steady-State	Dynamic Operation Redwing
I Beam (Drag)	2.03	2.52, Able
		2.82, Man-Made Island No. 2
		2.44, Dog
Angle Iron (Drag)	1.83	2.11, Able
		2.40, Man-Made Island No. 1
		2.61, Man-Made Island No. 2
Angle Iron (Lift)	2.07	2.28, Able
		2.73, Man-Made Island No. 1

18

SECRET

and two of the four gages gave usable lift data. Only the peak forces were read from the angle-iron recordings since they experienced signal shifts when loaded.

Steady-state drag and lift coefficients compare with those obtained on Operation Redwing as shown in Table 4.

The dynamic coefficients shown in Table 4 were obtained for beams at various angles of yaw by applying the correction method outlined in Equation 1.4. Since these values should closely approximate values which would have been obtained had the flow been normal to the beams, it is apparent that the method may be applied to predict the loading on angle beams and I beams at angular orientations to flow.

RECOMMENDATIONS

Although there is a paucity of data, the author makes the following recommendations:

1. In any further investigation of drag loading on structural members, participation should be only on ground bursts or tower detonations. This would assure flow normal to the members.

2. If, however, an angle of yaw is experienced on a unidirectional drag target, the measured free stream dynamic pressure should be corrected by the square of the cosine of the yaw angle before drag coefficients are computed.

3. Modifications should be made on the angle-iron instrumentation to prevent the signal shifts. Since horizontal and vertical forces are required, two angle stations should be instrumented. One station should measure the horizontal force while restricting the vertical force the other should measure the vertical force while restricting the horizontal force.

The I-beam instrumentation, as a whole, functioned adequately. Slight modifications of the sensor bearings, in order to facilitate installation, would be worthwhile.

4. If operationally feasible, further experimentation should be undertaken in order to supplement and verify the existing data under more ideal input conditions.

Part 2
SPHERICAL GAGES

OBJECTIVES

The objective of Part 2 of Project 1.5 was the study of the formation and nature of the drag forces exerted on spheres in the transient flow fields following long-duration, classical blast waves. In accordance with this objective, it was desirable to compare the results obtained on the Operation Teapot sphere tests (Reference 20) with those achieved here in an attempt to determine the effects of wave duration and dust loading. Also, it was of interest to test for scaling, between two sizes of spheres, based on Reynolds number.

BACKGROUND AND THEORY

The need for drag studies has arisen as the duration of blast waves has increased. The aerodynamic drag forces produced by the flow following a blast front assume increasing importance in causing damage to many targets (see, for example, Part 3 of this report) as the time interval over which they are exerted increases. Test shots in Nevada producing shock waves whose parameters were not apparently amenable to prediction by the Rankine-Hugoniot relations pointed up the need for direct measurements of drag forces. Such loading measurements would have to provide data which would allow theoretical or empirical predictions of damage from a given atomic detonation.

Accordingly, on Operation Teapot, two project groups were organized, one by the Naval Ordnance Laboratory (NOL) and one by the Ballistic Research Laboratories (BRL) and their purpose was to investigate methods for making the direct measurements required. Both groups chose to use simple geometrical shapes. BRL interest was restricted to spheres of 3-inch and 10-inch diameter, while NOL used, in addition to spheres of these two sizes, rectangular boxes and two-dimensional cylinders (Reference 23). The gages were arrayed on three blast lines whose surfaces were treated to give respectively, clean-air, classical blast waves; clean-air precursor blast waves; and dust-laden precursor blast waves. The effects measured in the clean-air, classical waves were to be used both as a standard for comparing the results from the other wave types as well as a basis for comparison between the drag characteristics of a sphere determined in steady-state wind-tunnel work with those found in the transient flow fields accompanying blast waves.

Because of unforseen loading of the clean-air shock waves and interaction between the waves on adjoining lines, need for further work with truly clean-air waves was indicated.

Consequently, participation on Operation Redwing at the EPG was planned, for there it was felt clean-air waves could be expected. BRL participation was planned for a multi-megaton shot giving long blast-wave durations (Reference 22), while NOL participation was planned for a multi-kiloton shot having durations more nearly comparable to those for the Operation Teapot MET shot. Thus, it was hoped that an indication of the effects of decay rates might also be shown.

The study of the formation and nature of drag forces on spheres in a transient flow field can be made most effectively by comparing the data taken under transient conditions with data from steady flow wind tunnels. To make such a comparison, one must simply present the two sets of data in compatible form.

It is usual to present drag data in a non-dimensional form to allow scaling between objects placed in flow fields of various characteristics. For low velocity flow (less than Mach 0.5) the

most general form is a plot of the logarithm of drag coefficient, C_D, versus the logarithm of Reynolds number, R (Reference 21)

$$R = \frac{d \rho V}{\mu} \tag{2.1}$$

Where d = A characteristic dimension of the object (the sphere diameter is used)

      ρ = The density of the medium

      V = The velocity of the medium

      μ = The viscosity of the medium

Since no gage to measure the viscosity of air has been developed for nuclear field tests, Reynolds number for these tests cannot be directly determined. Instead, as on Operation Teapot, the use of dynamic pressure, Q, instead of Reynolds number was decided upon. The resulting presentation is similar to the usual one and, when its limitations are considered, a number of inferences may be drawn from the comparison of the two (Reference 20). Figure 8 shows a
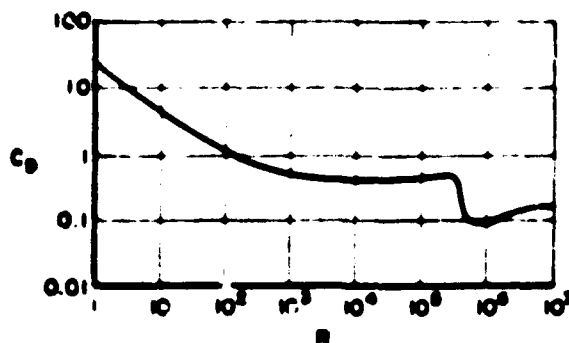
Figure 8 Typical logarithmic plot of drag coefficient
(C_D) versus Reynolds number (R) for spheres.

plot of log C_D versus log R taken from wind tunnel data while Figure 28 shows a plot of log C_D versus log Q taken from Operation Teapot data. It is apparent from its slope and position that the Operation Teapot curve is restricted to a plot of C_D values occurring at flows having Reynolds numbers less than critical. (The critical Reynolds number is usually defined as corresponding to a drag coefficient of 0.3 in the rapidly changing portion of the curve.)

Also, by plotting curves of log C_D versus log Q for various time segments, changes in the relation between the two variables during various stages of the blast wave may be illuminated.

Finally, the log C_D versus log Q_D presentation is useful in investigating the scaling relation between two spheres of different sizes at the same station. Since the Reynolds number depends on the object size, while the dynamic pressure does not, for a given Q, Reynolds number will vary in proportion to the sizes of the objects. Hence, at a given station the 3-inch sphere experiences a flow having a Reynolds number $\frac{3}{10}$'s of the Reynolds number for a 10-inch sphere. A plot of log C_D versus log Q for a 3-inch gage would then be translated along the log Q axis relative to a similar plot for a 10-inch gage, if Reynolds number scaling is applied.

OPERATIONS

Two drag gage stations were constructed, one on Site Able and one on Site Dog for exposure to Shot Cherokee. At each station, one 10-inch diameter gage and two 3-inch diameter gages were mounted. Upon completion of the necessary hookups to the recording equipment, the gages were statically calibrated over the range of forces predicted on the basis of their positions.

INSTRUMENTATION

Drag Gage. The gage was essentially a spherical shell coupled to a rigid support ating by a 3-dimensional sensing element (Figure 9). The sensing element was a sensitive, compact

unit made up of eight aluminum links held in place between the sting and a center ring (Figures 10 and 11) under a compressive force larger than any to be impressed upon the gage by external effects. The design resulted in a gage having a high natural frequency, a slippage-free action, and inherent ease of being damped.

In the at-rest position all links were equally stressed, but when an external force was applied to the gage, the stress in some links was increased and that in others was decreased. Strain gages mounted on the links sensed these changes and converted them to recordable electric signals. The gage was constructed with four links parallel to the axial direction (axis of the sting), two parallel to the vertical, and two parallel to the transverse.

Figure 12 is a schematic diagram of a drag gage suspended on three pairs of precompressed links anchored at the center of the sphere. It illustrates a system capable of sensing three-dimensional forces, but offering virtually no opposition to torsional forces. A small torsional force, such as could be produced by mount vibrations, would disassemble the gage.

To prevent this, the BRL gage was constructed with four link pairs. Instead of lying on concurrent lines, these translated outward from the center of the gage to allow production of moments opposing any torsional motion. Figure 13 is a schematic drawing showing the dis-
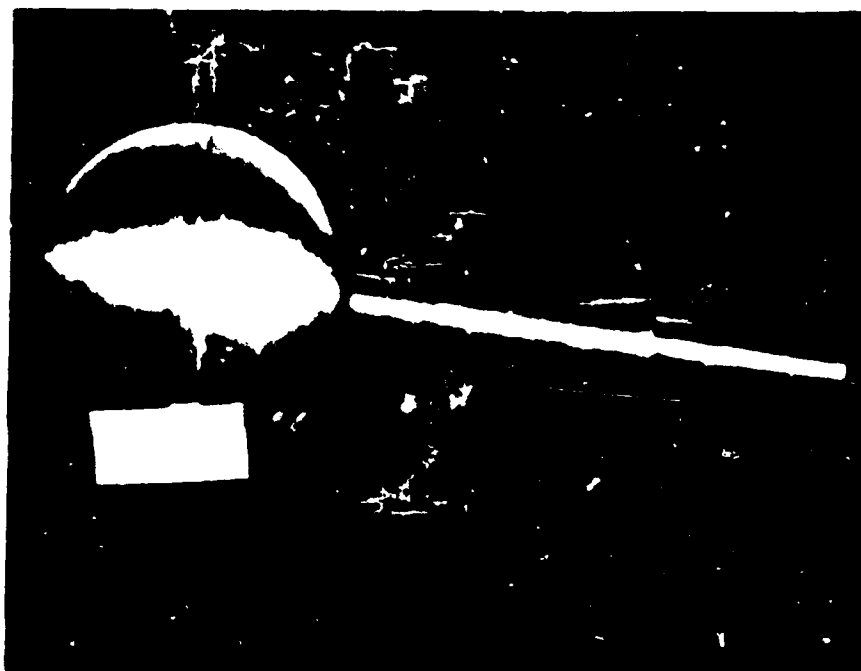
Figure 9 Three-inch spherical drag gage.

placement of the links from zero along the X and Y or X and Z axis. The links are represented by the arrows, the arrowheads point in the direction of the forces applied to the sting as a result of the precompression of the links. The spherical shell (not shown) was attached to the ring and completely surrounded the mechanism.

The configuration illustrated was stable, inasmuch as a force applied anywhere on the surface of the sphere would simply cause a redistribution of stresses in the various links so that an equal, opposing force was created.

When an external force was applied to the gage, it changed the length of the links parallel to its direction of action. Because the displacement of the gage was extremely small and because each link was mounted between pivots, action of this force on the links perpendicular to it was negligible. If a torsional force was applied to the shell, all of the links assumed new stresses, but no electrical output was registered, since the strain gage bridge connection giving most-sensitive output for pure force loads also gave zero output for torsion. The links, shown in

23

SECRET

Figure 10 Detail of link mounting and orientation for 3-inch sphere.
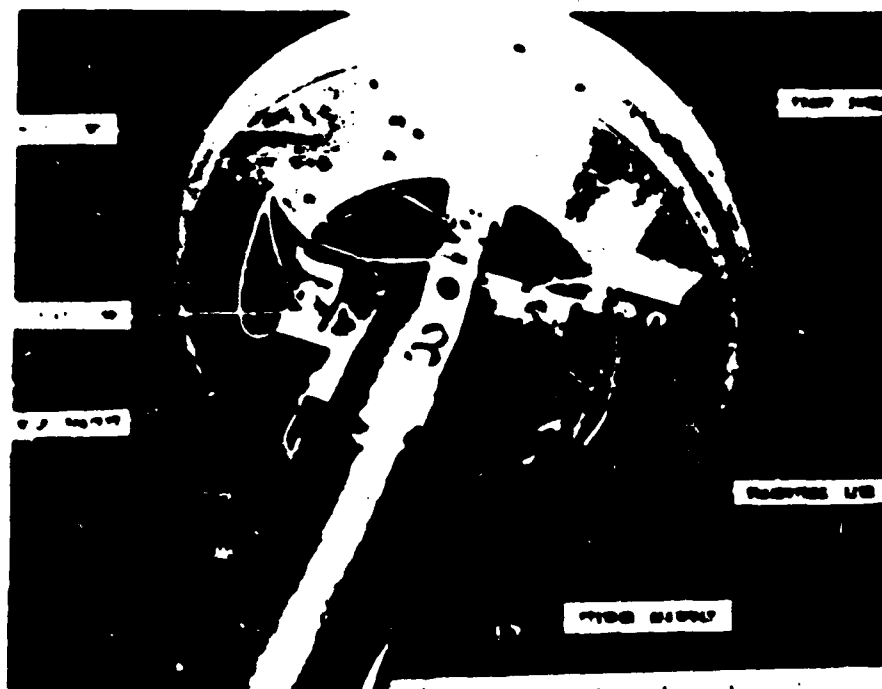
Figure 11 Detail of link sensing mechanism; 10-inch drag gage with rear half of shell removed.

24

SECRET
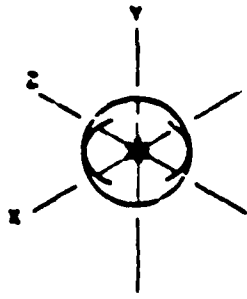
Figure 12 Schematic diaphragm, drag gage
suspended on three pairs of precompressed
links.
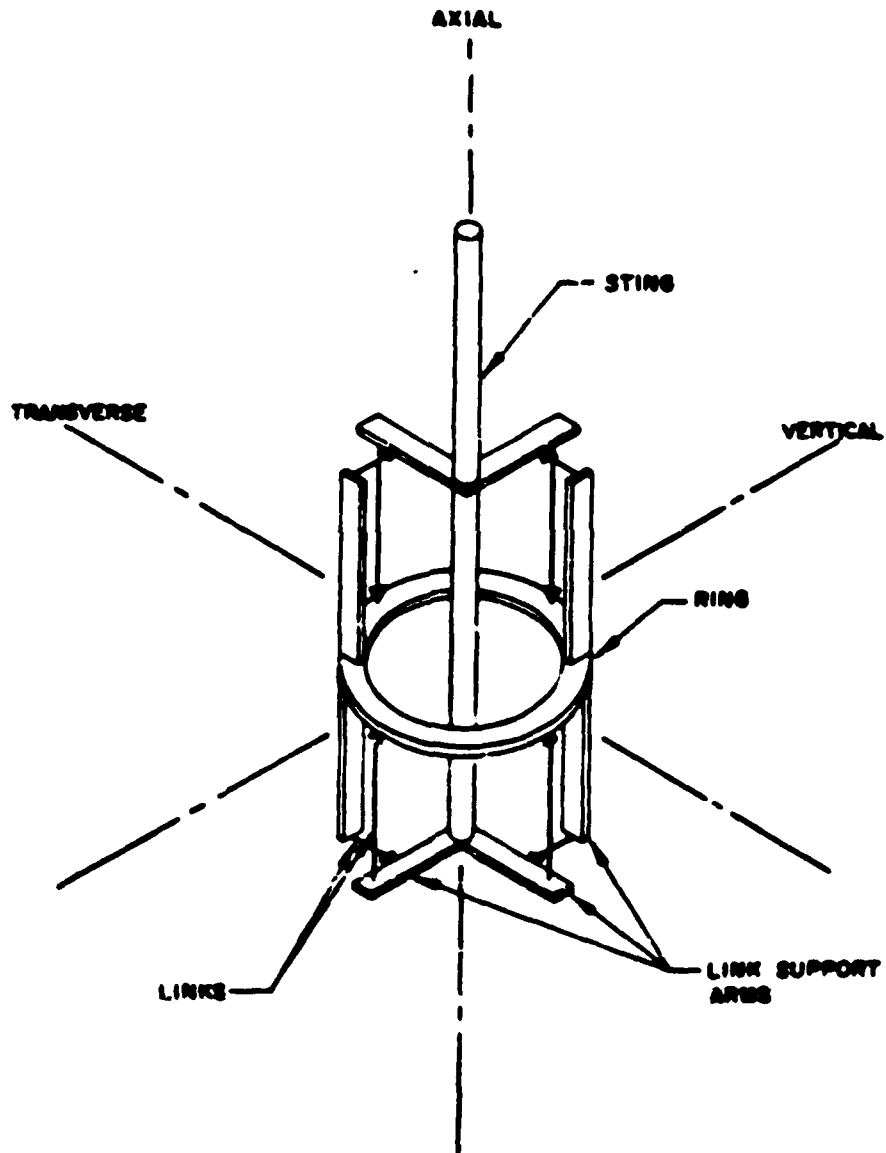
Figure 13 Schematic drawing, drag gage
showing displacement of the links along the
X and Y or X and Z axis.

26

SECRET

Figure 14, were loaded off their centroidal axes to give a beam-column effect. Damping of the gage oscillations was obtained by intermeshed brass leaves 0.004 inch thick attached alternately to opposite ends of the link. The surface of each strip was coated with Dow Corning high-viscosity silicone oil so that when relative motion between the brass strips occurred under fluctuating link loads, viscous damping forces were built up between the strips. There was almost no static friction between the strips, but on the very sensitive gages used at Site Dog there was enough present to cause slight gage hysteresis.

Shock-tube tests conducted on the 3-inch diameter gages showed that the gages had a higher natural frequency (900 cps) higher output (greater than 30 mv with a 20 v lt power supply) and more adequate damping than the BRL drag gages used during Operation Teapot.

Mounts. The gage mounts consisted of three 6-inch double extra heavy pipes extending 3 feet above ground and embedded 4 feet apart in concrete. The aboveground pipe ends were
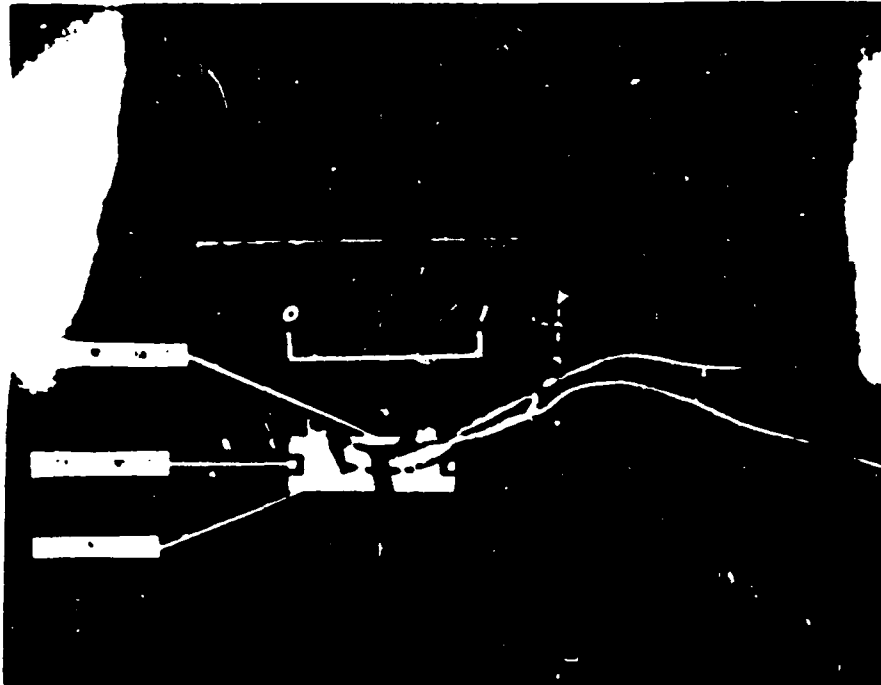
Figure 14 3-inch drag-gage sensing link.

cut at a 45 degree angle to allow the field-weld installation by the contractor of a tapered gage sting mount supplied by the project. The mount was constructed of 6-inch diameter solid steel stock and tapered to the diameter of the flared section of the gage sting (see Figure 15).

The gage sting was inserted into a bored hole in the mount and held in place with set screws.

A cable-junction box was installed in the concrete base with cable conduits running from the box to the pipe for facilitating cable hookup and calibration work. A typical station is shown in Figure 15.

Calibration. All spherical gages, after installation in the field and connection to the recording system cables, were statically calibrated in six directions along the three sensitive axes. The calibration rig, Figures 16 and 17, consisted of a rigid frame attached to the gage sting and supporting two pneumatically operated piston assemblies. The frame was rotated so that one piston applied force on the equator of a sphere at the proper points. The other piston was oriented to apply force along the axis away from ground zero. The piston was made airtight by the use of a Bellofram convoluted-diaphragm-type seal. Air was supplied to it from a 450 psi

28

Figure 15 Typical spherical drag-gage station.
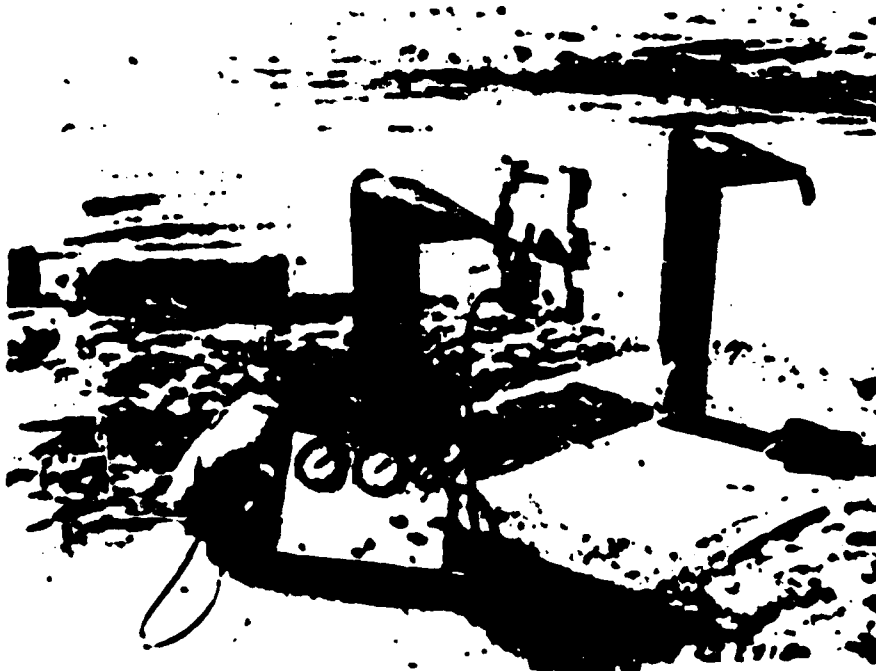
Figure 16 3-inch drag-gage calibrator in
position for field calibration of vertical-
gage component.

SECRET

tank through regulators giving a range of pressures from 0.2 inch of water to 300 psi. The
pressures were read on dial gages having 2 percent accuracy. The calibrator for the 10-inch
spheres was larger and heavier than that for the 3-inch spheres and it had a larger actuator-
piston area so that the same regulator and gage system could be used interchangeably. The
actual forces developed were found as the product of the pressure and the effective piston area.
An accurately calibrated (0.1 percent) Baldwin SR-4 load cell was used to double check the cali-
bration of the system.

Some loss of accuracy, noted for low-force calibrations, was attributed to stiffness of the
bellofram seal. However, by applying pressures to the calibrator which would produce a se-
quence of force values which oscillated about and slowly approached the desired value, the effect
of the stiffness, as well as the effect of static friction in the gage, could be minimized.
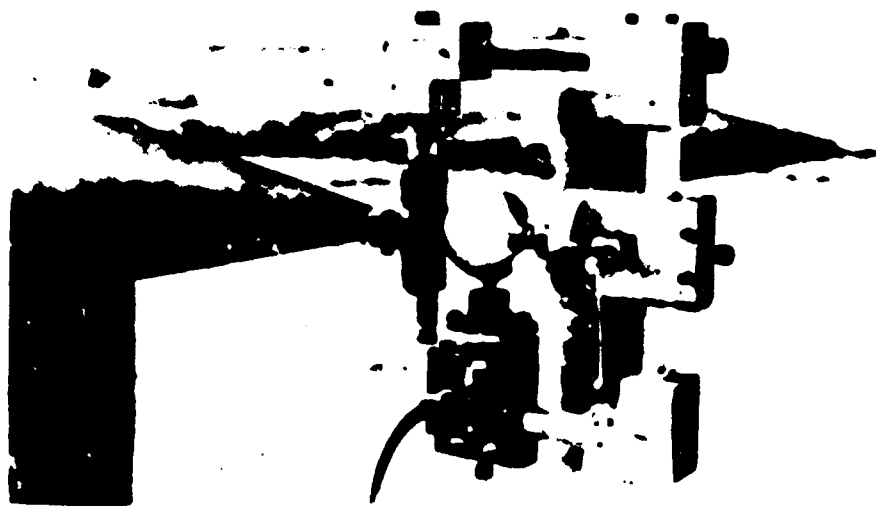
Figure 17 Detail of positioned 3-inch drag-
gage calibrator.

The calibrators were used in the field by adjustment of the regulators, the forces requested
from the recording shelter were applied and held constant until the proper recording mechanism
adjustments were made. Calibration forces in each direction were applied as shown in Table
5.

REQUIRED DATA

The only data required of the drag gages were curves of net force versus time along the
three mutually perpendicular axes of the gage.

The auxiliary data required was a plot of dynamic pressure versus time.

This data was recorded by the magnetic tape recorder system described in References 18
and 19. The magnetic tapes on which the data were recorded were played back through an
oscillograph recorder which presented the data on a roll of 7-inch-wide photographic paper.
Timing pulses marking 1^{1}_{2}-msec intervals and a zero time pulse were also displayed with the
data trace.

The data was read on a projection type data reader equipped with movable cross hairs. The
positions of the cross hairs were expressed numerically by an electronic device and the values
so obtained were automatically punched on IBM cards. In this manner, the coordinates of all

the peaks on the records were determined. The IBM cards were then fed into the ORDVAC high speed digital computer and, with the proper programming and the introduction of the calibration data, it linearized and smoothed the records. A description of this process is given in Appendix B of Reference 20.

As received from the ORDVAC. the data represented the forces measured along each of the three principal axis of the gage. It was originally thought that simple vector manipulations would suffice to determine the magnitude and direction of the total-force vector, however, recent shock tube tests performed in the BRL 24 inch shock tube have shown that the desired results may not be obtained by this method. As the angle between the flow and the axis of the sting increases above a few degrees, the sting seriously affects the flow and the total force changes as a function of the angle. It was found, as an empirical result, that the axial component of measured force varies little from the product of the predicted (theoretical) force and the cosine of the previously mentioned angle.

The method used in obtaining the total force from the field data was directly based on the shock tube experiments. the axial measured force value was divided by the cosine of the angle

TABLE 5 CALIBRATION POINTS FOR 3-INCH AND 10-INCH SPHERES

All values given in terms of equivalent drag pressure, psi.

Site	10-Inch Spheres					3-Inch Spheres				
	Axial	Transverse		Vertical		Axial	Transverse		Vertical	
		Left	Right	Up	Down		Left	Right	Up	Down
	plus	plus	minus	plus	minus	plus	plus	minus	plus	minus
Able	0	0	0	0	0	0	0	0	0	0
	3.22	2.97	2.97	2.97	2.97	3.6	3.6	3.6	3.6	3.6
	6.37	5.36	5.36	5.36	5.36	6.1	6.4	6.4	6.4	6.4
	9.27	7.31	7.31	7.31	7.31	9.3	9.3	9.3	9.3	9.3
	12.13	—	—	—	—	—	—	—	—	—
Dog	0	0	0	0	0	0	0	0	0	0
	0.15	0.15	0.15	0.15	0.15	0.17	0.18	0.19	0.18	0.18
	0.27	0.27	0.27	0.27	0.37	0.42	0.45	0.45	0.45	0.45
	0.37	0.37	0.37	0.37	0.37	0.62	0.62	0.62	0.62	0.62
	0.50	0.50	0.50	0.50	0.50	0.79	0.79	0.79	0.79	0.79
	0.64	0.64	0.64	—	—	1.05	—	—	—	—
	0.78	—	—	—	—	—	—	—	—	—

between the assumed flow direction and the direction of the axis of the gage sting. The supposed flow direction was radial, emanating from true ground zero.

A correction was also necessary to account for the difference in pressure between the inside of the gage (atmospheric) and that outside the gage (side-on) which tended to force the sting into the gage shell. This would be registered by the gage as a force in the same direction as the true drag force and having a magnitude $P_s a$, where P_s is side-on blast pressure and a is the circular cross sectional area of the sting. It is apparent that this sting correction force would have to be subtracted from the indicated force to give the true drag force.

RESULTS AND DISCUSSION

The results of this test were seriously affected by the great differences between the pressures predicted and those obtained (Table 6).

At Site Able the signal recorded was about $\frac{1}{20}$ that expected and was, consequently, little stronger than the system noise. Also, the corresponding forces did not exceed the small static forces which existed in the damping leaves by a large margin.

At Site Dog, the pressure was almost twice that expected and, while the averaged drag pressures did not exceed those calibrated for, in some cases, peak values caused by mount oscillation were high enough to overstress the links.

At Site Dog, some flaw in the 3-inch gage (No. 4) produced occasional abrupt changes in the record displacement. In such cases, the exact amount of the shift was apparent and based on the assumptions that the gage sensitivity was unaffected and that the output of the gage returned to zero, the segments of the curve were transposed to produce a continuous curve.

Sting corrections introduced a problem, for in some cases the product of side-on pressure and area was almost as large as the indicated force. Since the indicated force is expected to be the sum of the true force and the sting correction was, it may be assumed that one of these was small in the cases in question. The sting correction is dependent upon the difference between the pressure trapped ins de the spherical shell and that outside; here, the blast pressure.[1]

There was evidence that, during the 2-week period between the ready date and the actual shot date, the continuous action of the wind caused the silicone grease seal between the sting and the gage shell to flow and to rupture. Thus, air flow past the sting and into the shell was possible and the sting correction became a time dependent (as opposed to parametric) function

TABLE 6 MOST PROBABLE PEAK DRAG COEFFICIENT VALUES

| Site | Gage * | Predicted Values | | Actual Values [†] | | |
		Overpressure	Dynamic Pressure	Overpressure	Dynamic Pressure	Drag Coefficient
		psi	psi	psi	psi	
Able	10-1	23	10.6	4.1	0.395	0.53
Able	3-1	23	10.8	4.1	0.395	0.61
Able	5-2	23	10.8	4.1	0.395	0.55
Dug	10-2	3.2	0.26	4.5	0.475	0.91
Dog	3-3	3.2	0.26	4.5	0.475	0.47
Dog	3-4	3.2	0.26	4.5	0.475	0.38

* First number is gage diameter in inches, second number is serial number
† Dynamic pressure computed using Rankine-Hugoniot relations.

generally smaller than the simply obtained value for the sealed gage. Since the rate of pressure rise inside the shell was dependent on an unknown, the degree to which the seal had failed, and its description was not considered possible.

To investigate leak time, a gage with a faulty seal was placed in a chamber which was filled with air to a pressure of 5 psi. After a delay sufficient to allow pressure inside the gage to equalize with pressure external to it, a diaphragm on the chamber was ruptured to allow almost instantaneous dissipation of the pressure. The gage leak time was observed as the duration of output on the axial recording channel. This time was found to be a small portion of the Shot Cherokee blast wave duration. The test could be considered only an approximation of field conditions since there was no way of knowing the actual sizes of the leaks present in the field.

Since the existence of dynamic pressure seemed sufficient evidence for a drag force and since the failure of the pressure seals seemed quite certain, it was deemed prudent to neglect sting corrections. Thus, only a short portion early on the record of drag force would be in error.

The dynamic pressure gages suffered from the angle effects and the small signal amplitudes so that no direct measurements of Q were available.

The data is presented with all corrections made. Two forms of data presentation are used: the first gives time dependent plots of drag pressure measured along the three axes and the second gives a logarithmic plot of C_D versus Q. It should be noted that those plots of drag pressure versus time marked axial have been corrected by division by the cosine of the yaw

[1] Because fill time is difficult to predict accurately even under known conditions, it was considered preferable to seal the gage and use a sting correction.

angle, to give the best estimate of total drag pressure values. The form of the curve was precisely similar to the true axial drag pressure curve. The yaw angle measured on Site Able was 13 degrees, its cosine was 0.978. The yaw angle measured on Site Dog was 32 degrees, its cosine was 0.848.

The drag coefficients were computed using drag pressures taken from the corrected axial drag pressure plots and using dynamic pressures computed from side-on pressure values with the aid of the Rankine-Hugoniot relation. Drag-pressure values, taken at regular intervals (generally, each 500 msec) were divided by dynamic pressures computed for the corresponding times. The use of the Rankine-Hugoniot relation to determine dynamic pressure anywhere, except at the shock front was incorrect, but the approximate results obtained, where comparisons have been made, were not found to differ widely from directly measured values.

The results for the 10-inch gage at Site Able are given in Figures 18 and 24. Except for the correction to the axial drag pressure values, the plots of drag pressure versus time are exactly as received from the smoothing and linearizing process. In order of descending dynamic pressure, the drag coefficients were computed at the following times: using the peak drag pressure value; 75 msec, using a value which was the average of the spikes occurring at the first of the record; 200 msec, using a value corresponding to the height of the curve just following the occurrence of the spikes; and 500, 1,000, and 1,500 msec using corresponding computed dynamic pressure values. The 200 msec value was chosen as most probably correct.

The results for the 3-inch gage (No. 1) at Site Able are given in Figures 19 and 24. Except for the correction to the axial drag pressure values, the plots of drag pressure versus time are exactly as received from the smoothing and linearizing process.

Only one value of drag pressure, that at zero time, was used in computing a drag coefficient because the indicated values had become negative at 500 msec and would have indicated negative drag coefficients.

The results for the 3-inch gage (No. 2) at Site Able are given in Figures 20 and 24. In addition to the correction to the axial drag pressure values, several spikes on the axial and vertical records were smoothed through. These spikes first appeared long before the detonation and, because of their regularity in time and shape, they could be attributed to a tape-drive defect and smoothed with no fear of their being representative of an actual drag pressure. The values, in order of descending dynamic pressure, were taken at zero, 500, 1,000, 1,500, 2,000, and 2,500 msec. The value taken as most probably correct occurred at zero on the time scale.

The results for the 10-inch gage at Site Dog are given in Figures 21 and 25. In addition to the correction to the axial drag pressure values, the vertical drag pressure plot was shifted downward by 0.09 psi so that its final values coincided with the base line. Similarly, the transverse drag pressure plot was shifted upward by 0.02 psi.

Only two drag coefficient values were determined for this gage since drag pressure values became negative after 900 msec. The value of drag pressure corresponding to zero on the time scale was chosen as the first value occurring after the rise and not the spike which came slightly later.

The results for the 3-inch gage (No. 3) at Site Dog are given in Figures 22 and 26. In addition to the correction to the axial drag pressure values, the vertical drag pressure plot has been shifted upward by 0.07 psi so that its final values coincided with the base line. Similarly, the transverse drag pressure plot was shifted upward by 0.05 psi.

The indicated drag pressures dropped rapidly so that only the first of the four drag coefficient values computed appears plausible.

The results for the 3-inch gage (No. 4) at Site Dog are given in Figures 23 and 25. In addition to the correction to the axial drag pressure values, the segments of the curve defined by abrupt shifts in gage displacement were corrected as described previously.

Here, as in most of the previous records, the drag pressure appeared to drop rapidly and the drag coefficient values dropped with corresponding rapidity. The most probable value of drag coefficient was that occurring at approximately zero on the time scale.

Table 6 gives the most probable values of drag coefficient.
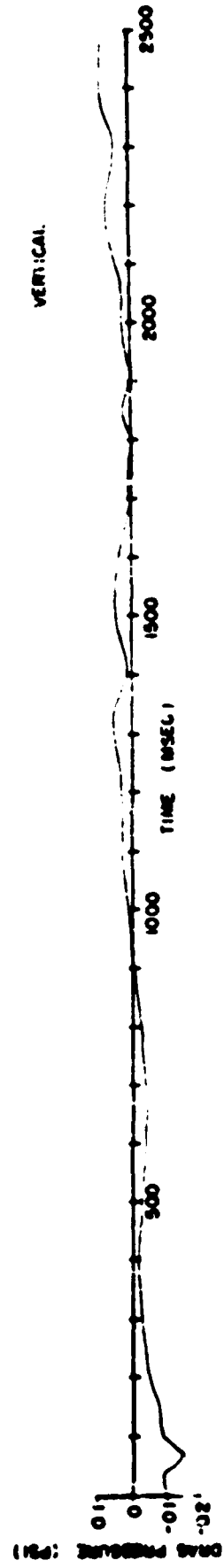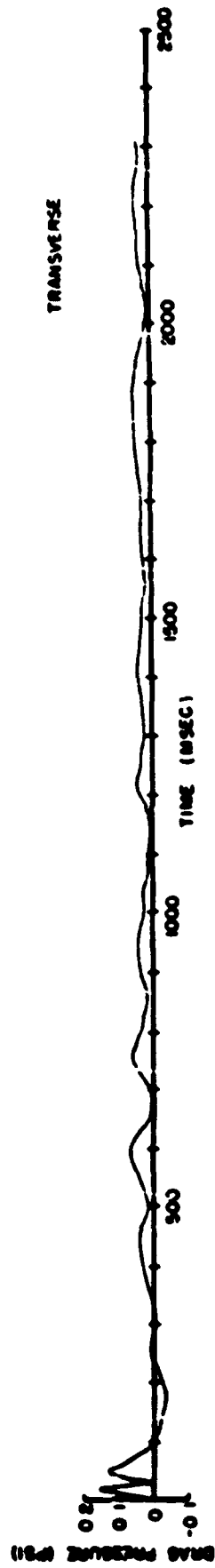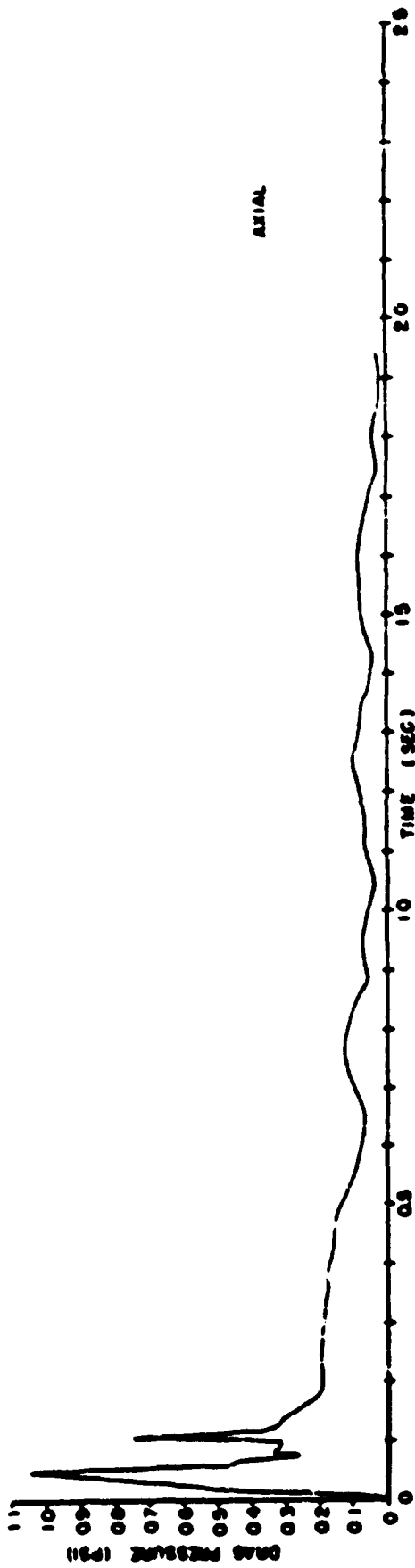
Figure 18 Drag pressure versus time from 10-inch drag gage on Site Able.
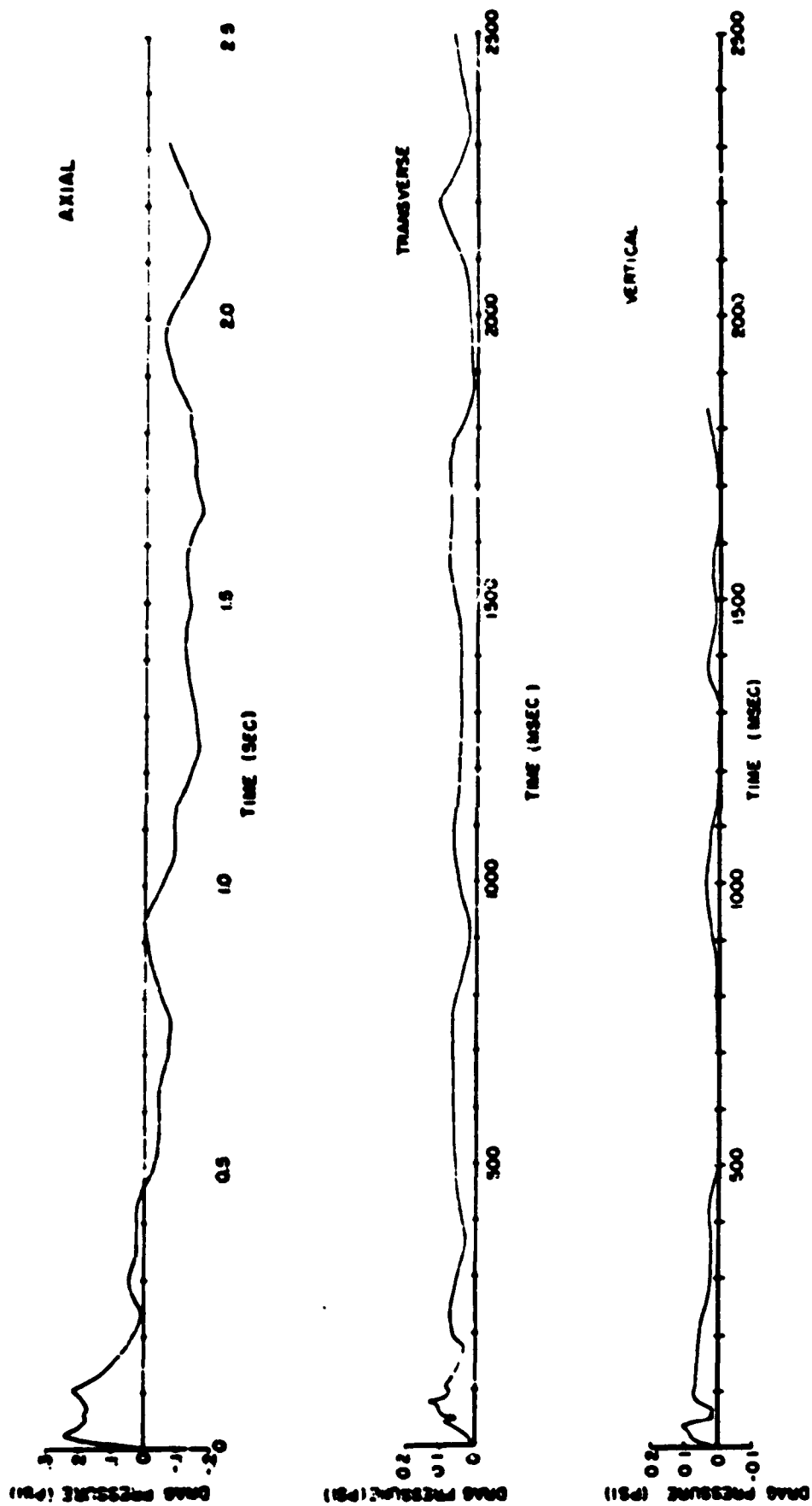
Figure 19 Drag pressure versus time from 3-inch spherical drag gage No.1 on Site Able.
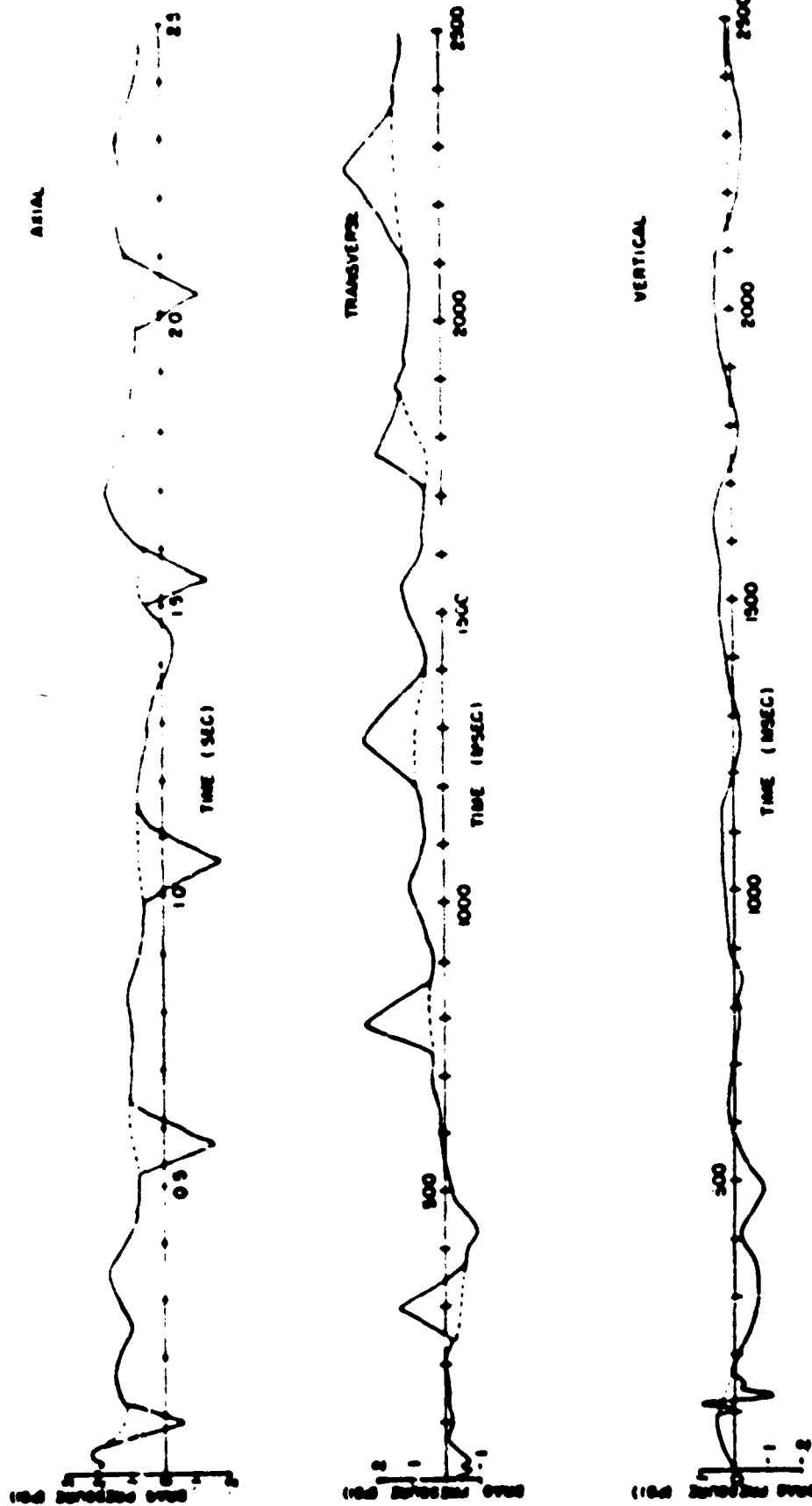
Figure 20 Drag pressure versus time from 3-inch spherical drag gage No. 2 on Site Able.

SECRET
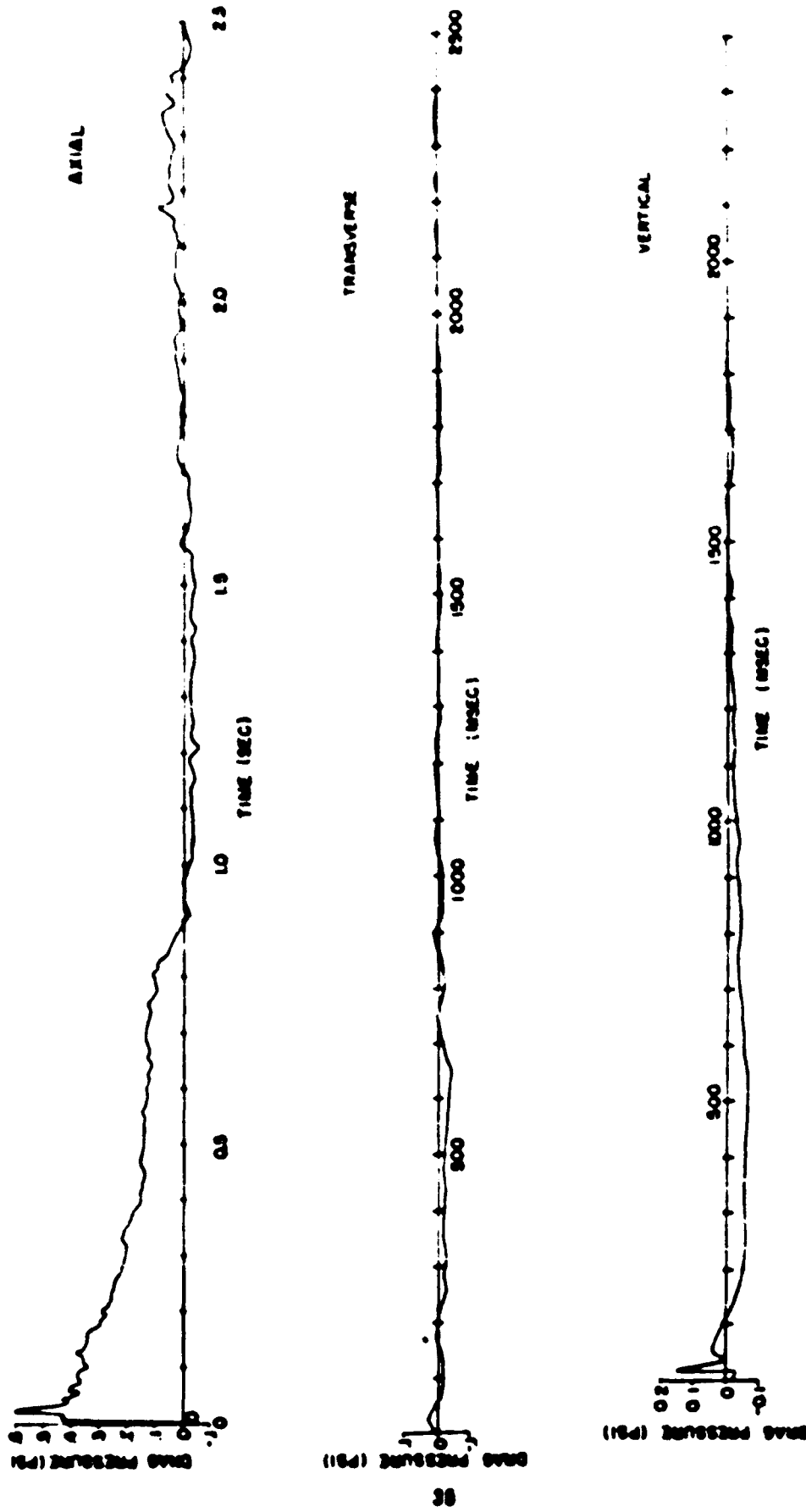
Figure 21 Drag pressure versus time for 10-inch spherical drag gage on Site Dog.

36
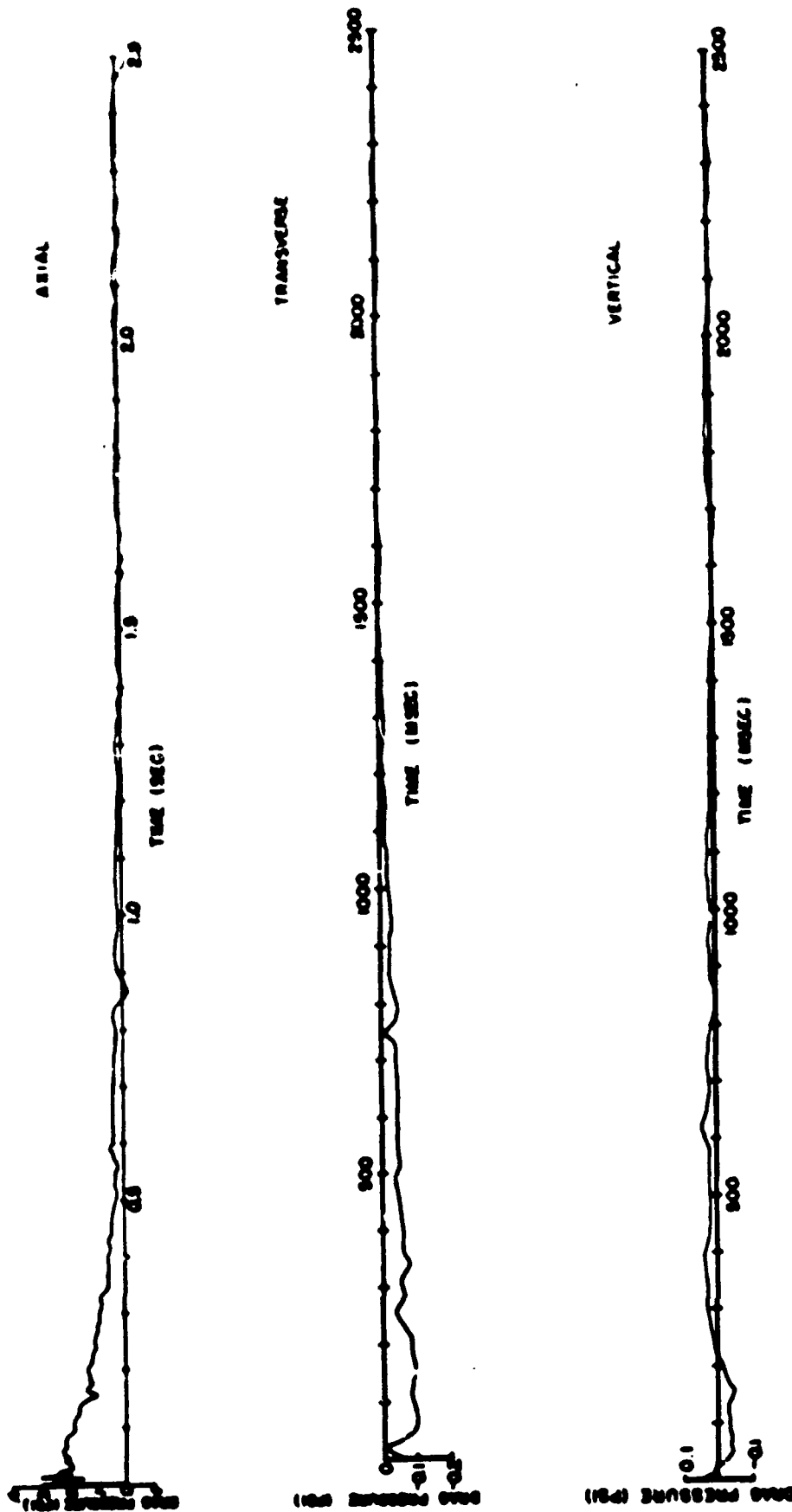
Figure 22 Drag pressure versus time from 3-inch spherical drag gage No. 3 on Sta Dig.
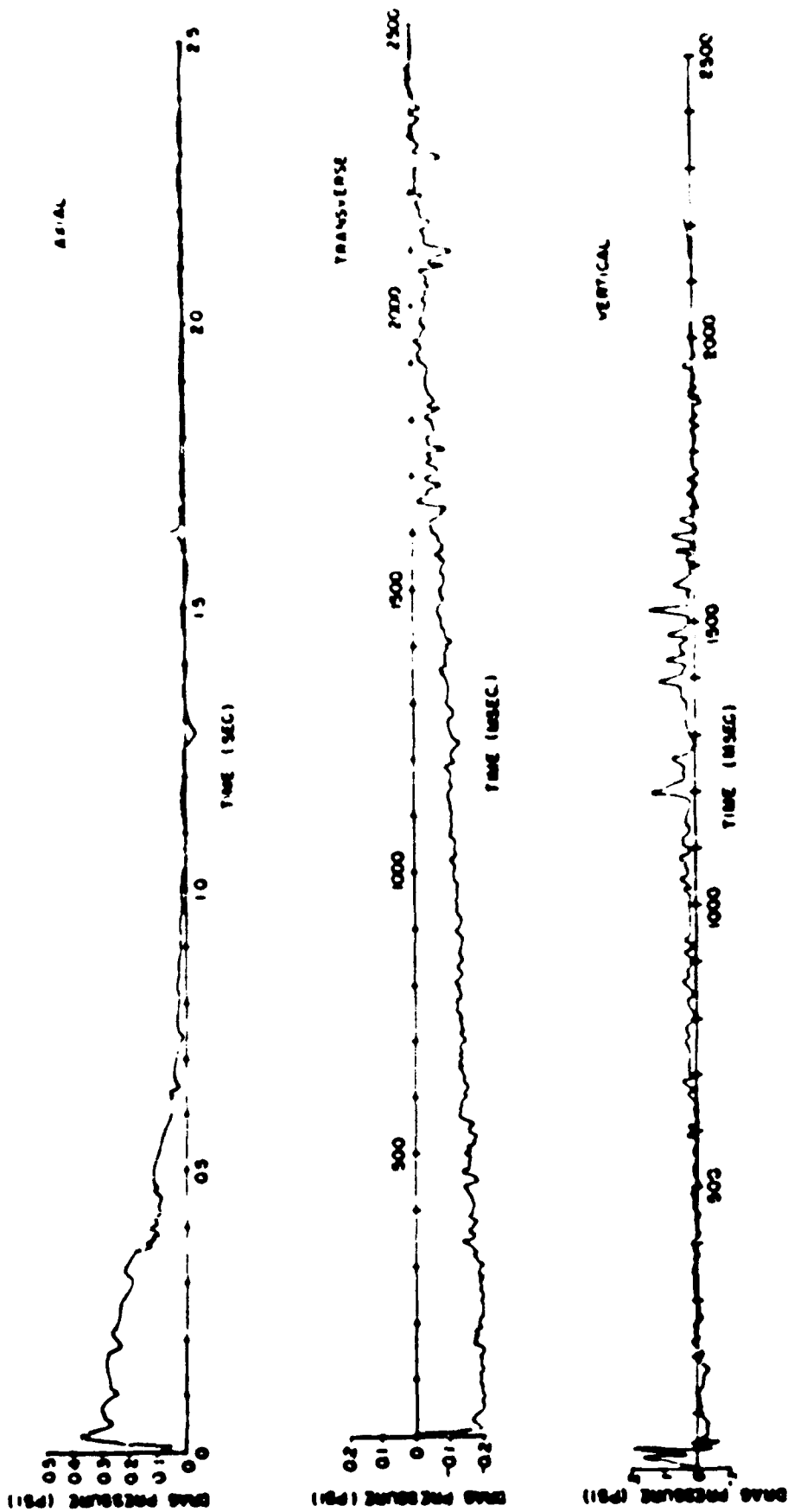
Figure 23 Drag pressure versus time from 3-inch spherical drag gage No. 4 on Site Dog

(c) 3-inch gage No. 2

DYNAMIC PRESSURE (PSI)

DRAG COEFFICIENT

(c) 3-inch gage No. 4

DYNAMIC PRESSURE (PSI)

DRAG COEFFICIENT

(b) 3-inch gage No. 1

DYNAMIC PRESSURE (PSI)
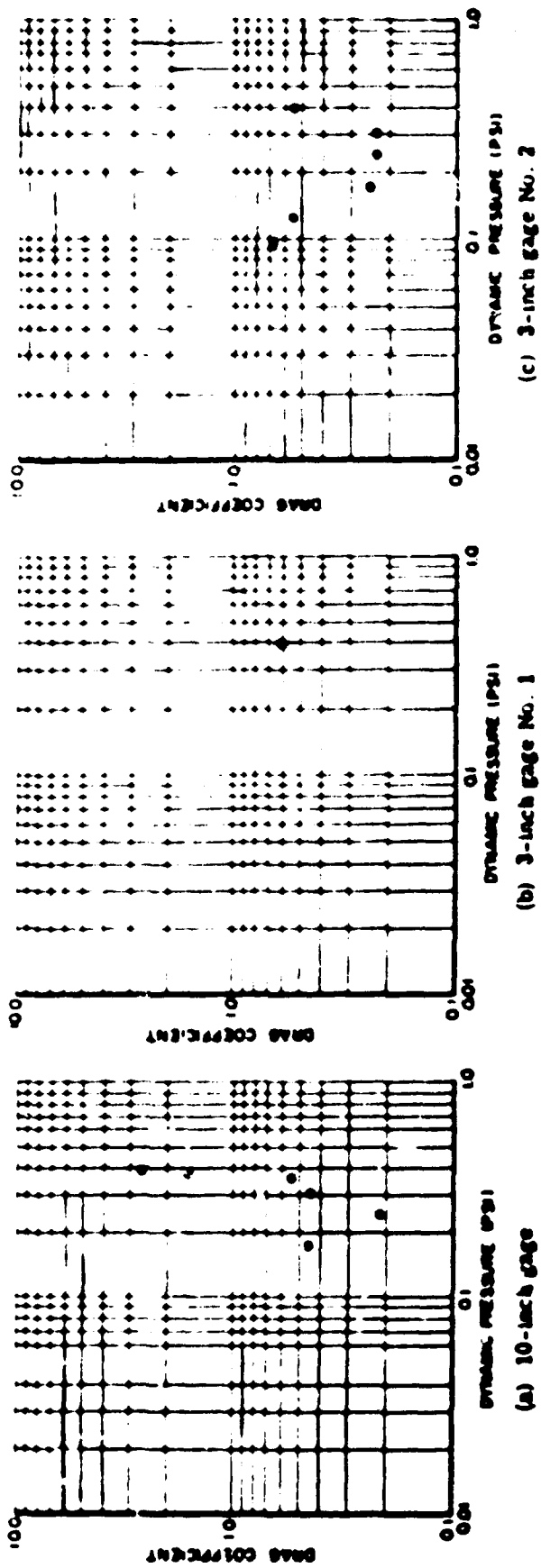
DRAG COEFFICIENT

Figure 24 Log C_D versus Q for drag gages on Site Able.

(b) 3-inch gage No. 3

DYNAMIC PRESSURE (PSI)
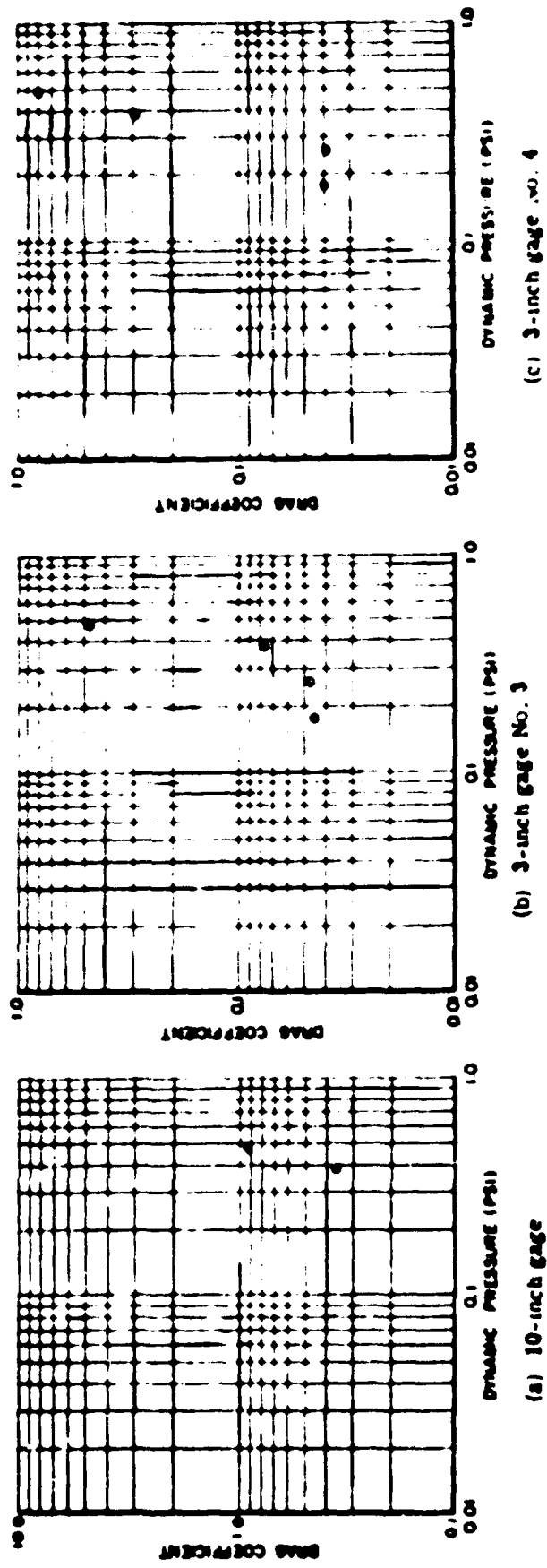
DRAG COEFFICIENT

Figure 25 Log C_D versus Q for drag gages on Site Dog.

(a) 10-inch gage

DYNAMIC PRESSURE (PSI)

DRAG COEFFICIENT

(a) 10-inch gage

DYNAMIC PRESSURE (PSI)
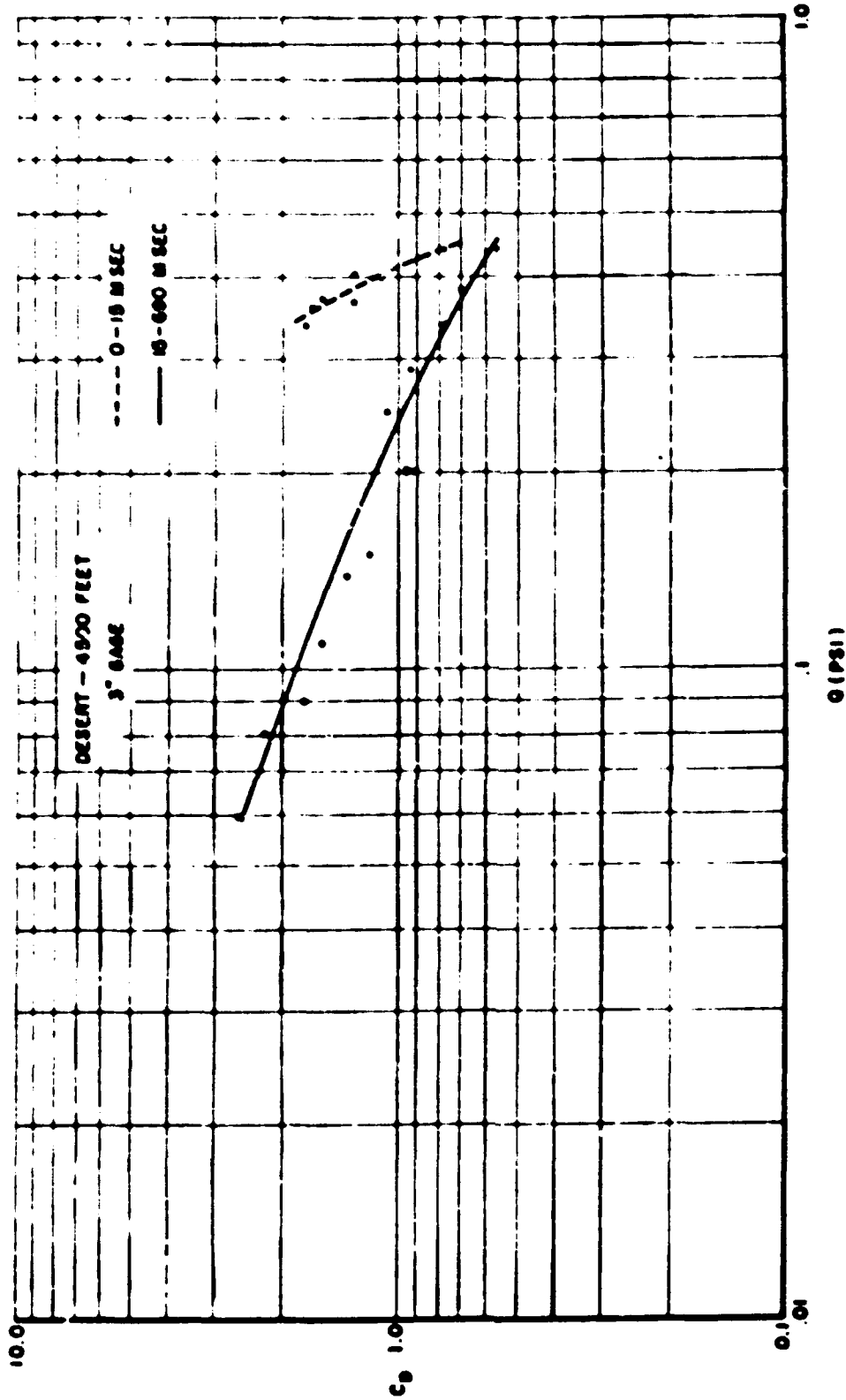
DRAG COEFFICIENT

Figure 26 *Logarithmic plot of drag coefficient versus dynamic pressure for 4.5 psi side-on pressure region (4,500 feet desert line station, Operation Teapot).*

SECRET

Figure 26 shows a plot of log C_D versus log Q for a 3-inch gage at 4,500 feet on the dust-laden-air line of Operation Teapot. Comparison of the Operation Teapot curve with those for the Operation Redwing curves shows little similarity except that drag coefficients for the Site Able gages are in the same general range for the peak values of Q, and for the Site Dog gages are considerably lower.

CONCLUSIONS

The objectives set down for the spherical drag gage investigations were not achieved. The taxing conditions under which it was necessary for the gages to operate coupled with dubious behavior on the part of the gages reduced attempts to interpret the data to speculation. A tabulation of Most Probable Peak Drag Coefficient Values (Table 6 is given; however, the values should not be considered authoritative but rather attempts to distill from the study any information which indicated trends and general behavior. The choice of these values was, in some respects, arbitrary with past experience in related studies serving as a guide.

RECOMMENDATIONS

Further testing should be carried out to obtain clean-air classical wave data in order to bridge the gap between steady-flow wind tunnel data and the data obtained on Operation Teapot. Such studies should not, however, be undertaken until a medium characteristic more adequate than dynamic pressure can be determined. Basic instruments for measuring such variables as medium density, dust density, flow velocities, and viscosity (which are necessary in determining Q and R) should be used in conjunction with the drag gages.

Part 3
MILITARY VEHICLES

OBJECTIVES

The primary objective of this part of Project 1.5 was to compare vehicle damage from a classical wave to vehicle damage from a nonclassical wave. Specifically, the variation of damage obtained from Shot Lacrosse (39.5 kt), Operation Redwing, and the damage obtained from Shot 4 (43 kt), Operation Teapot, was to be investigated. Both shots were approximately the same yield, but a precursor effect was observed on Shot 4, whereas on Shot Lacrosse no precursor effect was observed at the vehicle stations.

The secondary objective was to obtain further data from a wide range of yields (0.19 kt - 3,500 kt) and over the surfaces typical of the EPG.

BACKGROUND AND THEORY

The exposure of military vehicles under free field conditions dates back to Operation Buster-Jangle. Data from this and succeeding operations have been used to construct damage prediction charts. For certain blast conditions, further significant data were desired. The three shots on Operation Redwing used for jeep exposure were chosen to supplement the previous data.

In past operations it has been shown that different size trucks placed the same distance from ground zero experienced approximately the same degree of damage. On Operation Redwing, the exposed vehicles were all old-type (WW II) $\frac{1}{4}$-ton trucks, but the damage data are applicable to all $\frac{1}{4}$-ton through 5-ton trucks and serve as a basis for estimating damage to similar drag-sensitive targets.

OPERATIONS

Eighteen World War II jeeps (trucks, $\frac{1}{4}$-ton, 4 by 4, utility, Model M38) were used on Operation Redwing. A preshot vehicle-condition inspection was performed, and numbers were stenciled on all major components, sheet metal sections, and vehicles to facilitate postshot identification. The windshields, canvas, and bows were removed before the vehicles were placed in position. Station ranges from ground zero were chosen on the basis of TM 23-200 (Reference 24). Steel stakes were driven into the ground beside the wheels of each positioned vehicle to facilitate displacement measurements, and each vehicle was secured in that position by placing the transmission in reverse gear, the transfer case in low range, four-wheel drive, and by engaging the hand brakes. The postshot evaluation consisted of inspecting each vehicle and measuring displacements. An attempt was made to start and operate each vehicle where practical. Vehicles which could be operated within one man-hour of maintenance time were considered to be immediately combat usable. Damage levels (light, moderate, and severe) as well as type of maintenance were selected on a basis of man-hours required for repair:

Damage Level	Man-hours	Type of Maintenance	Man-hours
Light	0 - 1	Organizational	0 - 6
Moderate	1 - 32	Field	6 - 32
Severe	>32	Depot or Salvage	>32

INSTRUMENTATION

Ten vehicles were exposed to Shot Lacrosse, a surface burst of a 39.5 kt device. The vehicles were placed in pairs at five stations ranging from 2,500 to 4,378 feet from ground zero,

41

with one vehicle facing into the blast (FO) and the other broadside to the blast (SO). These
stations are indicated in Figure A.2 (Appendix). Figures 27 and 28 show the vehicles in place
and the general ground conditions before the blast.

The exposure of jeeps to Shot Zuni was a continuation of the collection of damage data from
multi-megaton devices begun during Operation Castle. Ten vehicles, including two recovered
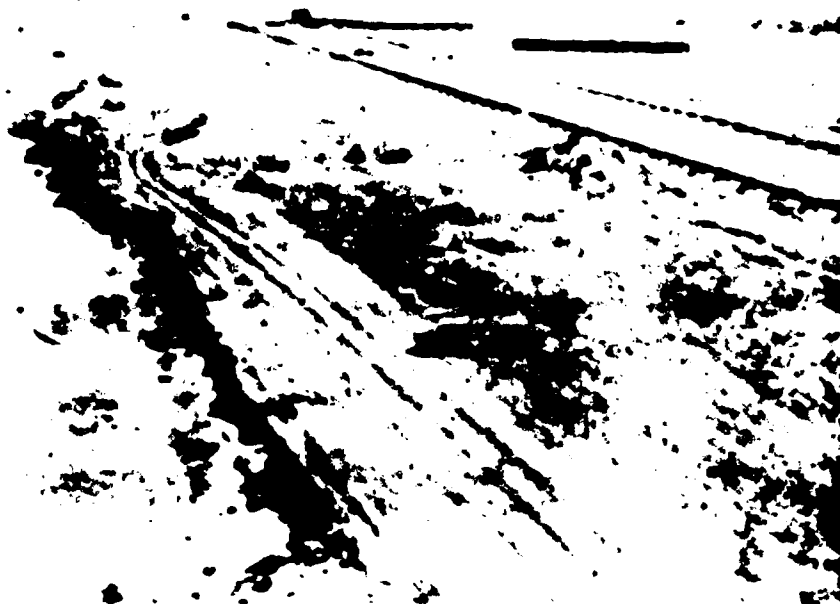
(a) Stations 154.09 and 154.10
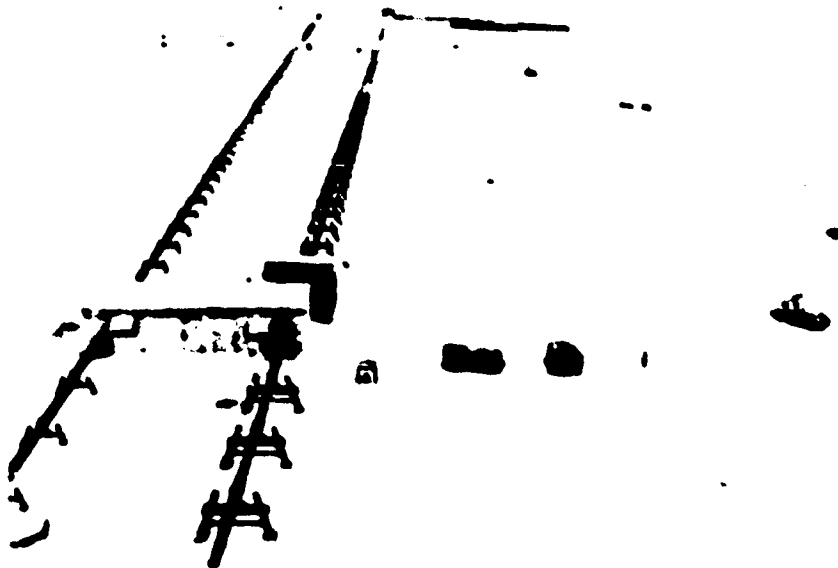
(b) Stations 154.11 and 154.12

Figure 27 Ground conditions before Shot Lacrosse (toward ground zero).

from Shot Lacrosse, were exposed to Shot Zuni. Eight vehicles were placed in pairs (one face-
on and one side-on) at four locations ranging from 8,300 to 13,800 feet. One side-on vehicle
was placed at 7,000 feet and one side-on vehicle was placed at 16,500 feet. Figure A.4 shows
the approximate location of these stations, while Figure 29 shows the vehicles in position before
the blast.

42

SECRET

(a) Station 154.09

(b) Station 154.11

Figure 26 Vehicles in place before Shot Lacrosse.

SECRET

(c) Station 154.02

(d) Station 154.03

(a) Station 114.07

(b) Station 154.01

Figure 29 Vehicles in place before shot Zuni.

44
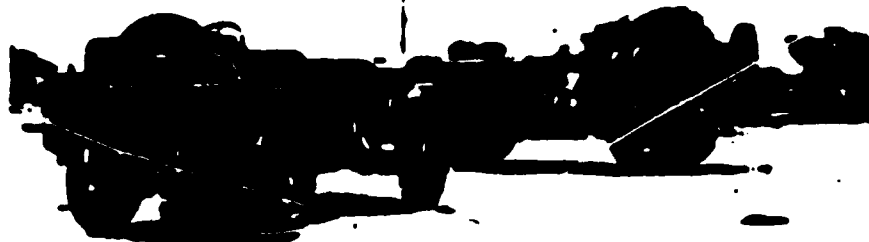
(e) Station 154.04

(f) Station 114.09

Figure 29 Continued.

Eight vehicles were exposed to Shot Yuma, a 0.19 kt device detonated from a 200-foot tower. Previous to this shot the lowest yield weapon to which vehicles had been exposed was approximately 1 kt, and it was desirable to extend damage prediction charts to the fractional kt region. The vehicles were placed in pairs at four stations ranging from 150 feet to 400 feet from ground zero. Figure A.3 indicates the approximate locations of the vehicle stations. Figure 30 shows vehicles in place before the shot.

RESULTS AND DISCUSSION

Tables 7, 8, and 9 give the damage evaluation of data obtained on Shots Lacrosse, Zuni, and Yuma, respectively. Figures 31, 32, 33, 34, and 35 show the vehicle damage experienced on these shots.

COMPARISON WITH TM 23-200

The report "Capabilities of Atomic Weapons" (Reference 24) contains a chart of isodamage contours for scaled height of burst (HOB) versus scaled ground range for use in the prediction

(Text continued on Page 55.)

SECRET

Burst Range	Station	P_o	P_d	Displacement	Final Position	Degree of Damage	Description of Damage	Man hours Reqd to Restore Combat Usability	Man hours Reqd for Complete Restoration	Type of Maintenance
										Organization
					Upright	Moderate				Field
						Light				Organization
					On left side	Moderate				Field
						Light				Organization
					Upright	Light				Organization
						Light				Organization
						Light				Organization
						Light				Organization
					Upright	None				Organization

*Computed

SECRET

47

TABLE 8 DAMAGE EVALUATION OF TRUCK, 1/4-TON, 6 x 6, UTILITY, MODEL M8 (or M), 2007 V1MA

Station	Range	Orientation	P_6	P_d	Emplacement	Final Position	Degree of Damage	Description of Damage	Man hours Required for Combat Usability	Man hours Required for Complete Restoration	Type of Maintenance
336.05	150	70	185	150.0°	13	Right side up	Severe	Frame damaged. Body, cowl, and hood (hull) damage severe. Instrument panel, wiring, conduit and wires destroyed by fire. Radiator, transmission, fuel tank, steering wheel and headlights also damaged.	0.0	63½	Depot
336.06	150	80	105	130.0°	35	Left side up	Severe	Frame damaged. Body, fender and cowl damage severe. Brake guard, radiator and fan damaged. One spring, two shocks and three wheels broken or damaged. The transmission, transfer, steering, fuel tank and clutch system also damaged.	...	63½	Depot
336.06	200	70	25.0	24.0	11%	Right side up	Moderate	Vehicle damaged severely by fire from Bomull to rear of cab. Instrument panel burned out. Body damage moderate. Brake guard, radiator, fuel tank and steering damaged.	15%	33½	Field
336.06	200	80	25.0	24.0	37%	Left side up	Severe	Floor, sides, cowl and rear panel of body damaged severely. Transmission and transfer cracked. Engine and crankcase broke cracked. One spring broken. Fenders, radiator, steering and fuel tank damaged.	...	26%	Depot
336.07	200	70	25	3.3	0%	Right side up	Light	Radiator leaking. Light body damage. Light body damage.	—	3%	Field
336.07	200	80	25	2.3	0%	Up side down	Light	Radiator leaking and sheared slightly damaged. Light body damage.	3	0	Field
336.08	400	72	3.0	3%	Right side up	Light	Rool blown off. Light body damage. Fuel tank and radiator top tank partially collapsed.	%	3½	Organization
336.08	400	80	3.0	0%	Up side down	Light	Rool blown off. Light body damage.	%	3½	Organization

*Computed

48

SECRET

Figure 30 Vehicles in place before Shot Yuma.
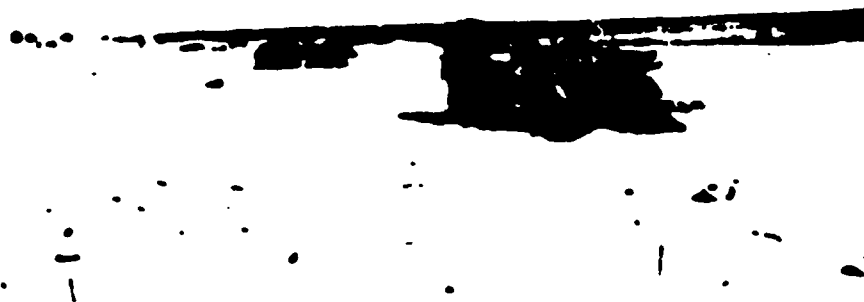
(a) Station 154.09, 2,500 feet

(b) Station 154.10, 2,770 feet

Figure 31 Vehicle damage obtained on Shot Lacrosse.

48
SECRET
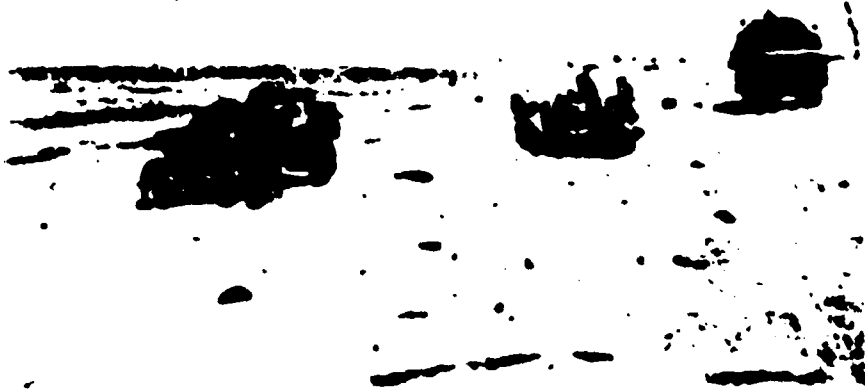
(c) Station 154.11, 3,350 feet
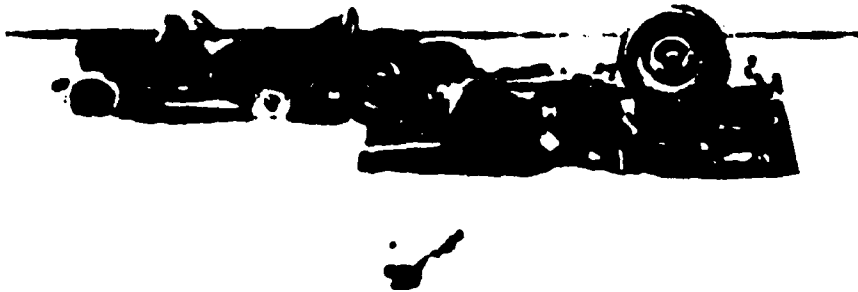
(d) Station 154.12, 3,900 feet

(e) Station 151.13, 4,370 feet

Figure 31 Continued.

(a) Station 114.07, 6,900 feet, SO vehicle

(b) Station 154.01, 8,300 feet, FO vehicle

(c) Station 154.01, 8,300 feet, SO vehicle

Figure 32 Vehicle damage obtained on Shot Zuni.

SECRET

(c) Station 154.03, 11,700 feet, FO vehicle

(d) Station 154.03, 11,700 feet, SO vehicle

(a) Station 154.02, 10,400 feet, FO vehicle
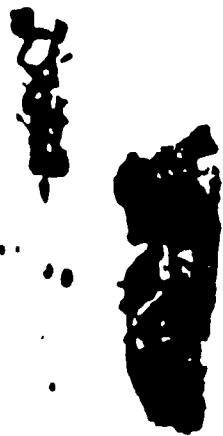
(b) Station 154.02, 10,400 feet, SO vehicle

Figure 33 Vehicle damage obtained on Shot Zuni.

(b) Station 154.04, 13,800, FO vehicle

(c) Station 114.09, 16,500 feet, SO vehicle

(a) Station 154.04, 13,800 feet, SO vehicle

Figure 34 Vehicle damage obtained on Shot Zuni.
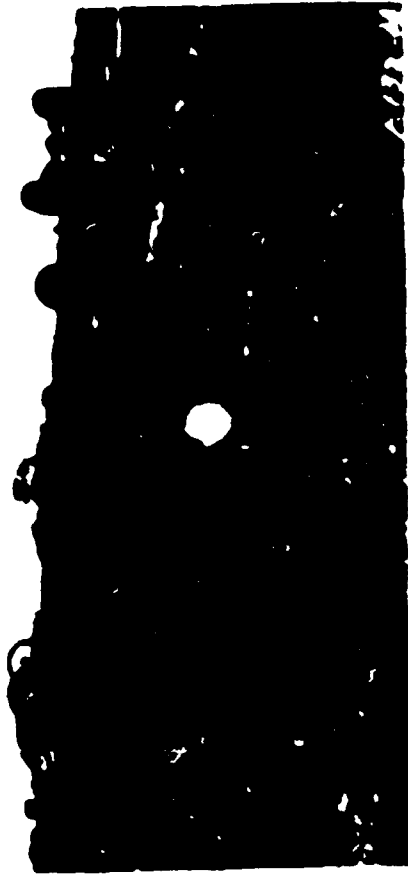
(c) Station 154.07, 350 feet

(d) Station 154.08, 400 feet

(a) Station 154.05, 150 feet

(b) Station 154.06, 250 feet

Figure 35 Vehicle damage obtained on Shot Yuma.

of damage to military vehicles. This chart, shown in Figure 36, was constructed by use of damage versus ground range curves derived from the data accumulated through Operation Teapot. The isodamage contours in the regular reflection region for the higher HOB were determined by considering the damage sensitivity of vehicles to peak overpressure as well as to the mass flow component of the blast wave. The isodamage contour for the low scaled HOB were essentially vertical. Below a scaled HOB of 100 feet, only a few data points were available so the isodamage contours were extended to zero HOB by constructing them parallel to the contours of ideal dynamic pressure. Almost all the NTS vehicle damage data on which this chart was based were obtained in a precursor region where pressure wave shapes were distorted.

The ground range for a given level of damage and a given HOB has been found to vary with the yield, w, approximately as $w^{0.4}$. A detailed discussion of the chart construction and the entire problem of damage prediction for vehicles is contained in AFSWP 311 (Reference 25).

The damage data obtained on Operation Redwing and Operation Teapot, Shot 4, are shown in Figure 36 for comparison with the prediction chart. The yield (43 kt) of Shot 4, Operation Tea-
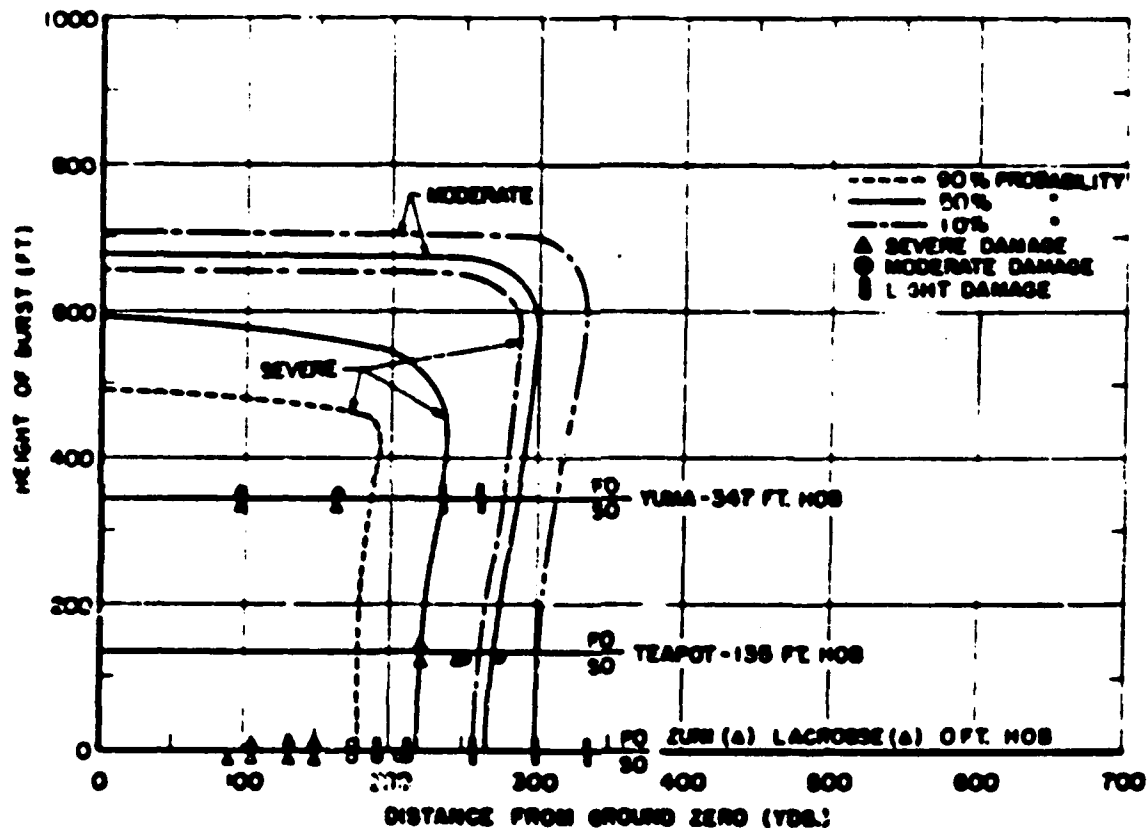
Figure 36 Height-of-burst chart for damage to military vehicles (TM 23-200).

pot, was similar to the yield of Shot Lacrosse (39.5 kt) of Operation Redwing. Damage to the vehicles was expressed as severe, moderate, or light in accordance with the level of maintenance required to restore the vehicles to combat use. The HOB for the shots was scaled as $w^{1/3}$ and the ground range was scaled as $w^{0.4}$.

As shown in Figure 36, the data from Shot 4, Operation Teapot, fits the predicted waves very well. However, a significant decrease in damage radii for the EPG shots is indicated.

Also shown in Figure 36 is the orientation of each test vehicle, whether side-on (SO) or face-on (FO) to the blast. There was an indication of extended damage radii for the SO vehicles, as would be expected for a drag-sensitive target. This effect appeared well in the overlap of the

57

data points for Shots Zuni and Lacrosse even though no severe damage was obtained on Lacrosse. A similar scheme was indicated by the Shot Yuma data points.

COMPARISON OF DAMAGE RADII VERSUS YIELD

In Reference 25 (AFSWP 511) the damage radii for selected levels of damage observed on a number of shots on previous operations were examined as a function of weapon yield. The damage radius for a selected level of damage for a given shot was determined by expressing the vehicle damage in terms of 10 categories, and plotting damage category versus ground range. The category for light damage was equated to 0.1, moderate damage to 0.5, and severe damage to 0.8. Further description of the categories and definitions of light, moderate and severe damage are given in Appendix B.

Damage category versus ground range curves were plotted for the Operation Redwing surface shots. The ground range for 50 percent probability of moderate damage and 50 percent probability of severe damage were then estimated. These damage radii are shown versus yield of device in Figure 37 together with damage radii of NTS shots. All damage radii except for Shot
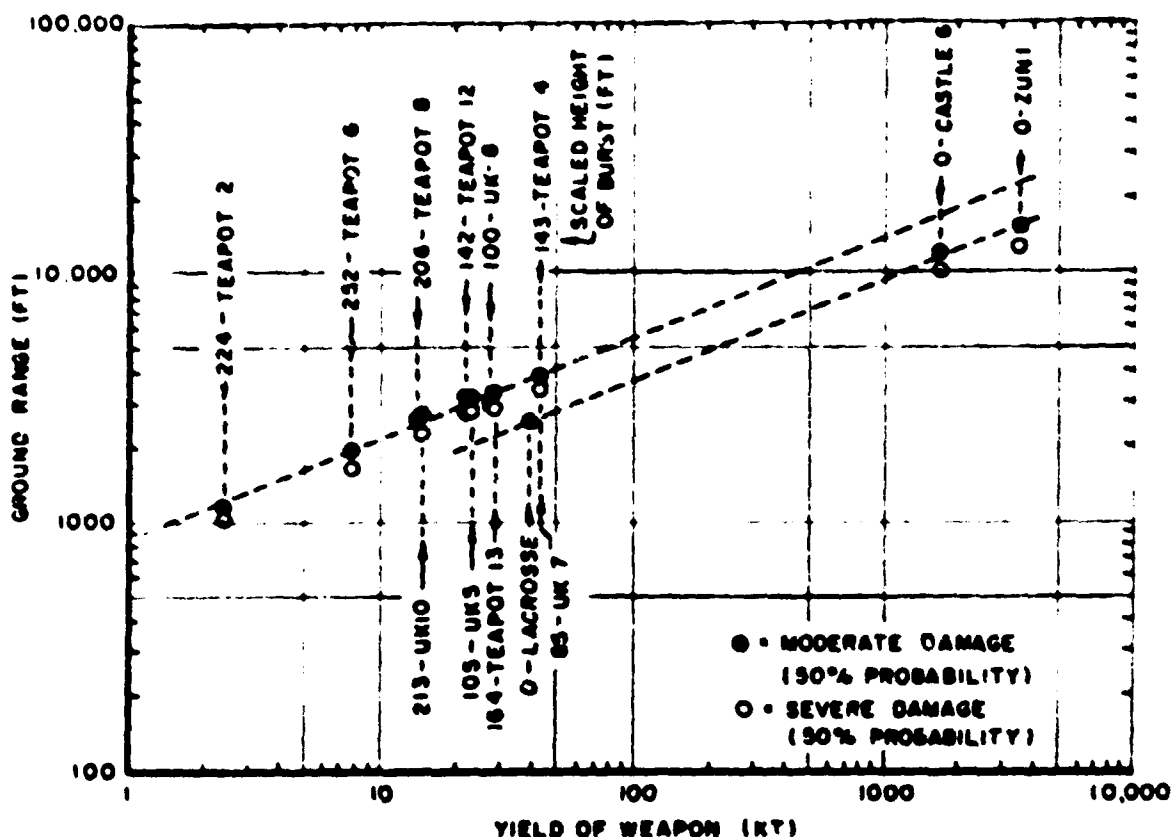
Figure 37 Ground range versus yield for various damage levels for EPG surface shots and NTS shots of low scaled height of burst.

13, Operation Teapot, and the Operation Redwing shots were taken from AFSWP 511, Figure 20.

A line showing the variation of damage radius with yield raised to the 0.4 power was drawn through the NTS data points in Figure 37. The line fits the data points well and substantiates the use of this scaling factor for the range of yield measured. The damage radius for Shot Lacrosse was significantly less than that of the corresponding NTS shots. When a line corresponding to scaling damage radius of $w^{0.4}$ was drawn through the point for Shot Lacrosse, it

58

intersected the data points for the other EPG surface shots. Hence, the NTS shots and the EPG shots formed two groups with difference damage radii but with similar scaling properties.

The NTS shots were detonated primarily at a scaled HOB between 100 and 300 feet, while the EPG shots considered were surface shots. However, under ideal conditions the data of the two groups should overlap, since the ideal dynamic pressure and dynamic impulse contours are essentially vertical for a range of HOB from 0 to 300 feet. The conclusion that the difference in damage radii observed is due primarily to the nonclassical disturbed wave shapes which occurred at the ranges of significant vehicle damage on the NTS shots and the essentially classical wave shapes which occurred on the EPG shots is further developed in succeeding paragraphs.

DYNAMIC PRESSURE EFFECTS ON DAMAGE

The peak dynamic pressure data obtained at the NTS showed considerable variation from the ideal values in the range of interest for damage to vehicles. The peak dynamic pressure data

Figure 38 Peak dynamic pressure versus scaled
ground range $(W^{1/3})$.

recorded at the EPG are shown compared to the peak dynamic pressure curve for ideal conditions in Figure 38. The pressures have been corrected for compressibility effects. The data points are scattered about the ideal curve and show that the peak values of dynamic pressure correspond to those of a classical wave.

Examination of the pressure-time wave forms showed disturbed wave shapes and hence a precursor formation on Shots Zuni and Lacrosse. It was not strong and did not extend into the region where effects on vehicle damage radii could be produced. No disturbed wave shapes were observed on Shot Yuma. Hence, the damage data obtained was for essentially classical type blast waves.

Figure 38 shows that peak dynamic pressure scales well from a large range of yields. The fact that the Shot Yuma data obtained a scaled HOB of 347 feet overlap the data obtained for

57

surface shots confirms that for essentially classical blast waves the scaled ground range for a given value of peak dynamic precursor remains essentially constant for a range of HOB from 0 to 3?0 feet.

Although previous operations have shown that peak dynamic pressure correlates well with damage (References 26 and 27) this was experimentally confirmed over a limited range of yields. The EPG shots provided a comparison of peak dynamic pressure over a wide range of yields for essentially classical waves. Table 10 gives vehicle orientation, vehicle damage, and corresponding peak dynamic pressure for Shots Yuma, Zuni and Lacr'sse.

On Shot Lacrosse, light damage was received primarily in the 0.8 to 2.2 psi dynamic pressure region. However, on Shot Yuma, light damage was received in the 9.2 to 9 6 psi dynamic pressure range. Moderate damage was received in the 5.3 to 7.4 psi region on Shot Lacrosse but at 24.8 psi on Shot Yuma. The moderate damage level was noted on Shot Zuni at 1.6 to 3.3 psi. Severe damage was noted on Shot Yuma from 24.8 to 136.8 psi. Severe damage was obtained on Shot Zuni from 6.4 to 24.6 psi.

The significance of this increase in peak dynamic pressure required for a given level of damage on a low yield shot compared to a high-yield shot becomes evident when the duration of

TABLE 10 DYNAMIC PRESSURE COMPARED WITH DAMAGE

Shot	Orientation	Dynamic Pressure (psi) for Damage which is:		
		Light	Moderate	Severe
Yuma	FO	9.2, 9.6	24.8	136.8 *
	SO	9.2, 9.6	—	24.8, 136.8 *
Zuni	FO	— —	3.3	6.4, 7.5, 16.9
	SO	— —	1.6, 3.3	6.4, 7.5, 16.9, 24.6
Lacrosse	FO	0.8, 1.0, 2.2, 5.3, 7.4	—	—
	SO	0.8, 1.0, 2.2	5.3, 7.4	—

* Computed

the wave is considered. Severe damage was obtained on Shot Zuni at 6.4 psi with a wave duration of 3,500 msec. On Shot Yuma the same damage occurred at 24.8 psi with a wave duration of 45 msec.

The requirement for an increase in peak dynamic pressure with a decrease in wave duration for constant damage was to be expected from the satisfactory use of scaling of damage radii with $w^{0.4}$, since the radius for a given peak dynamic pressure scales as $w^{1/3}$, and wave duration varies with yield. The calculations in WT-911, Appendix A, (Reference 26) in which damage radii are calculated for a classical blast wave for a wide range of yields, imply that for large yields the peak dynamic pressure is most important, while for small yields the dynamic impulse becomes of equal importance.

DIFFERENCE IN DAMAGE RADII FOR CLASSICAL AND NONCLASSICAL
    BLAST WAVES

A difference in damage radii is shown for NTS shots and EPG shots in detail in Figure 39. This figure shows a plot of the damage versus scaled ground range for $1/4$-ton trucks exposed on the NTS tower shots and the EPG surface shots. No distinction of orientation was made for these data. The short vertical bars at the 1.0 damage level mark the maximum ground range for which no damage less than 1.0 was obtained. The dashed curves represent the estimated average curves. The location of the predicted curve for surface bursts from TM 23-200 (Figure 3d) is indicated. The decreased ground range for this predicted curve represents a reduction incorporated to account for probable shielding effects on average terrain.

Considerable differences in damage radii between the NTS and EPG data is evident in Figure 39. At the severe damage level (0.8) the reduction in damage radius from the NTS curve is 35 percent for the EPG curve, and the reduction below the TM 23-200 curve is 28 percent.

The difference in HOB for the two groups is appreciable. However, under ideal conditions (classical blast waves) the ground range for a given value of dynamic pressure varies less than 10 percent for HOB from 0 to 300 feet scaled HOB. This range of HOB includes both groups of data.

If the effective yield for blast was reduced by interaction between the fireball and the ground, then the yield used in scaling the EPG data should be reduced to provide the proper comparison with the NTS data. However, a reduction to 80 percent of the yield (0.6 w) will increase the scaled damage radii by only 10 percent.

Some reduction in damage radii may be due to the soft, sandy surface at the EPG. This would have the effect of decreasing the force of impact of the vehicles with the surface as they
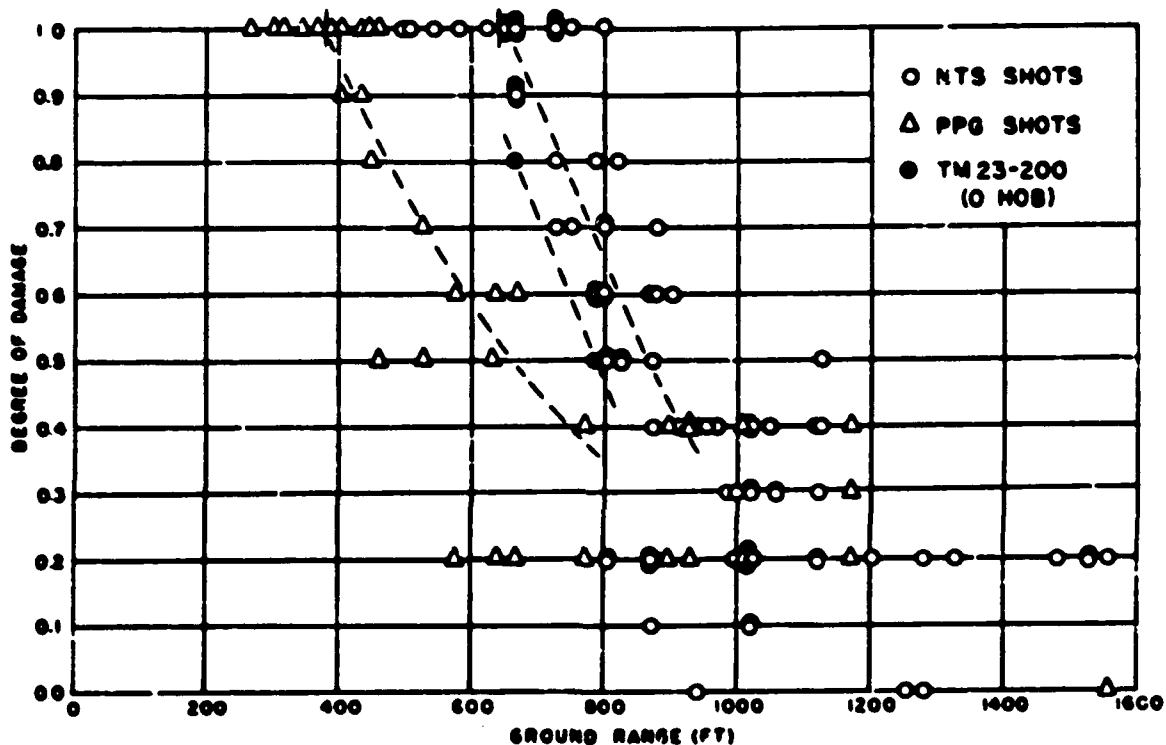
Figure 39 Degree of damage for $\frac{1}{4}$-ton truck versus scaled ground range ($1/W^{0.4}$) for EPG surface shots and NTS shots of low scaled heights of burst.

were tumbled by the blast wave. However, this effect was probably less than the effect due to the orientation of the vehicles.

Differences due to the atmospheric pressure have not been considered, since the change in damage radii with changes in atmospheric pressure are small (Reference 25).

Therefore, it is concluded that the large difference in damage radii shown in Figures 37 and 39 is due primarily to the occurrence of nonclassical wave shapes and associated higher drag forces on the NTS shots and classical wave shapes on the EPG shots. Hence, image radii can be changed significantly by the presence and extent of a precursor.

DISCUSSION OF SHOT YUMA DAMAGE DATA

Shot Yuma was a fractional kiloton weapon (0.19 kt) with a scaled HOB of 347 feet. The NTS tower shot data were for scaled HOB ranging from 100 feet to 252 feet and the lowest yield was

higher than Shot Yuma by a factor of 10. Since Shot Yuma was a tower shot with no precursor effect and was well below the yields of either the EPG or the NTS data, it was of interest to examine the correlation of the groups indicated in Figure 37.

Figure 40 shows the 50 percent probability of moderate damage and the 50 percent probability
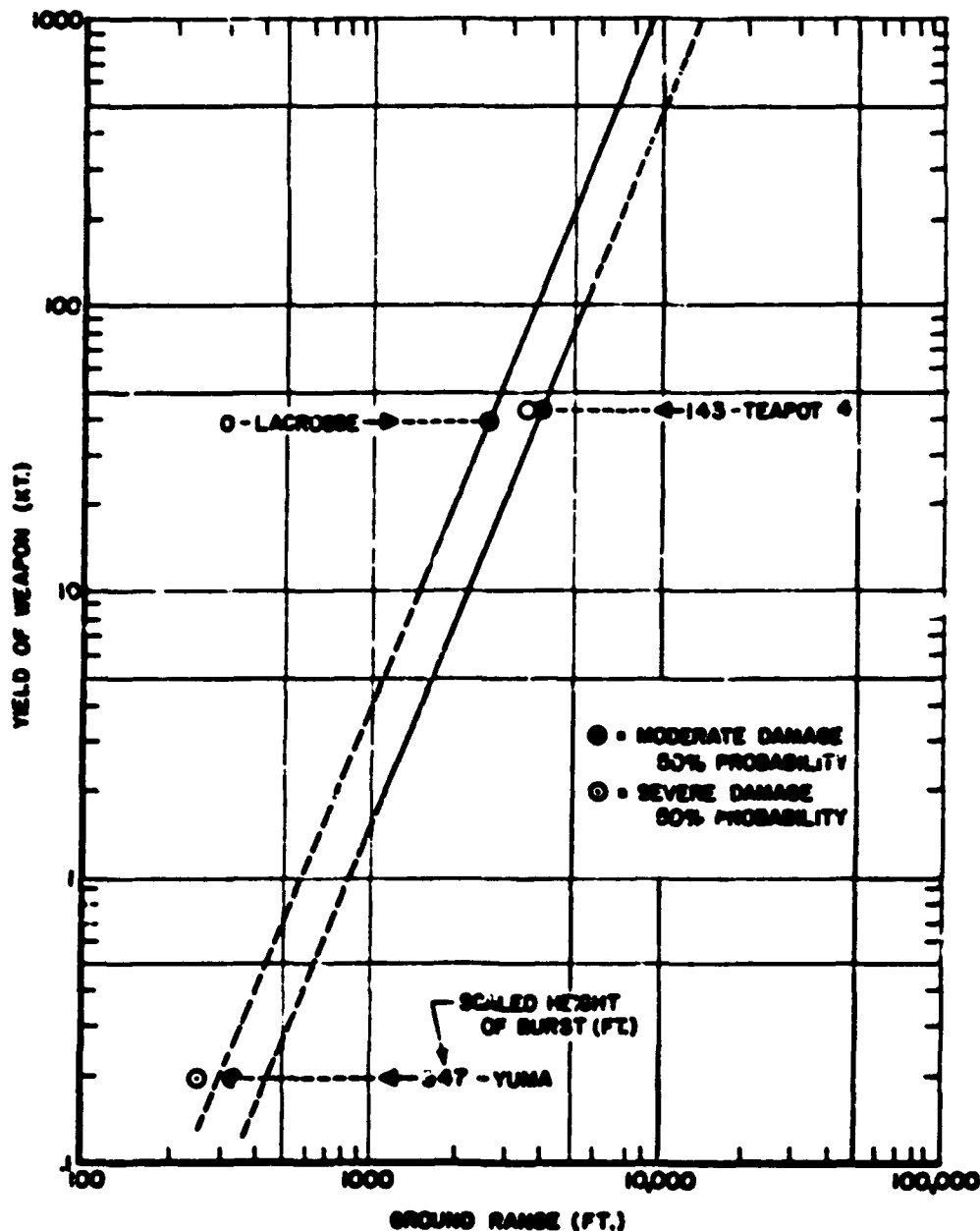
Figure 40 Ground range versus yield for various damage levels for EPG tower Shot Yuma as compared with NTS tower shot and EPG surface shot data.

of severe damage obtained from Shot Yuma. These data are presented along with the extrapolated curves of Figure 37.

As indicated in Figure 40, the Shot Yuma data points fit the extrapolated curve for the EPG surface bursts fairly well. However, the shot was of a relatively high scaled HOB and more properly belongs in the NTS group. The decrease in range shown may result both from the lack of precursor formation and the short duration of the blast wave produced by the low yield. A

62

SECRET

surface burst of a similar low yield may show a similar decrease in range; and scaling by yield varied to a constant power may be unsatisfactory for such low yields.

DISPLACEMENT OF ¼-TON TRUCKS

Since displacement, like damage, is a result of exposure to a blast wave, the displacements measured for the vehicles were examined for indication of a grouping of NTS and EPG data. Plots of displacements versus ground range were made for each shot, and the probable ground ranges for 10, 20, 50, and 100 feet displacements were selected. These are shown plotted versus yield in Figure 41. The lines shown in Figure 41 are of slope 0.4, and fit the points for each group very well.

Assuming that the NTS tower shots and the EPG surface shots were two groups distinguished primarily by type of blast wave (nonclassical versus classical) with scaling as $W^{0.4}$ applying to each, the consistency within a group of the displacements data were examined. Ground ranges were reduced by the factor $(1/W^{0.4})$ and the displacements were plotted versus the scaled
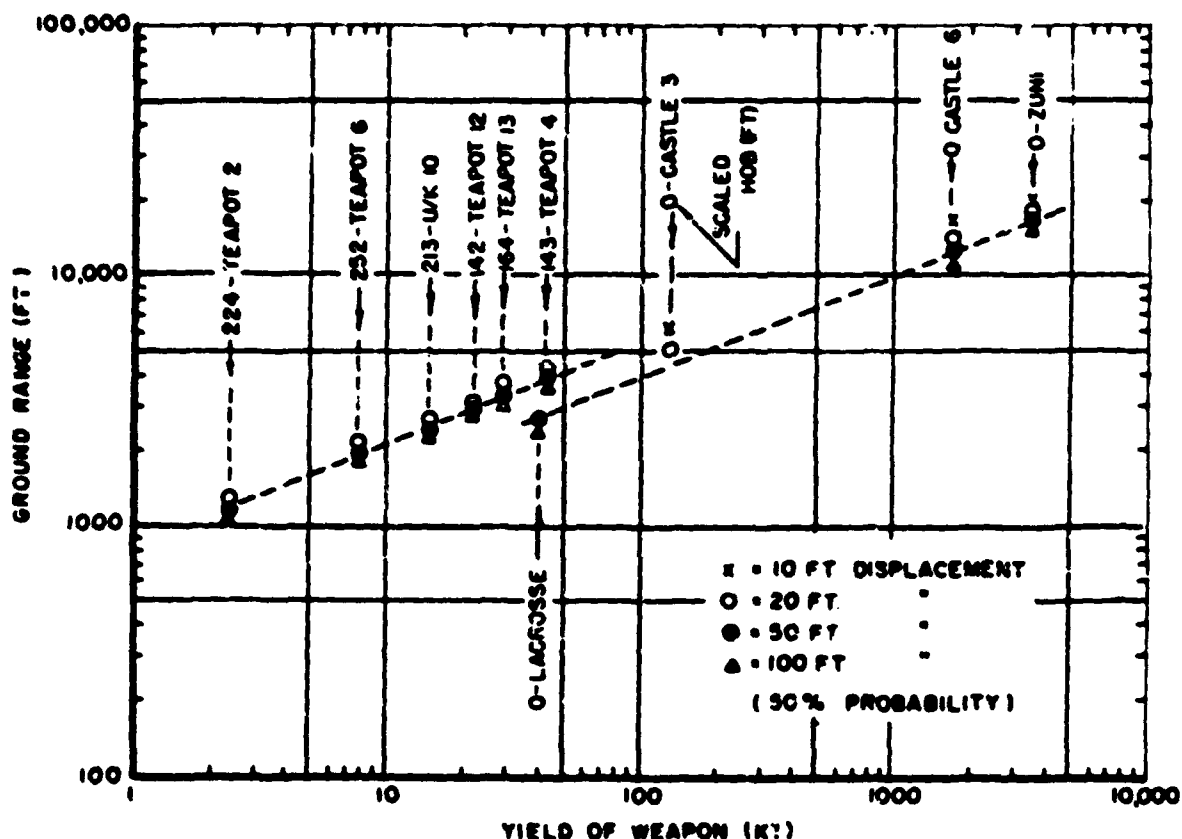
Figure 41 Ground range versus yield for various displacement levels for EPG surface shots and NTS shots of low scaled height of burst.

ground ranges. The results for the EPG surface shots are shown in Figure 42. The displacements merge well for the four shots considered. The plot of the NTS data are shown in Figure 43. A line indicates the center of the EPG distribution of points. In both Figure 42 and Figure 43 the separation of SO from FO vehicles at the same ground range illustrates a larger displacement for SO vehicles. This is expected because of the larger presented area exposed to the blast wave by the SO vehicles as compared to the FO vehicles.

The consistency of division of the displacement data between the EPG surface and the NTS tower shots again indicate that they belong to two groups with approximately the same scaling

Figure 43 Displacement of ¼-ton trucks versus scaled ground range (1/W^{0.4}) for NTS shots.

Figure 42 Displacement of ¼-ton trucks versus scaled ground range (1/W^{0.4}) for EPG shots.

factor. There is evidence to support the idea that the FO vehicles of each group and the SO vehicles of each group may be scaled by the same factor but be represented by different lines. Further analysis of existing data is necessary to define this separation.

CONCLUSIONS

The damage radii for surface bursts at the EPG in the yield range of 40 kt to 3.5 Mt have been determined and scaling of ground range for a given damage level is as $W^{0.4}$, where W is the yield.

The damage data indicate an appreciable reduction in damage radii for non-precursor conditions (classical wave shapes). Non-precursor conditions usually occur with surface bursts especially at the distances represented by the vehicle target locations.

The displacement data indicate that the radii for a given displacement are significantly reduced for non-precursor conditions (classical wave shapes).

Light damage was produced by a fractional kiloton device at scaled ground ranges associated with severe damage for a nominal device.

Peak dynamic pressure associated with a given trend of damage varied considerably over a wide range of yields. When considered alone it was not a satisfactory parameter for predicting the level of damage sustained by wheeled vehicles.

RECOMMENDATIONS

1. It is recommended that further analysis considering the duration and dynamic impluse of the blast wave be conducted to confirm the amount of reduction in damage radii of vehicles exposed under non-precursor conditions.

2. It is recommended that the extent of the precursor region be determined over the entire range of device yields, and for the surface burst in particular.

3. It is recommended that the HOB versus range isodamage curves be revised to reflect the damage radii for surface bursts.

4. Further investigation of displacement data (considering the jeep as a response gage) with blast wave characteristics and vehicle damage is recommended.

Part 4
CUBICLE STRUCTURE

OBJECTIVES

The primary objective of this part of Project 1.5 was to obtain diffraction and drag data on a nonresponsive structure at a higher pressure and longer positive duration than had previously been recorded. A secondary objective was to validate model-scaling methods at higher pressures and longer durations.

BACKGROUND

Measurements of air-blast loading on full-scale structures and cubicles were made on Operation Greenhouse, Upshot-Knothole, and Castle. The greatest effort was made on Operation Upshot-Knothole, where a large array of nonresponsive cubicles were used (see Reference 28). A limited number of structures were instrumented on Operation Teapot and reported in Reference 35. Scaled models of cubicles have been instrumented in the BRL shock tube and reported on in References 30, 31, and 32. The work in the shock tube has been confined until recently to the initial or diffraction loading. The advent of multi-megaton devices with long positive-pressure durations has placed more emphasis on drag loading as a damage criterion.

Operation Redwing afforded an excellent opportunity to instrument a structure exposed to a megaton yield device. The structure used during Operation Castle (Reference 29) was available, and Project 1.5 accepted the responsibility for obtaining pressure-time records on a limited number of positions (see Figures 44 and 45). It was hoped that this information would correlate with field data already available from previous operations. Scaled three-dimensional model studies in the shock tube had checked with field results for low pressure and it was hoped that this data would further validate model scaling in the moderate pressure range (15 to 20 psi).

The validity of scaling the diffraction phase of air-blast loading on a model to a full-size structure for incident free-field overpressures of 3 psi and 6 psi has been well established in reports from BRL (References 30 and 31). Prediction methods were made using the shock tube records from scaled models of the Project 3.1 structures exposed on Operation Upshot-Knothole but they had not been checked at the higher overpressures. An attempt was made to predict the loading expected on a concrete cubicle exposed during Operation Teapot. Here again the predicted curves could not be checked, because of the non-ideal blast wave which enveloped the structures on all blast lines. The method used to predict the curves presented in this chapter is outlined in the following section.

THEORY-LOADING PREDICTIONS

__Scaled Model Method.__ A $\frac{1}{30}$-scale model of the Operation Redwing structure was exposed in the PRL shock tube to record the air blast loading from a shock wave of the same peak overpressure as recorded near the field structure. The model was instrumented with miniature piezo-electric gages flush with the surface of the various faces of the model and in locations corresponding to similar positions on the field structure. From a large yield device such as Shot Zuni there was little decay in a free-stream-pressure-time record during the diffraction loading phase and therefore a record from the step shock produced in the shock tube should correlate well with field records when the time scaling factor is applied.

__Free-Stream Pressure Versus Time.__ To predict the air-blast loading expected on a field structure, it is first necessary to predict the free-stream-pressure-versus-time curve ex-

pected to envelope the structure. The method used in this chapter has been published in Reference 31. The parameters which must be known or assumed are: device yield, height of burst, distance from ground zero and type of surface. The pretest prediction of the free-stream-pressure-time curve was based on a yield of 2.5 Mt and a distance of 9,700 feet from ground zero, which gave an expected peak overpressure of 17.5 psi. This value was established from the height-of-burst curves presented in TM 23-200 (Reference 24). The actual yield was 3.53 Mt and a peak overpressure of 23 psi was measured near the field structure. The measured values of yield and pressure will be used to establish a predicted curve of pressure versus time by the method outlined in Reference 33.

After determining the peak pressure expected at a given distance, it is necessary to predict the wave shape. A semi-empirical equation from Reference 31 is thought to be the best available at present:

$$P_s(t) = P_s(1 - \frac{t}{t_+})_e - C \frac{t}{t_+} \tag{4.1}$$

Where: $F_s(t)$ - Overpressure in the blast wave at any time (t).

P_s - Peak overpressure (23 psi).

t_+ = Total positive duration (sec).

C = Decay constant.

The positive duration (t_+) is obtained from Reference 31 and is 200 msec for a 1 kt yield or 3,038 msec for a 3.5 Mt yield. The measured duration from the two curves presented in Figure 46 approximately 2,500 msec. The impulse (I_+) expected from a pressure-time curve with a peak overpressure of 23 psi and a duration of 200 msec was determined from Reference 33 and was found to be 1,500 psi msec. The factor still to be determined is the decay constant C, which is a function of P_s, t_+ and I_+. The value of C as determined from Reference 33 was 1.45. Equation 4.1 may now be written as follows:

$$P_s(t) = 23(1 - \frac{t}{3.038})_e - 1.45 \frac{(t)}{3.038} \tag{4.2}$$

From this equation, values of pressure from any time t_0 to t_+ can be determined. Enough values were calculated to plot a curve of pressure versus time. These values are listed in Table 11 and plotted in Figure 46. The predicted or theoretical curve in Figure 46 was used to correct the step shock records from the shock tube.

Time Scaling. When scaling records of pressure versus time from models to compare with records from full-scale structures, it is first necessary to scale the time units. This is a straightforward procedure since the velocity of the shock front in the field may be assumed to be the same as the velocity of the shock front in the shock tube for a given incident overpressure. Therefore, to scale it is necessary to consider only the difference in the size of the model and field structure as the size-scaling factor. The field structure was 36 times the size of the model, therefore, 1 msec on a shock tube record should represent 36 msec of a field record.

Pressure Scaling. The shock wave produced in the shock tube is a step shock in which the initial portion of the wave is flat topped with no decay in pressure. The flat-topped portion of the wave envelopes the model, and the pressure-time records obtained must be adjusted pressure wise to correlate with the decaying wave produced in the field. The shock-tube record is adjusted by multiplying by a ratio of $P_s(t)/P_s$ from the predicted free-stream field wave.

$$P_s(t) = P_s(0) \left(1 - \frac{t}{t_+}\right) e^{-C \frac{t}{t_+}} \tag{4.3}$$

65

SECRET

Figure 45 Back-quarter view of structure and gages at Station 111.

Figure 44 Front-quarter view of structure and gages at Station 111.
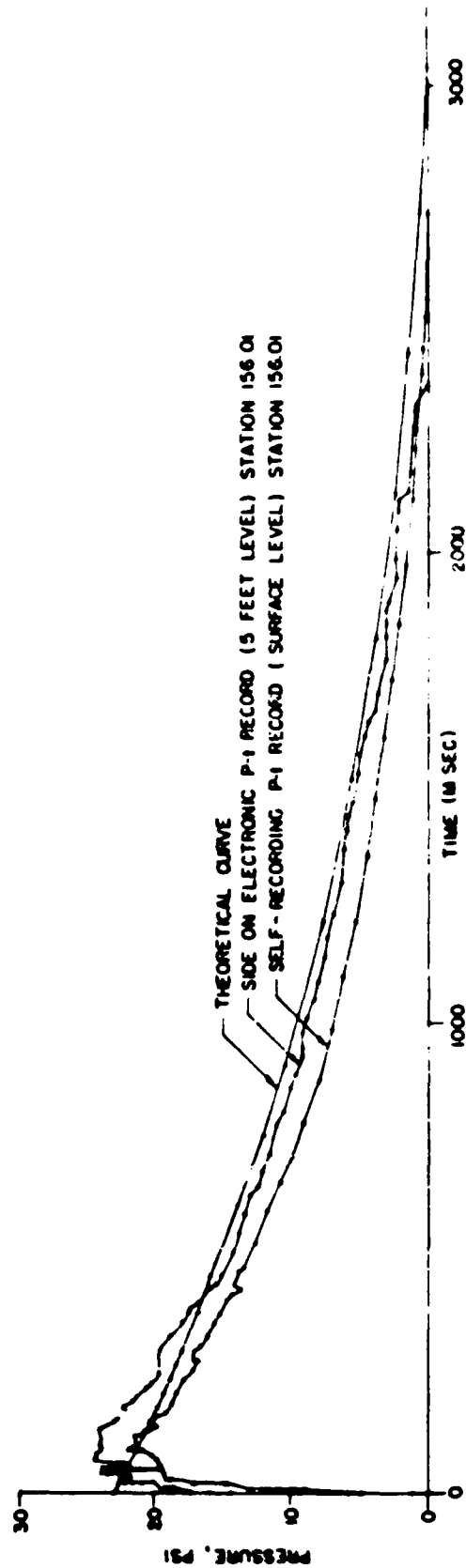
Figure 46 Comparison pressure-time curve, theoretical, measured side pressure, electronic and self-recording gage.

Where: $P_s(O)$ Peak overpressure   23.0 psi

C   Decay parameter   1.45

t_+ Positive Duration   200.0 msec for 1 kt - 3,038.0 msec for 3.5 Mt.

t - Any time interval during the positive phase.

Presentation of Predicted Records. The same positions from which field records were ob-
tained were instrumented in the scaled model, with one extra position on the rear face. The
records from the model were first scaled for time and then for pressure decay. These records
are presented in Figures 17 through 50. The first portion of the records have been expanded so
the diffraction loading can be analyzed.

OPERATIONS

The 6 by 6 by 12-foot target structure utilized by Operation Castle Project 3.1 was renovated
for use on Shot Zuni. The structure, located on Site Uncle (9,700 feet from ground zero), is
designated as Station 111 in Figure 51. Nine positions were instrumented with Wiancko pressure
transducers. The predicted pressure records were used to select gage ranges for the different
locations. The positions selected to instrument are given in Figure 49 and Table 12.

INSTRUMENTATION

Free-Field Measurements. Two stations, 156.01 and 156.02 were established in the free-
stream region. Station 156.02, located 100 feet in front of the structure, was instrumented by
Project 1.1 with one ground-baffle gage and a q gage 7 feet above the ground surface. Station
156.01 was located at the same ground range as the structure and had a self-recording ground
baffle, an electronic q gage at a 5-foot elevation, and an electronic free-stream pressure gage
at a 10-foot elevation above the surface (Figure 51).

Types of Gages, Mounts, and Calibration. Wiancko type 3 PAD, variable-reluctance pres-
sure gages were used to instrument the structure. This type of gage had an undamped natural
frequency higher than 2,000 cps. The gages used were damped to 0.7 of critical. This amount
of damping limited the amount of overshoot to 5 percent, while permitting maximum response
of the recording system. With this application of the Wiancko gage, the recording system, with
a rise time of approximately 0.4 msec, is the limiting factor in recording pressure versus
time.

The electronic recording q gage placed at Station 156.01 was of the type used by Stanford
Research Institute during Operation Teapot (Reference 33). However, damping was added to
the gage.

Mounts for the Wiancko gages in the structure were those used during Operation Castle.
The contractor repaired and renovated the mounts before gage installation. The gages were
mounted with the face of the gage flush with the structure.

After installation and connection with the recording system, the gages were calibrated by the
application of several increments of static pressure. The pressure was applied from a portable
air-supply tank. All gages were calibrated in 20-percent steps up to 100 percent of the pre-
dicted values. Added as a safety factor in event the yield went higher than predicted were a
125- and a 150-percent step.

DATA REQUIRED

The data required for a thorough analysis of the air-blast diffraction and drag loading would
be a complete instrumentation of the field cubicle. The time between Shot Cherokee and Shot
Zuni was not sufficient to calibrate all the 29 planned gage positions. The nine instrumented
positions were chosen as the most representative over the four surfaces but not necessarily
adequate for determining the average pressure over a surface or a drag coefficient (Figure 52).

67

SECRET

TABLE 11 VALUES OF PREDICTED FREE-STREAM PRESSURE-TIME CURVE

t/t_+	$1 - \dfrac{t}{t_+}$	$C\dfrac{t}{t_+}$	$e^{-C\frac{t}{t_+}}$	$(1 - \dfrac{t}{t_+})\,e^{C\frac{t}{t_+}}$	P_s psi	t msec
0.00	1.00	0.000	1.000	1.000	23.0	00.0
0.01	0.99	0.014	0.986	0.976	22.4	30.4
0.02	0.98	0.029	0.971	0.952	21.9	60.8
0.03	0.97	0.044	0.956	0.927	21.3	91.1
0.04	0.96	0.058	0.944	0.906	20.8	121.5
0.05	0.95	0.073	0.929	0.882	20.3	152.0
0.06	0.94	0.087	0.917	0.862	19.8	182.3
0.07	0.93	0.102	0.903	0.840	19.3	212.7
0.08	0.92	0.116	0.890	0.819	18.8	243.0
0.09	0.91	0.131	0.877	0.798	18.4	273.4
0.10	0.90	0.145	0.864	0.778	17.9	303.8
0.15	0.85	0.218	0.806	0.685	15.8	455.7
0.20	0.80	0.290	0.748	0.598	13.8	607.6
0.25	0.75	0.363	0.692	0.519	11.9	759.5
0.30	0.70	0.435	0.647	0.453	10.4	911.4
0.40	0.60	0.580	0.560	0.336	7.7	1,215.2
0.50	0.50	0.725	0.484	0.242	5.6	1,519.0
0.60	0.40	0.870	0.419	0.168	3.9	1,822.8
0.70	0.30	1.015	0.362	0.109	2.5	2,126.6
0.80	0.20	1.160	0.313	0.063	1.5	2,430.4
0.90	0.10	1.305	0.271	0.027	0.6	2,734.2
1.00	0.00	1.450	0.235	0.000	0.0	3,038.0

TABLE 12 STRUCTURE GAGE LOCATIONS

Gage	Distance from Front Face	Distance from Top Face	Distance from Left Side *
	in	in	in
P-1	60	—	72
P-9	30	—	42
P-13	12	—	10
P-24	—	12	12.5
P-27	—	33.25	42.5
P-28	—	34.25	72.25
P-34	—	12.25	74.50
P-44	36.5	36.75	—
P-50	—	48.25	12.25

* Left side as viewed from ground zero.
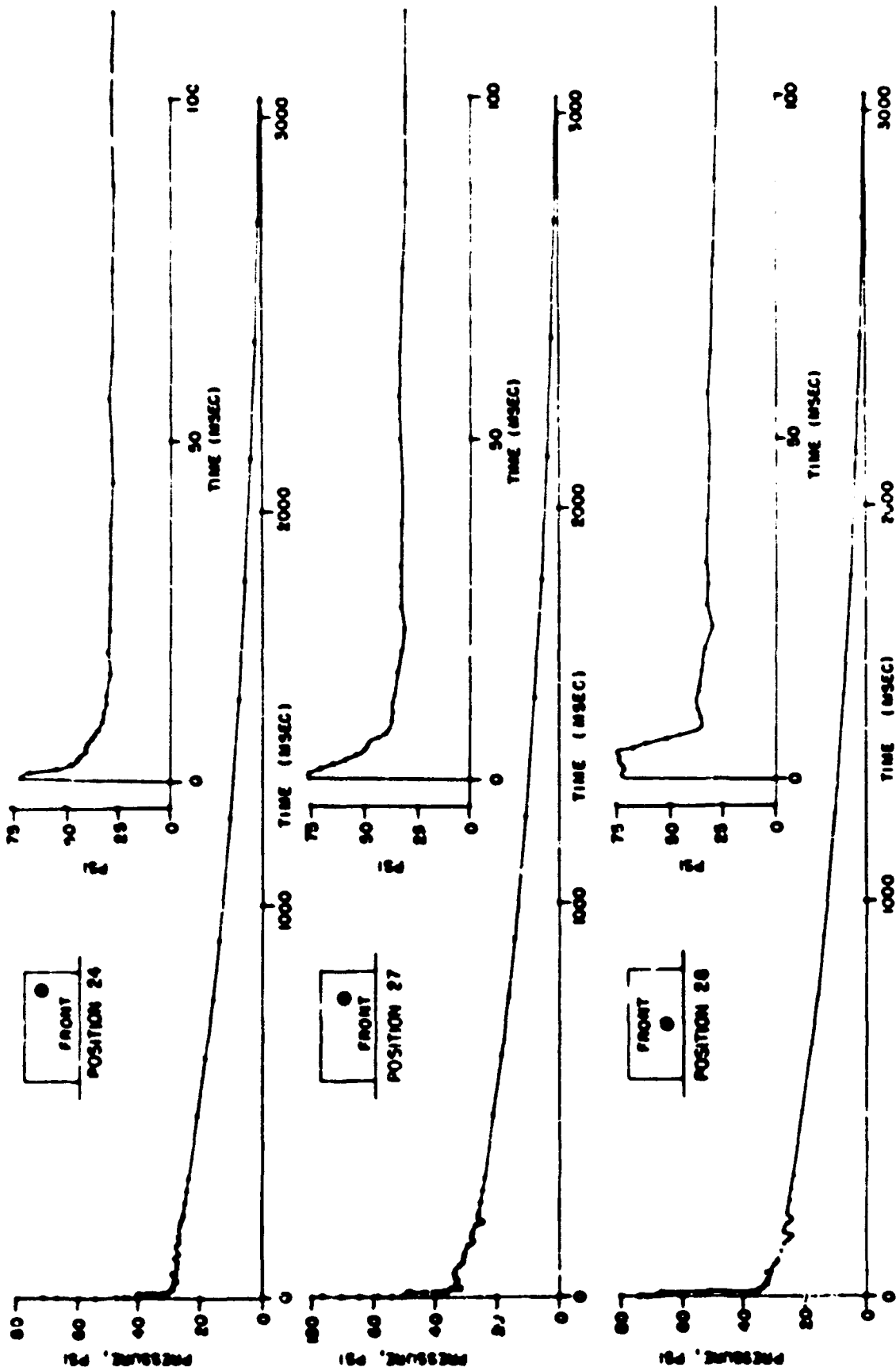
Figure 47 Pressure-time loading prediction curves, Positions 24, 27, 28.

SECRET
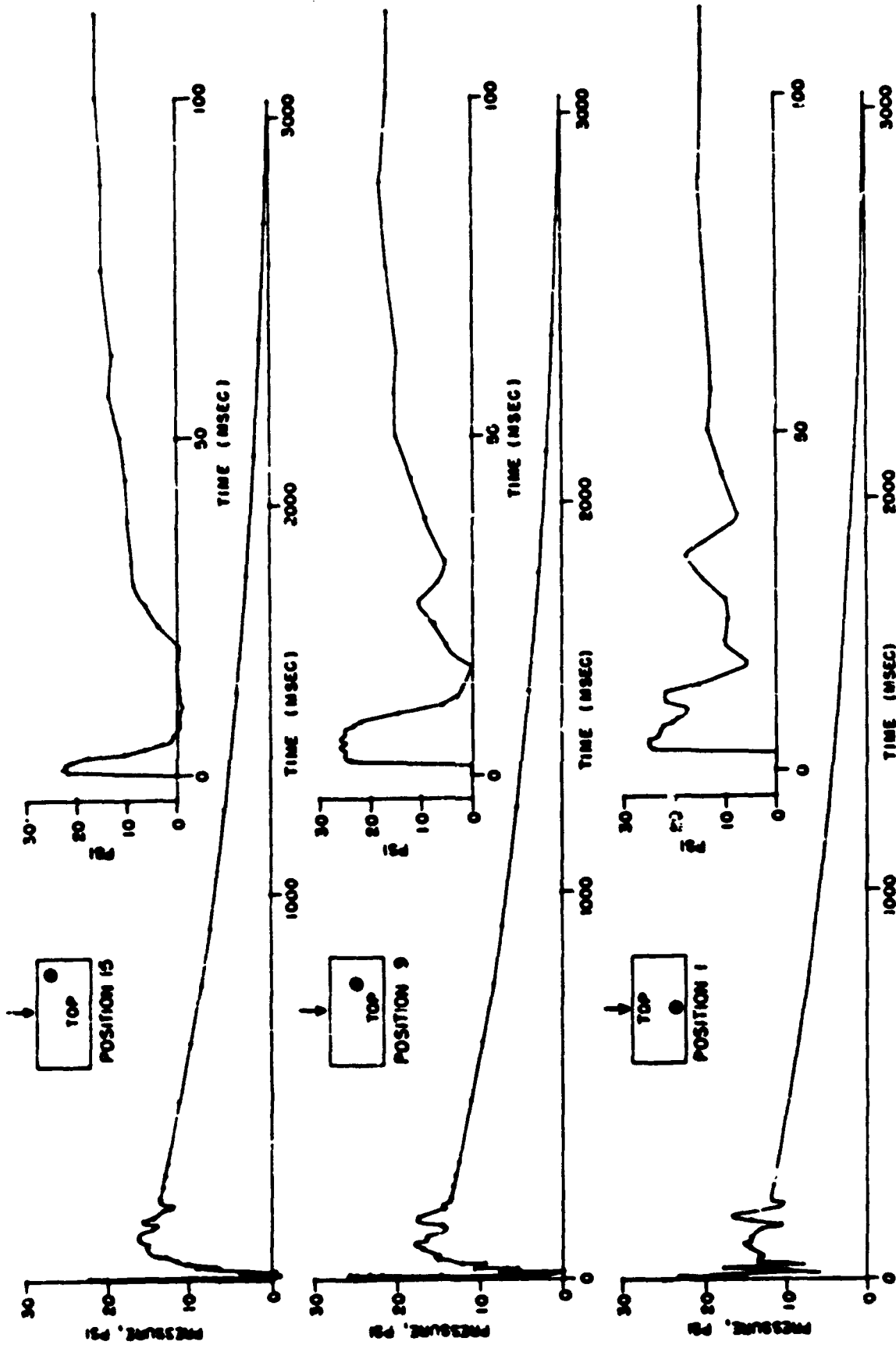
Figure 48 Pressure-time loading prediction curves, Positions 15, 9, 1.
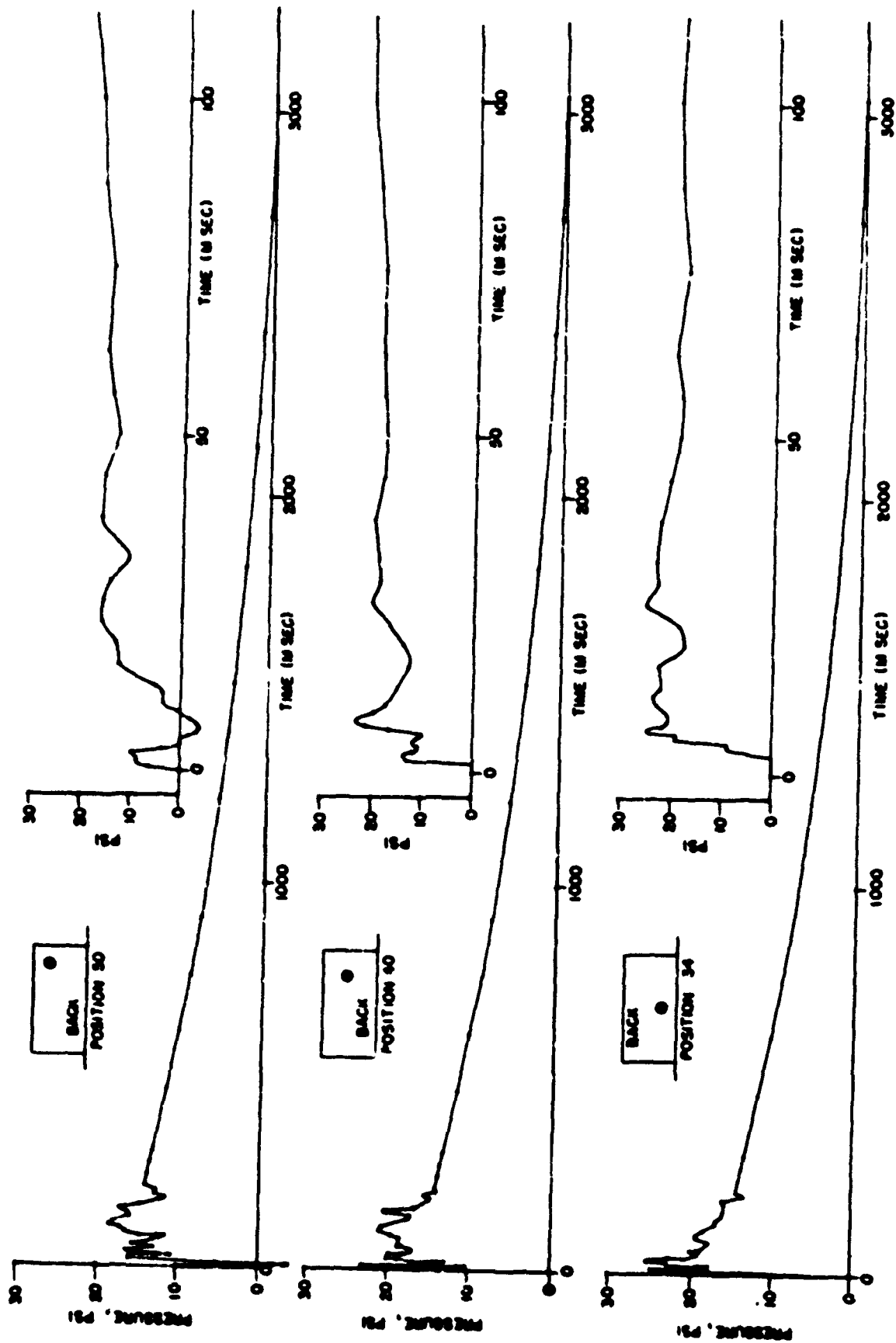
Figure 49 Pressure-time loading prediction curves, Positions 50, 40, 34.

73
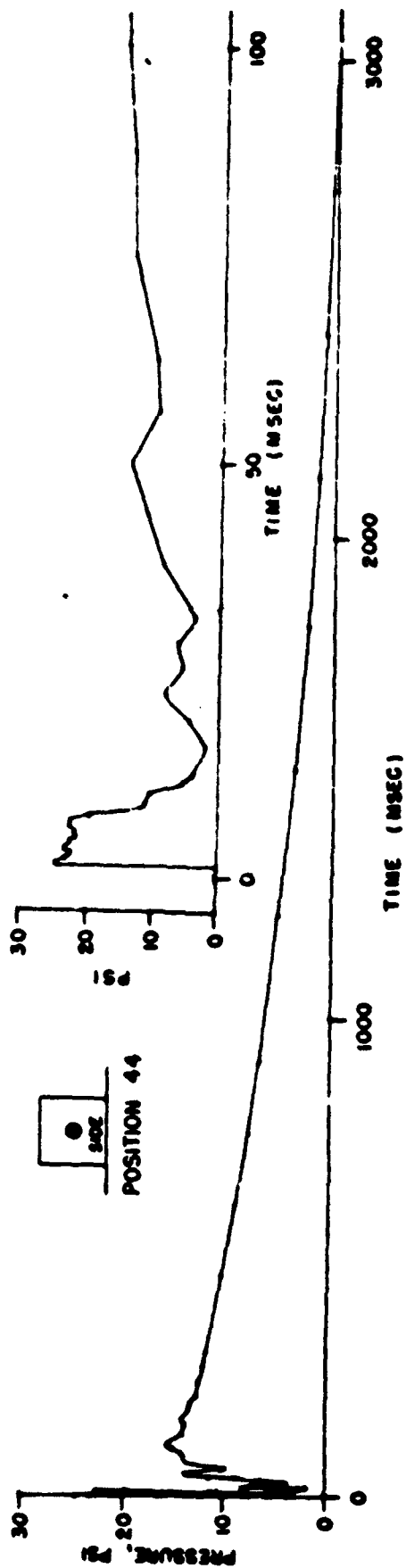
Figure 50 Pressure-time loading prediction curves, Position 44.
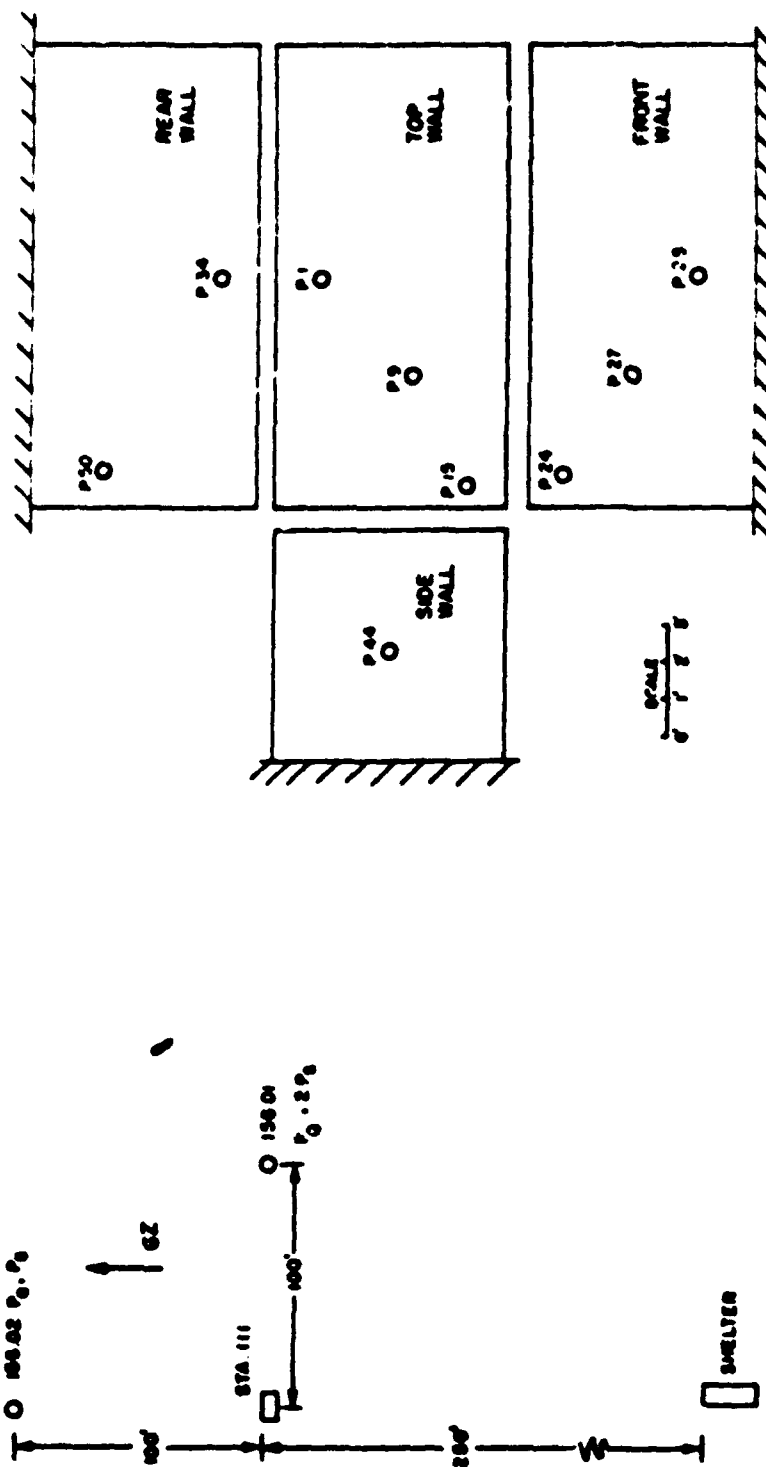
Figure 51 Free-field pressure gage layout.

Figure 52 Station 111 pressure gage positions.

To meet the primary objective of the project it was necessary to measure the pressure-time history at selected positions over the various faces of the target structure. A record of pressure versus time can then be analyzed to determine from the pressure fluctuations, the time of occurrence and strength of the vortex action and reflected waves that effect the air-blast diffraction and drag loading of a structure.

RESULTS

Front Face Measurements. The records of pressure versus time from the front face positions are presented in Figure 53. Here it can be seen that the records do not follow the trend expected for a classical shock wave input. For a peak overpressure of 23 psi the reflected pressure on the front face under ambient conditions just prior to shot time should be approximately 72 psi. The reflected pressure measured on the front face gages satisfy the predicted value within the limits of error that might be expected. The deviation from what might be expected from a classical shock wave can be seen in the rate of decay of the reflected to a stagnation pressure. The reflected pressure on the front face of a structure should decay to stagnation pressure within the time shown on the scaled up shock tube records shown in Figure 47 that
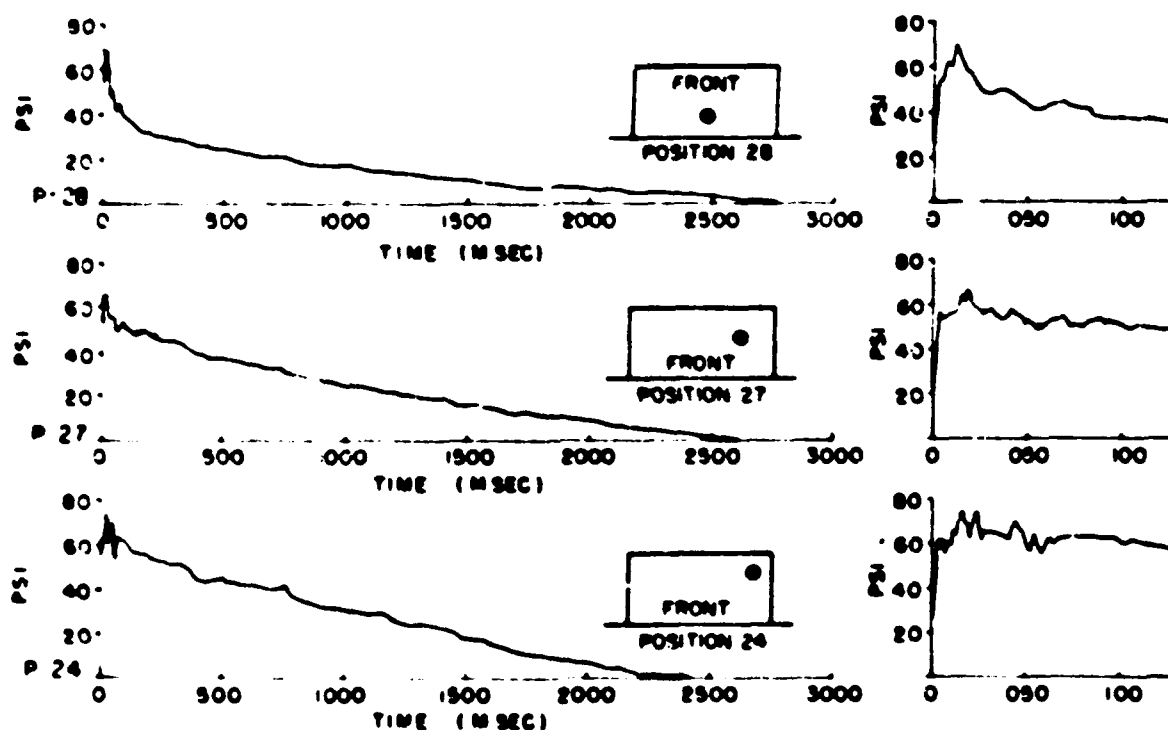
Figure 53 Structure front face records, Positions 24, 27, 28.

is approximately 25 msec. It can be seen in Figure 53 that there is little or no decay within the first 100 msec at positions 24 and 27, while at position 28 the pressure had decayed to approximately 40 psi which is still much higher than would be predicted from a classical wave shape. The total impulses measured at positions 24, 27 and 28 were 6,535, 5,763 and 3,902 psi-msec respectively. The positive durations reported in the same order were 2,410, 2,608 and 2,608 msec.

Top Face Measurements. Good pressure measurements were made at the three positions instrumented along the top face. The pressure time history from Position 9 was not valid. As can be seen in Figure 54, there appeared to be a gage malfunction beyond the first 200 msec. The diffraction phase of the record is believed to be valid when compared with the other two

73

positions. The attenuation of the initial pressure rise by the vortex action is seen in the record from Position 15. This effect becomes weaker as the shock front moves across the top tr Positions 9 and 1. Some decrease in pressure after the initial rise is also contributed to the rarefaction wave moving from the rear edge back over the top face. The effect because of the rarefaction wave was greater at position 1 while the effect because of the vortex was greater at Position 15. The impulses from Positions 1 and 15 were 1,611 and 1,905 psi/msec while the durations were 2,581 and 2,870 sec.

Back Face Measurements. Two positions were instrumented on the back face. The records from Positions 34 and 50 are presented in Figure 55 and both appear to be valid. The records show the slow build-up of pressure to a peak slightly less than the incident side-on pressure. Position 50 built up to a peak pressure sooner than Position 34 and also decayed much slower. The impulse from Position 50 was 2,386 psi/msec which was also much greater than Position 34, which was 1,797 psi/msec. The duration of the record from Position 50 was 2,887 sec as compared to 2,749 sec from Position 34.

Side Face and Free-Stream Measurements. One position was instrumented on the side of the structure. This was Position 44 and the record is presented in Figure 55. The record appears to be valid and the initial position compares with the record from Position 9 on the top face.

The side-on pressure record from the q gage is presented in Figure 56 along with the dynamic pressure record. The measured dynamic pressure is much greater during the first 100 msec than would be expected from calculating the values from side-on pressure.

Presentation of the surface level pressure record, Station 155.01, is made in Figure 46. No usable record was obtained from the pressure gage at the 10-foot elevation because of mount failure.

The side-on pressure records from the q gage and the ground baffle gage at the Project 1.1 instrumented station 156.02 are presented in Figure 57.

DISCUSSION

Field Records. The records of pressure versus time measured on the field structure were excellent so far as noise level, readability and playback techniques were concerned. There were no base line shifts at zero time and therefore the calibration curves were applied to the records without the necessity of correction. With all the factors mentioned above in favor of reliable records there still appeared some inconsistencies. On the front face the relief of reflected pressure was slow and Position 24 which should have shown the fastest decay of reflected pressure actually recorded the slowest decay while Position 28 which should have held the reflected pressure longer, recorded the fastest pressure decay of the three gages.

The records from the top position appeared to be the most consistent. No explanation can be given for sudden pressure decay of the record at Position 9, but as mentioned before, the first 200 msec appeared valid.

Positions 34 and 50 on the back face showed some inconsistency in pressure and impulse values. Based on shock tube data, Position 34 should have recorded a peak overpressure higher than that recorded at Position 50 and also recorded a greater impulse. From the actual field record, just the reverse was recorded. These inconsistencies are mentioned to point out the difficulty in checking the validity of shock tube scaling and establishing any prediction method based on shock tube data that could predict the records obtained from this structure.

Shock Tube Records. The records of pressure versus time measured on the scaled model exposed in the shock tube were excellent and it is felt that if the field structure had been enveloped by a classical shock wave the records presented in Figures 47 through 50 would have been representative of the field records. Actually the front face field records showed the greatest dissimilarity from the shock tube records, which followed patterns similar to those set up and reported in Reference 32.
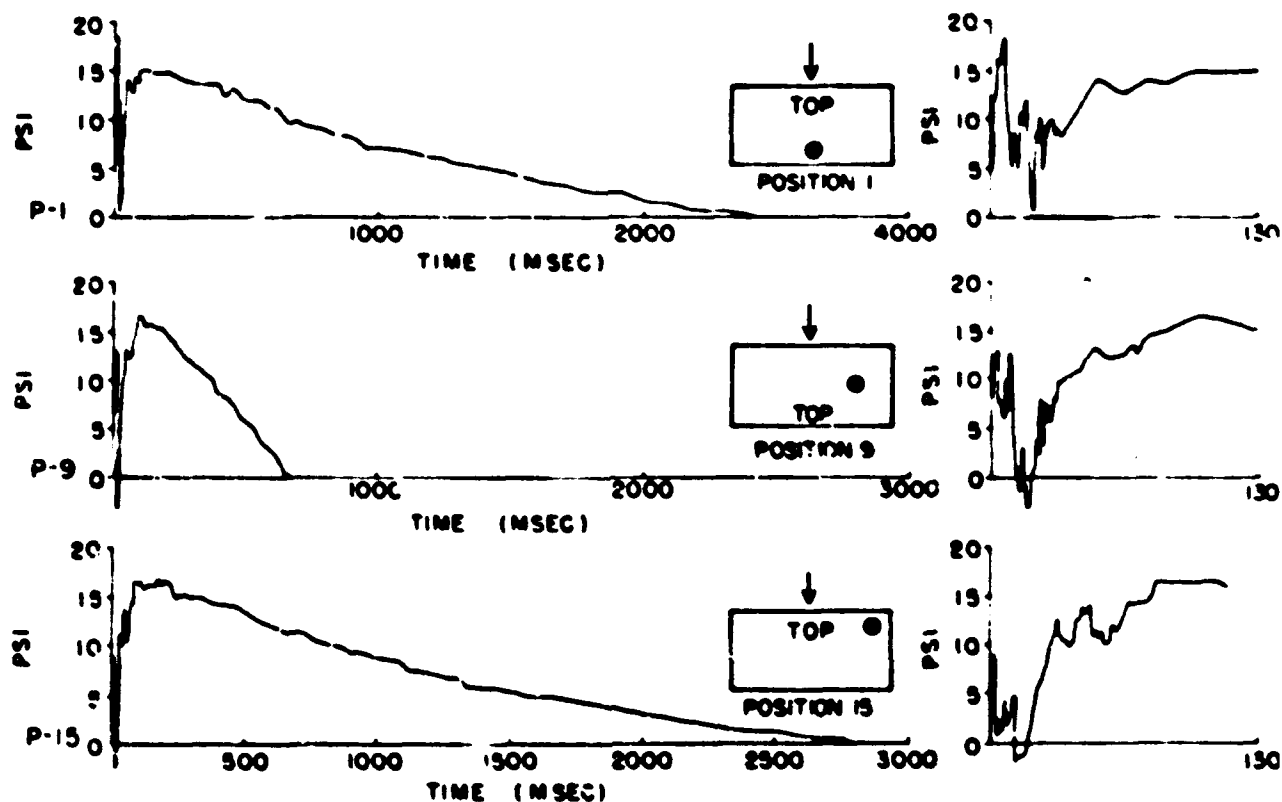
Figure 54 Structure top face records, Positions 15, 9, 1.
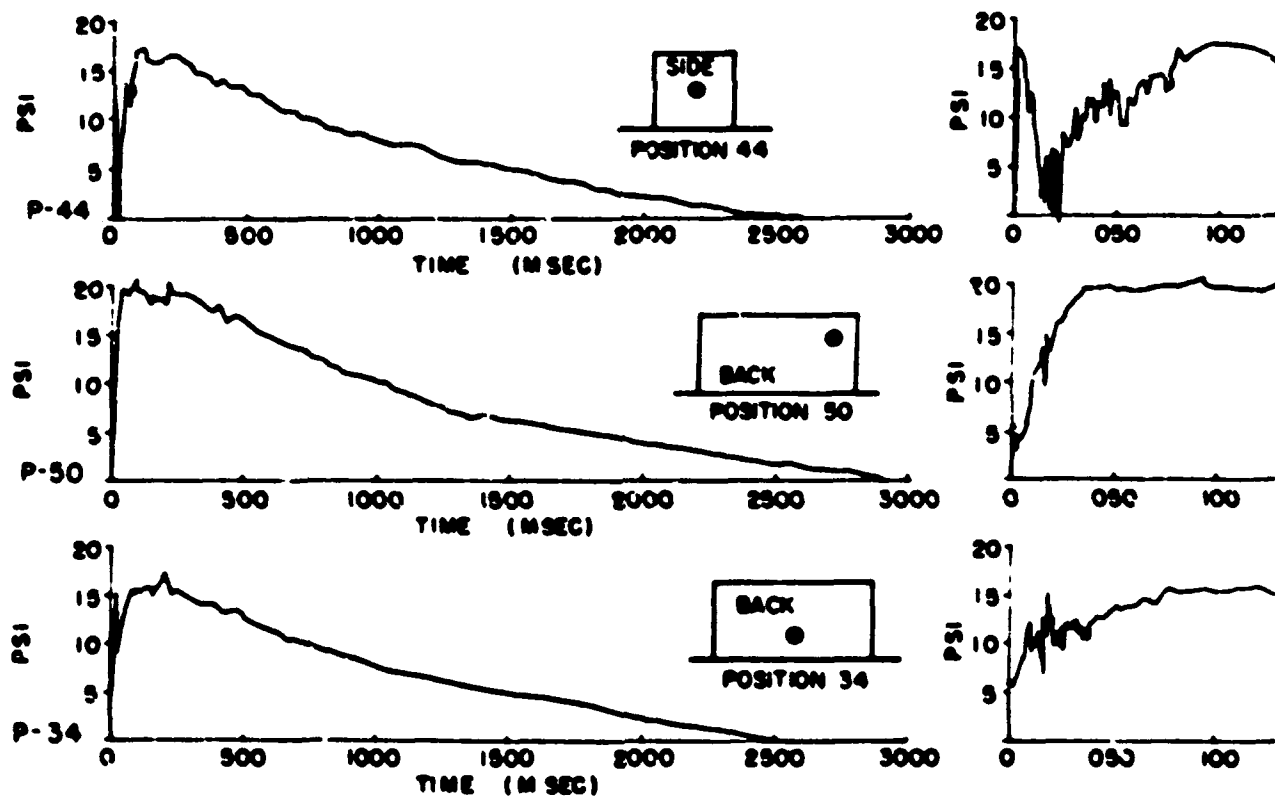
Figure 55 Structure back face and side face records, Positions 50, 34, 44.

SECRET

<u>Comparison of Predicted and Measured Records.</u> No comparison has been attempted for the front face records, except for the reflected pressure. The peak reflected pressures check, but that is the only similarity throughout the rest of the record.

The top face records showed a much better correlation in the diffraction phase, but not in the drag phase. It is felt that part of the initial peak shown on the shock tube records was lost on the field records because of the response time of the gages. In Position 15, which was affected quickly by the vortex, the field records did not reach 10 psi while the shock tube record reached approximately incident pressure as expected. Positions 9 and 1 records were not affected as soon by the vortex. Therefore, they reached higher pressures. It should be noted that the incident free stream record required approximately 75 msec to reach a peak value. Therefore, the vortex or rarefaction wave can cause a decay in the initial rise before it can reach the peak value.

The back positions also compared favorably when the two input conditions were considered. The field pressure wave with its slow rise will not reflect and form the strong vortices over the
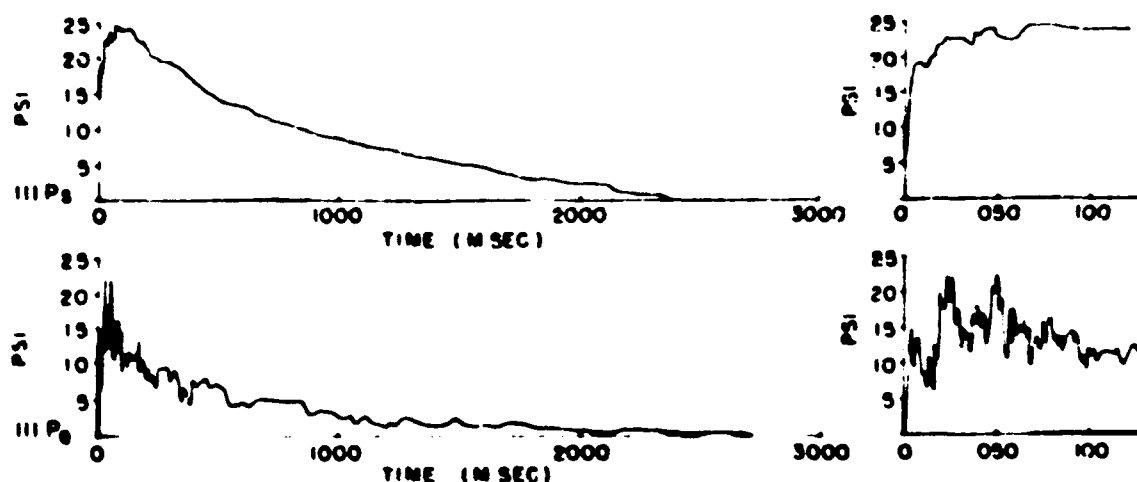
Figure 56 Dynamic and side-on records from Station 156 U1.

back face as shown on the shock tube records. Therefore, a slow build-up of pressure over the back face of the field structure would be expected.

The side face Position 44 showed excellent correlation between the field and shock tube records in the diffraction phase, but as found in the other records, the drag phase loading was much higher.

CONCLUSIONS AND RECOMMENDATIONS

The conclusions reached by the authors are stated as follows:

1. The field structure was enveloped by a non-ideal shock wave.
2. The field instrumentation is believed to be reliable and it reproduced the pressure time history acting on the structure.
3. The number of positions instrumented was inadequate to obtain an average pressure over the surfaces for translational force.
4. The diffraction phase loading on the top, back and side was similar to what might be expected from shock tube data, but the loading on the front face was quite different.
5. The drag phase loading was much higher on all faces than would be predicted from shock tube data which was based on a classical wave shape.
6. The dynamic pressure was higher than would be predicted from the measured side-on pressure, but it was not as high as indicated from the drag loading measured on the structure.
7. The input conditions were based on the side-on pressure from a q gage, 100 feet to the

78

SECRET
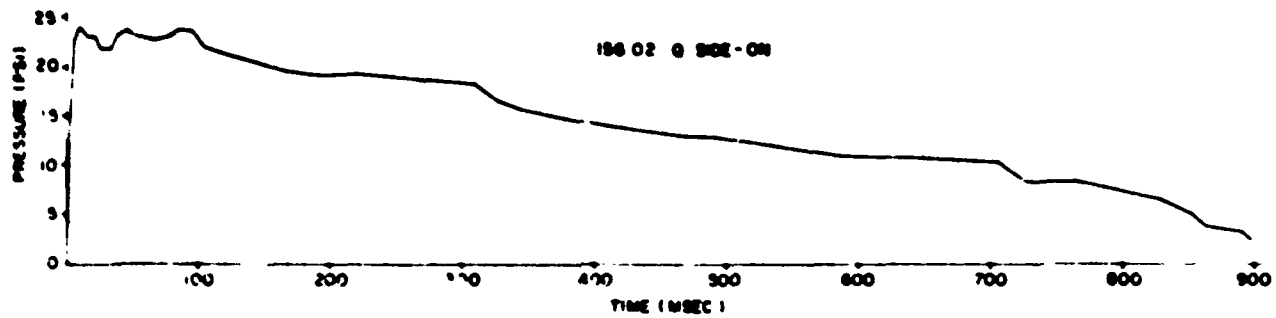
(a) Q Side-on
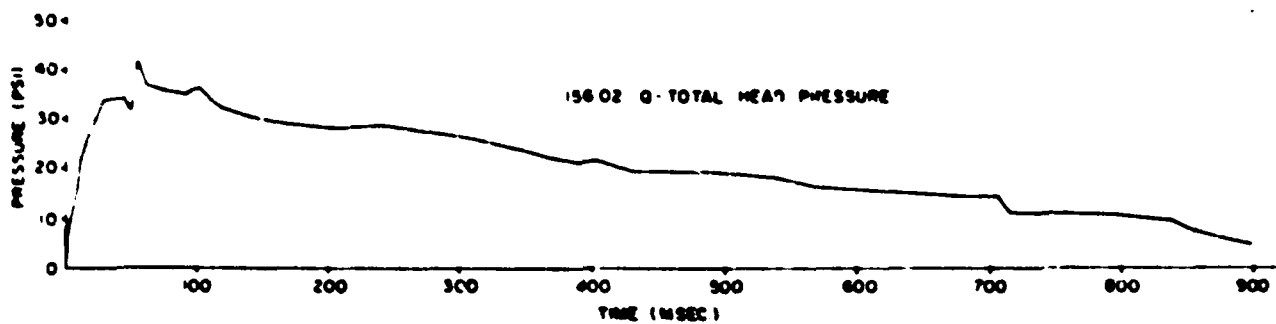
(b) Q total head pressure
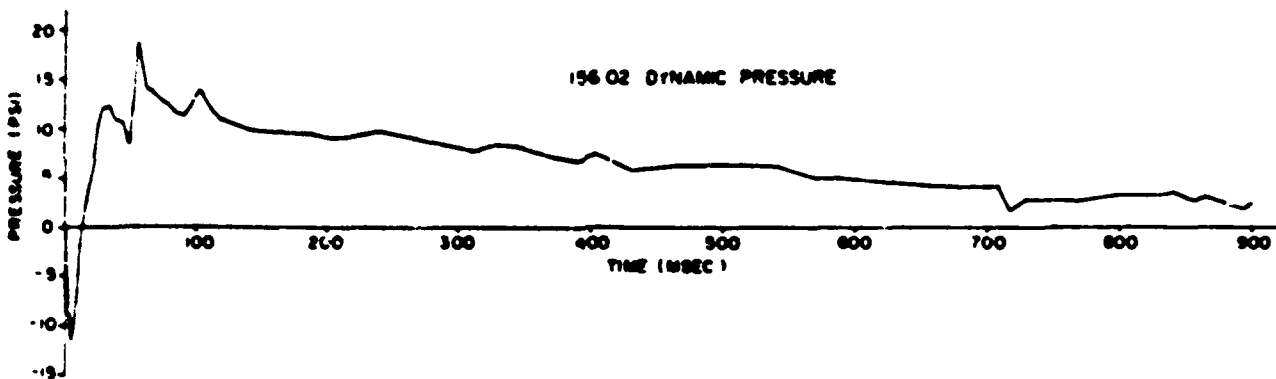
(c) Dynamic pressure
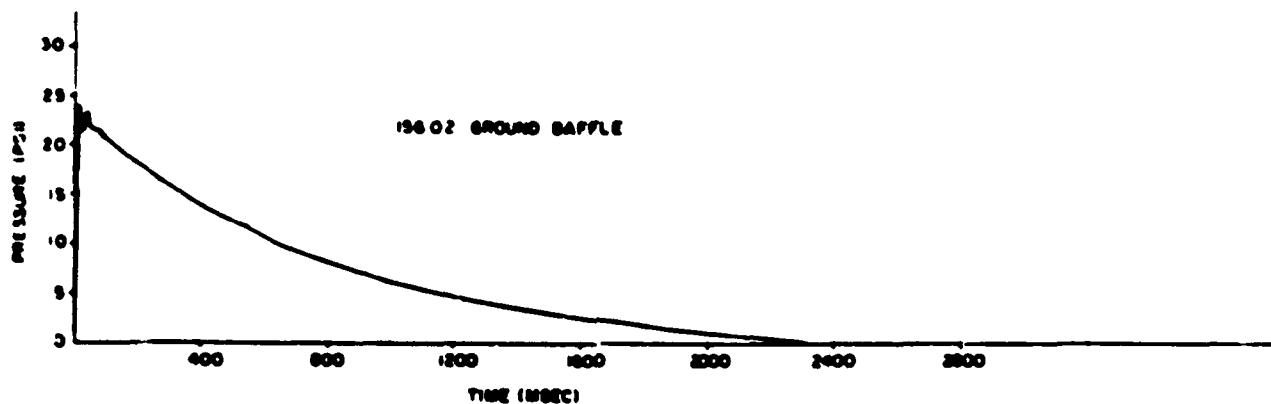
(d) Ground baffle

Figure 57 Ground baffle and dynamic pressure records, Station 156.02.

SECRET

side of the structure, which may or may not have been the true conditions at the structure.

The recommendations presented for consideration are as follows:

1. Full instrumentation should always be carried out whenever there is a possibility of a precursor being formed or a non-ideal wave shape enveloping the target structure.

2. Free-stream measurements should be as close as possible to the structure as insurance that the true input conditions are known.

3. A greater emphasis should be made to simulate in the shock tube the actual field conditions, expecially wave shaping techniques.

Part 5
ELECTRONIC INSTRUMENTATION

OBJECTIVES

Project 1.5 provided electronic instrumentation for Project 3.1, as well as the other phases of Project 1.5. Data required by these projects necessitated the measurement of each of the following, versus time: dynamic pressure, side-on pressure, column deflection, column strain, column acceleration, time of break of the frangible siding, and the acceleration of the footing at each of the four Project 3.1 locations.

Project 1.5 provided electronic recording and instrumentation on Shots Cherokee and Zuni.

BACKGROUND AND HISTORY

The instrumentation requirements of Project 3.1 were similar to those of Project 3.7, Operation Teapot. The instrumentation for Project 1 5 included recording data from various types of drag gages and instrumenting Station 111, a 6 by 6 by 12 foot cubicle described in Part 4. The drag gages are described in Parts 1 and 2.

The multi-channel magnetic tape recording equipment used during Operation Teapot was modified to correct some of the difficulties encountered and used for Operation Redwing.

Representatives from Projects 3.1 and 1.5 met and decided on the type, location, and ranges of the gages for both projects. Instrumentation for Project 1.5 drag gages was designed to insure compatibility of the transducers with the multi-channel magnetic tape recording system.

OPERATIONS

Project 1.5 (electronic measurement portion) participated in two events, Shots Cherokee and Zuni.

The installation of the instrumentation and recording equipment was started as soon as construction had progressed sufficiently. Instrument cables were installed after all heavy equipment was removed from the area The end-instrument calibration was accomplished upon completion of the cable installation. Faulty gages, recording equipment, and calibration techniques were detected by analyzing the playback of the calibration records.

INSTRUMENTATION

The Project 3.1 structures were all instrumented in a similar fashion. Measurement of dynamic and side-on pressures were made 10 and 25 feet aboveground. Accelerometers were mounted near the top of the center columns farthest from ground zero (Figure 58). Strain gages were located on both the front and rear center columns at 4, 8, and 15 feet above the column footing (Figure 59).

The inner three front columns of the b-type structures and all three front columns of the a-type structures were instrumented for deflection. The measurement was made between the point of the column where the bottom chord of the truss was attached and a piling driven into the coral at a point 17 feet in front of the column. A fourth deflection measurement was made between the front and rear center columns immediately below the bottom chord of the truss. Figure 58 gives details of the deflection gage locations.

There were three time-of-break gages installed on each of the a-type structures, one on each side of the center on the front wall, and one centered on the rear wall. The gage wires
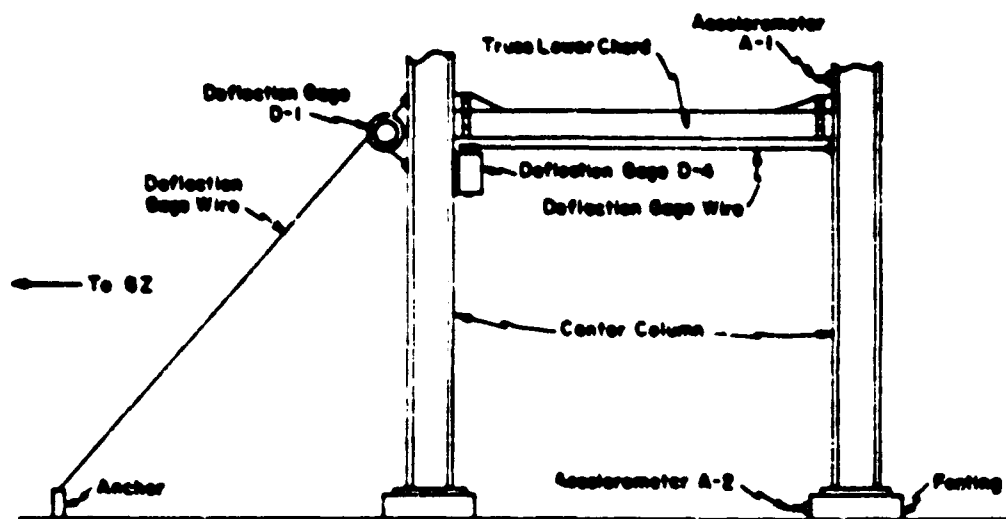
Figure 58 Locations of accelerometer and deflection gages.
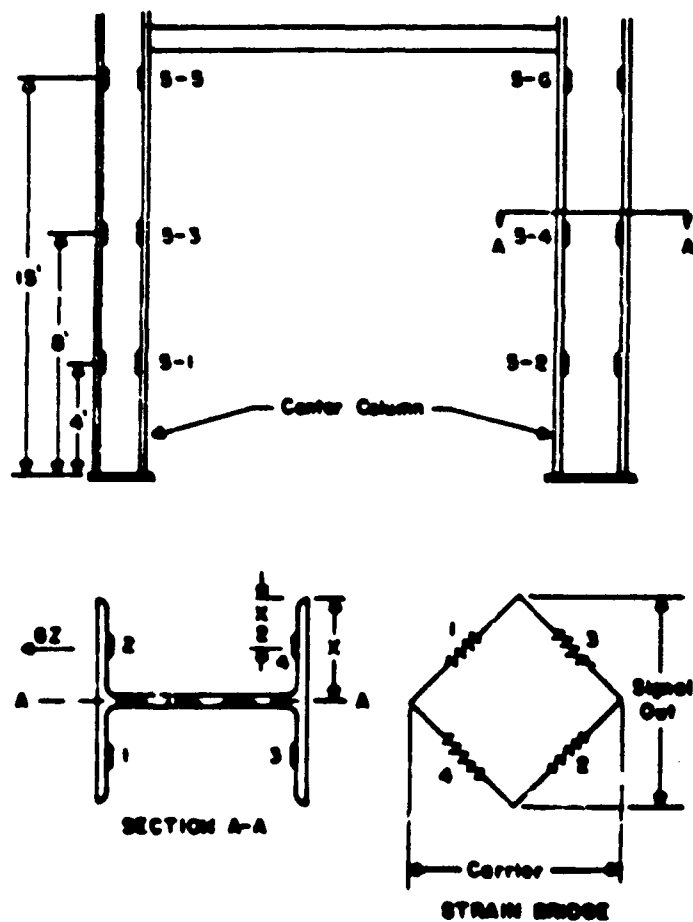
Figure 59 Locations of strain gages and bridges.

SECRET

for the front wall were run horizontally 8 feet aboveground and were 12 feet long. The gage wire for the rear wall was run in a similar fashion and was 20 feet long. All three break times were recorded on the same channel. The footing acceleration was measured by an accelerometer placed on the center rear footing of the b-type structures. This accelerometer was located at the same point on the Project 3.1 a-1 structure to measure its footing acceleration. Figure 58 shows the position of the footing accelerometer.

The Project 1.5 Station 111 was instrumented with nine pressure gages, three in the front wall, three in the top wall, two in the rear wall, and one in a side wall. See Part 4 for details. A pressure gage in a disc-baffle and two q gages were supplied to make free field pressure measurements. One of the two q gages was oriented with its axis at an angle of 45 degrees to a line from ground zero.

Dynamic pressure measurements were made with q gages developed by Sandia Corporation and furnished to the Ballistic Research Laboratories by the Stanford Research Institute. Blast type pressure measurements utilized Wiancko Engineering Company type 3PAD-R Pressure
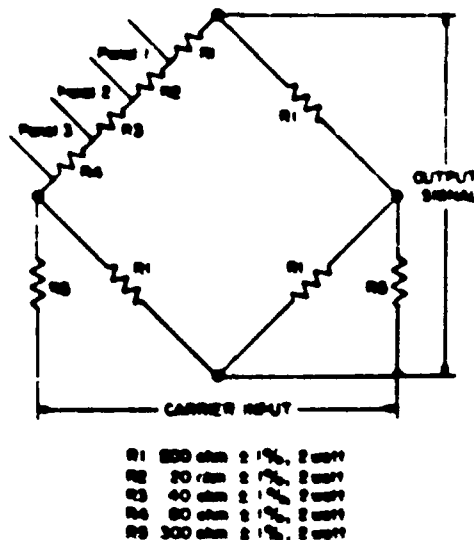
Figure 60 Time-of-break gage.

Gages. The accelerometers used were Wiancko Engineering Compary, type 3AA-T. The deflection gages were the type developed by BRL and described in Reference 18. The column strain measurements were made using C-5-1, SR-4 strain gages, arranged to measure the bending moment at three levels on a column (See Figure 59). The strain gages were applied to the column with Duco cement. After a suitable drying time the gages were moisture proofed with a liberal coat of hot petrosene wax, followed by a coat of Dow Corning DC-4 silicone grease.

The time-of-break gage was developed by BRL. It consisted of a resistance bridge arranged as indicated in Figure 60. R2, R3 and R4 were each shunted by a No. 32 wire stretched over the frangible siding in such a manner that at the breaking of the siding would break the wire. Breaking the wire would cause an unbalance of the resistance bridge and a corresponding voltage output. The value of the three shunted resistors was chosen so that the breaking of each wire would produce a unique output voltage amplitude.

Prior to the shot, all gages were statically calibrated in conjunction with the entire recording system in its field setup. Pressure and acceleration gages were calibrated by applying known values of pressure and acceleration and recording the output. Deflection gages were calibrated by using a simple analog converter to simulate deflection. Expected values of strain were simulated by shunting certain arms of the bridge with appropriate resistors. The time-of-break gage was calibrated by simulating the breaking of the frangible siding panels. All acceleration, displacement, and strain channels were calibrated in the positive and negative directions. A

81

SECRET

posi ive signal is defined as that signal which is the initial output of the gage because of the effect of the blast on the structure or gage.

An electrical calibration signal was provided at the recording shelter and recorded immediately prior to both the calibration record and the shot record. The electrical calibration signals were used to determine the drift of the recording system.

The recording equipment used was a multi-channel, magnetic-tape recording system. This system used the phase modulation principle. As many as 20 channels of data could be recorded on a 35 mm magnetic tape. The recording system received its power from storage batteries.

An Edgerton, Germeshausen and Grier (EG&G) blue box provided a zero time signal which was recorded by each recording system.

During the shot, EG&G remote-controlled relays operated the recording system sequence timer which provided appropriate times and relay closures to operate the system.

In laboratory tests, the error in making dynamic measurements with the multi-channel magnetic tape equipment had been found to amount to a maximum of ± 6 percent. This error arose

TABLE 13 KEY TO SYMBOLS USED

Symbol	Gage Type	Meaning
A	Accelerometer	A-1 top of column, A-2, footing
a, t, v	Drag Gage	A, axial, t, transverse, v, vertical. First digit or pair of digits, diameter of gage, last digit, gage serial
D	Displacement	1, right, 2, center, 3, left, 4, differential
F	WF-Beam	Front Bridge.
H	Angle-Beam	Horizontal Bridge
P	Pressure-time	Overpressure measurement.
FAP_1	Pressure-time	Overpressure measurement free air
Pq	q-gage	Dynamic pressure
PQ₄	q-gage	45 degree orientation dynamic pressure (Station 111)
PS	q-gage	Side-on or overpressure
PS₄	q-gage	45 degree orientation side-on pressure (Station 111)
R	WF-Beam	Rear Bridge
S	Strain Gage	1, 2, 5 - front, 4 R, 6 R, 12 R positions, 3, 4, 6 - rear, 6 R, 8 R, 10 R position
TB	Time of Break	
V	Angle-Beam	Vertical Bridge.

primarily from static sources, such as noise, drift, and cross talk. Under field conditions it was expected that these errors might be twice as great, resulting in a probable accuracy of the data of ± 12 percent.

To utilize the data recorded on magnetic tape, the latter was played back along with the appropriate calibration record and reproduced on oscillographic photo-sensitive paper. To determine the time differential between the breaking of the frangible siding and the arrival of the blast wave, the time-cf-break record and a pressure record from the nearest q gage on the same recording system were played back simultaneously and displayed on the same oscillograph record.

RESULTS

Table 14 lists each channel instrumented by Project 1.5 together with remarks resulting from examination of the records. Table 13 explains symbols used in Table 14. Those records

TABLE 10 SUMMARY OF INSTRUMENTATION RESULTS

Location	Gage	Remarks	Location	Gage	Remarks	Location	Gage	Remarks
3.1-a1	PQ1	Good Record	3.1-a3	A1	Good Record	3.1-b3	PS1	Good Record	152.02	R2	Questionable
	PS1	Good Record		T.B	Fair Record		PQ2	Good Record	152.03	F1	Fair Record
	PQ.	Good Record		b1	Good Record		PS2	Good Record		R1	Partial Record
	PS2	Questionable		b2	No Record		D1	No Record		F2	Good Record
	D1	No Record		b3	Good Record		D2	No Record		R2	Good Record
	D2	No Record		b4	Fair Record		D3	No Record	152.04	F1	Good Record
	D3	No Record		b5	Good Record		D4	Good Record		R1	Good Record
	D4	Questionable		b6	Good Record		A1	Good Record		F2	Good Record
	A1	Good Record	3.1-b1	PQ1	Good Record		A2	Good Record		R2	Good Record
	A2	Questionable		PS1	Good Record		S1	Good Record	153.01	H1	Fair Record
	T.B	Fair Record		PQ2	Good Record	151.01	S2	Partial Record		V1	Fair Record
	S1	Questionable		PS2	Good Record		S3	Good Record		H2	Fair Record
	S2	Questionable		D1	No Record		S4	Good Record		V2	Fair Record
	S3	Questionable		D2	No Record		S5	Good Record	153.02	H1	Questionable
	S4	Questionable		D3	No Record		S6	Good Record		V1	Good Record
	S5	Questionable		D4	Good Record		a31	Good Record		H2	Good Record
	S6	Questionable		A1	Good Record		t31	Questionable		V2	Partial Record
3.1-a2	F.1	Good Record		A2	Good Record		v31	Good Record	153.03	H1	Questionable
	PS1	Good Record		S1	Good Record		a32	Questionable		V1	Questionable
	PQ2	Good Record		S2	Fair Record		t32	Questionable		H2	Good Record
	PS2	Good Record		S3	Questionable		v32	Good Record		V2	Questionable
	D1	No Record		S4	Questionable		a101	Good Record	153.04	H1	No Record
	D2	No Record		S5	Good Record		t101	Good Record		V1	No Record
	D3	No Record		S6	Partial Record		v101	Good Record		H2	No Record
	D4	Good Record	3.1-b2	PQ1	Good Record	151.02	a33	Good Record		V2	No Record
	A1	Good Record		PS1	Good Record		t33	Good Record	111	P1	Good Record
	T.B	Fair Record		PQ2	Good Record		v33	Good Record		P9	Good Record
	S1	Good Record		PS2	Good Record		a34	Good Record		P15	Good Record
	S2	No Record		D1	No Record		t34	Questionable		P24	Good Record
	S3	Good Record		D2	No Record		v34	Good Record		P27	Good Record
	S4	Good Record		D3	No Record		a102	Good Record		P28	Good Record
	S5	Good Record		D4	Good Record		t102	Good Record		P34	Good Record
	S6	Questionable		A1	Good Record		v102	Good Record		P44	Good Record
3.1-a3	PQ1	Questionable		A2	Good Record	152.01	F1	Good Record		P50	Good Record
	PS1	No Record		S1	Good Record		R1	Good Record		PQ	Good Record
	PQ2	Good Record		S2	No Record		F2	Good Record		PS	Good Record
	PS2	Good Record		S3	Partial Record		R2	Good Record		PQr	Good Record
	D1	No Record		S4	Good Record	152.02	F1	Fair Record		PSr	No Record
	D2	Good Record		S5	Good Record		R1	Questionable		FAP;	Questionable
	D3	No Record		S6	Good Record		F2	Questionable			
	D4	Good Record	3.1-b3	PQ1	Good Record						

85

indicated as partial records were records which appeared reasonable up to a certain time and then became unusual in some respect. Those records indicated as questionable were records that had drifted out of the calibrated range or showed some anomaly that could affect the validity of the record. Those records indicated as fair record were records that were abnormally noisy, or of low amplitude.

DISCUSSION

The bombing error on Shot Cherokee caused the loss of some strain gage channels and influenced the validity and utility of several other instrumentation channels. The lost or questionable channels caused by the bombing error were due to the thermal energy and the shock wave coming in from an angle widely different from that expected, and of a different magnitude than that expected. The loss of the deflection gage records resulted from the corrosive effects of the salt atmosphere on the gage wire.

CONCLUSIONS AND RECOMMENDATIONS

Eleven of the no record or questionable records of the Project 3.1 strain gage channels were directly attributable to thermal damage resulting from the thermal energy coming in from an angle widely different from that expected.

It is recommended that the BRL deflection gage should utilize a gage wire that is not effected by the salt atmosphere when it is used at the EPG.

REFERENCES

1. "Transient Drag and Its Effect on Structures". Final Report MR 1013, Contract No. AF 33(616)-2285, February 1955; American Machine and Foundry Company.

2. B. L. Tucker; "Transient Drag and American Machine and Foundry Project MR1013", TM 260-55-51, Sandia Corporation.

3. O. Flachsbart and H. Winter; "Model Research on the Wind Loading of Lattice Structures"; (Translated from the German by B. L. Tucker), AFSWP – 404, Sandia Corporation, Sandia Base, Albuquerque, New Mexico; Unclassified.

4. E. C. Campbell; "A Comparison of Method from Calculating the Response of a Beam to a Suddenly Applied Load"; Report Structures 155 (c), April 1954.

5. D. Williams; "Displacements of a Linear Elastic System Under a Given Transient Load"; The Aeronautical Quarterly, Vol. I, Part II, August 1949.

6. W. T. Thomson and J. A. Cheney; "Response of Elastic Beams to Impulsive Loading"; UCLA Report 51.13, December 1951.

7. P. T. Hsu and G. S. Ram; "The Effect of Shock and Impact Loads on Elastic and Rigid-Plastic Beams"; MIT/ASRL TR-25-15, September 1954.

8. A. C. Eringen; "Impact on Elastic Beams"; TR No. 1, Contract N7-ONR-32909, May 1952; Illinois Institute of Technology.

9. P. D. Flynn; "Elastic Response of Simple Structures to Pulse Loading"; Report No. 525, November 1950; Ballistic Research Laboratories, Aberdeen, Maryland.

10. F. J. Allen and F. Nally; "A Plastic-Rigid Theory of the Response of Beams to Air Blast Loading"; MR Report No. 811; Ballistic Research Laboratories, Aberdeen, Maryland.

11. R. G. Locklin and S. M. Mills, Jr.; "Dynamic Response of Thin Beams to Air Blast"; Report No. 787, September 1954; Ballistic Research Laboratories, Aberdeen, Maryland.

12. W. E. Baker and J. F. Detlef; "Initial Accelerations of Simple Structures Under Blast Loading"; MR Report No. 583, November 1951; Ballistic Research Laboratories, Aberdeen, Maryland.

13. A. J. Hoffman; "The Shapes of Circular and Square Membranes Under Air Blast Loading"; Report No. 556, August 1951; Ballistic Research Laboratories, Aberdeen, Maryland.

14. W. J. Francy and N. M. Newmark; "A Study of Blast Loading Transmitted to Building Frames"; Civil Engineering Studies, SRS No. 89, December 1954.

15. W. J. Francy; "An Instrument Design for a Nuclear Test"; TM 268 54-51.

16. Journal of Applied Mechanics; Vol. 20, No. 4, December 1953.

17. "Criteria for Dynamic Net Force Sensor Selection"; MR 1021-03, Call No. 3, Contract No. AF 33(616)-2457; American Machine and Foundry Company.

18. J. J. Messaros and J. I. Randall; "Structures Instrumentation"; Project 3.28.1, Operation Upshot-Knothole, WT-736, February 1955; Explosion Kinetics Branch, Terminal Ballistics Laboratory, Ballistics Research Laboratories, Aberdeen, Maryland; Confidential Restricted Data.

19. P.H. Lorrian and E.G. Schwartz; "Structures Instrumentation"; Project 3.1°, Operation Teapot, WT-1107, May 1958; Explosion Kinetics Branch, Terminal Ballistics Laboratory, Ballistics Research Laboratories, Aberdeen, Maryland; Unclassified.

20. H.S. Burden; "Transient Drag Characteristics of a Spherical Model"; Project 1.14a, Operation Teapot, WT-1114, October 1959; Explosion Kinetics Branch, Terminal Ballistics Laboratory, Ballistics Research Laboratories, Aberdeen, Maryland; Confidential.

21. S.F. Hoerner; "Aerodynamic Drag"; Published by the Author, 1951.

22. C.N. Kingery, C.H. Hoover and Others; "Basic Surface Blast Measurements"; Project 1.1, Operation Redwing, WT-1301, not published; Ballistics Research Laboratories, Aberdeen, Maryland, Secret Restricted Data.

23. J.F. Moulton, Jr. and E.R. Walthall; "Shock Wave Photography"; Project 1.2, Operation Teapot, WT-1102, May 1958; U.S. Naval Ordnance Laboratory, White Oak, Silver Spring, Maryland; Confidential Formerly Restricted Data.

24. "Capabilities of Atomic Weapons"; TM 23-200, June 1955; Armed Forces Special Weapons Project, Washington, D.C.; Confidential.

25. R.J. Hesse, Major, CE, USA; "Damage to Field Military Equipment from Nuclear Detonations"; AFSWP 511, February 1956, Headquarters, Armed Forces Special Weapons Project, Washington 25, D.C.; Secret Formerly Restricted Data.

26. L.J. Bryant; "Dynamic Pressure Investigation"; Project 1.8, Operation Castle, WT-911, March 1957; Explosion Kinetics Branch, Terminal Ballistic Laboratory, Ballistic Research Laboratories, Aberdeen, Maryland; Secret Formerly Restricted Data.

27. E.J. Bryant, N.H. Ethridge and Others; "Response of Drag Type Equipment Targets in the Precursor Zone"; Project 3.1, Operation Teapot, WT-1123, October 1959; Explosion Kinetics Branch, Terminal Ballistics Laboratory, Ballistics Research Laboratories, Aberdeen, Maryland, Secret Formerly Restricted Data.

28. E.V. Gallaher and T.H. Schiffman; "Tests on the Loading of Buildings and Equipment Shapes"; Project 3.1, Operation Upshot-Knothole, WT-721, July 1955; Air Materiel Command, Wright-Patterson Air Force Base, Ohio; Secret

29. L.M. Swift and E.J. Wells; "Air Pressure Measurements"; Project 5.1, Operation Castle, WT-919, May 1955; Stanford Research Institute, Menlo Park, California; Confidential Formerly Restricted Data.

30. C.N. Kingery and J.H. Keefer; "Comparison of Air Shock Loading on Three Dimensional Scaled and Full-Size Structures"; Part II, Structure 3.1a, BRL Technical Note 976; AFSWP-775; Terminal Ballistics Laboratory, Ballistics Research Laboratories, Aberdeen, Maryland; Confidential.

31. C.N. Kingery and J.H. Keefer; "Comparison of Air Shock Loading on Three Dimensional Scaled and Full-Size Structures"; Part I, Structures 3.10o and 3.1p, BRL Technical Note 929, AFSWP 770, July 1955; Explosion Kinetics Branch, Terminal Ballistics Laboratory, Ballistics Research Laboratories, Aberdeen, Maryland; Confidential Formerly Restricted Data.

32. C.N. Kingery and J.H. Keefer; "Air Blast Loading on a Scaled Three Dimensional Structure"; BRL Report 953, AFSWP-813, July 1955; Explosion Kinetics Branch, Terminal Ballistics Laboratory, Ballistics Research Laboratories, Aberdeen, Maryland; Confidential.

33. L.J. Vortman; "Prediction of Incident Pressure Time Curves for Nuclear Explosions"; Ref. Syn.: 5112-(82); Supplement to AFSWP Report No. 226, January 1954; Sandia Corporation, Sandia Base, Albuquerque, New Mexico.

34. L.M. Sw?, D.C. Sachs and Others; "Air Blast Overpressure and Dynamic Pressure

Over Various Surfaces", Project 1.10, Operation Teapot, WT-1109, September 1957; Stanford Research Institute, Menlo Park, California; Confidential Formerly Restricted Data.

35. L. A. Schmidt; "Study of Drag Loading of Structures In and Out of the Precursor Zone"; Project 3.2, Operation Teapot, WT-1124, May 1955; Headquarters, Field Command, Armed Forces Special Weapons Project, Sandia Base, Albuquerque, New Mexico. Confidential Formerly Restricted Data.

SECRET

Appendix A
INSTRUMENTATION SUMMARY

A.1 STATIONS AND INSTRUMENTATION

A total of 28 stations were instrumented on four shots; 13 of the stations were electronically recorded, and 15 were ¼ ton vehicle stations. These utilized, in all, 42 electronically recorded channels (including duplicate back-up channels used for the WF-Beams) and an effective total of 28 jeeps and were located on a total of 11 islands (three man-made) in the two atolls.

Contractor support was given in the construction of mounts, recording shelter, and cable ditching. Also provided were the surveyed vehicle positions and renovation of the Operation Castle 3.10 structure and instrument shelter.

A.2 STATION LOCATIONS

The station locations, ground distances, azimuths from ground zero, type and numbers of gages used for the beams, spheres, cubicle, and jeeps for each shot are indicated in Tables A.2 through A.5.

A.3 FIELD LAYOUT

The blast line layout for the instrumentation covered in Table A.1 is shown in Figures A.1, A.2, A.3, and A.4.

TABLE A.1 STATION AND INSTRUMENTATION SUMMARY

Shot	Number of Stations	Type of Stations	Number of Gages or Sensors per Station	Number of Channels	Type of Transducer
Cherokee	4	WF Beam	2	16	Strain
Cherokee	4	Angle Iron	4	16	Strain
Cherokee	2	3-in-dia. Spheres	2	12	Strain
Cherokee	2	10-in-dia. Spheres	1	6	Strain
Zuni	1	6 x 6 x 12-ft Structural Target	9	9	Wiancko Static Pressure
			2	4	Dynamic Pressure
			1	1	Pressure-Time
Zuni	6	$\frac{1}{4}$ ton Jeeps	-	-	—
Lacrosse	5	$\frac{1}{4}$ ton Jeeps	-	-	—
Yuma	4	$\frac{1}{4}$ ton Jeeps	-	-	—

TABLE A.2 STATION LOCATIONS FOR SHOT CHEROKEE

Station Number	Island	Distance from Ground Zero, Intended ft	Azimuth from Ground Zero, Intended deg	min	sec	Type and Number of Measurements 3-in. Sphere	10-in. Sphere	WF-Beam	Angle Iron
151.01	Able	12,000	247	24	38	2	1	-	-
152.01	Able	12,000	247	14	18	-	-	1	-
153.01	Able	12,000	247	20	54	-	-	-	1
152.02	Man-Made No. 1 Reef Island	20,455	105	57	31.2	-	-	1	-
153.02	Man-Made No. 1 Reef Island	20,455	105	52	08.6	-	-	-	1
152.03	Man-Made No. 2 Reef Island	23,955	103	42	09.2	-	-	1	-
153.03	Man-Made No. 2 Reef Island	23,955	103	37	33.6	-	-	-	1
151.02	Dog	35,580	94	23	42	2	1	-	-
152.04	Dog	35,580	94	20	12	-	-	1	-
153.04	Dog	35,580	94	22	26	-	-	-	1

TABLE A.3 STATION LOCATIONS FOR SHOT LACROSSE

Station Number	Island	Distance from Ground Zero	Azimuth from Ground Zero			Type and Number of Measurements Vehicles	
		ft	deg	min	sec	SO *	FO †
154.09	Yvonne	2,500	156	48	44	1	1
154.10	Yvonne	2,770	155	52	50	1	1
154.11	Yvonne	3,350	147	16	4s	1	1
155.12	Yvonne	3,900	149	58	42	1	1
154.13	Yvonne	4,400	148	46	17	1	1

* Side-on orientation.
† Face-on orientation.

TABLE A.4 STATION LOCATIONS FOR SHOT YUMA

Station Number	Island	Distance from Ground Zero	Azimuth from Ground Zero			Type and Number of Measurements Vehicles	
		ft	deg	min	sec	SO *	FO †
154.05	Sally	150	12°	41	09	1	1
154.06	Sally	250	124	57	18	1	1
154.07	Sally	360	122	22	13	1	1
154.08	Sally	400	120	31	03	1	1

* Side-on orientation.
† Face-on orientation.

TABLE A.5 STATION LOCATIONS FOR SHOT ZUNI

Station Number	Island	Distance from Ground Zero	Azimuth from Ground Zero			Type and Number of Measurements			
						Structural P_t *	Target P_q †	Vehicles SO ‡	FO §
		ft	deg	min	sec				
111	Uncle	10,018	267	41	12	9	—	—	—
114.07	Roger	7,004	83	32	23	—	—	1	—
154.01	Roger	8,300	84	17	39	—	—	1	1
154.02	Peter	10,400	84	26	19	—	—	1	1
154.03	Peter	11,700	82	55	02	—	—	1	1
154.04	Peter	13,800	82	21	21	—	—	1	1
114.09	Oboe	16,500	82	30	24	—	—	1	—
156.01	Uncle	9,700	267	41	12	2	1	—	—
156.02	Uncle	9,600	267	41	12	1	1	—	—

* Pressure time.
† Dynamic pressure time.
‡ Side-on orientation.
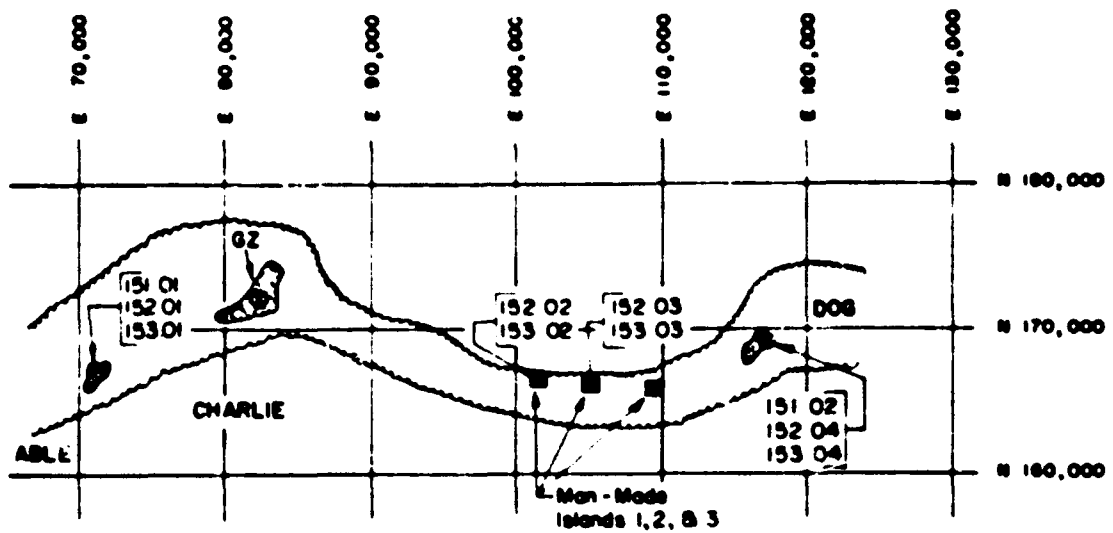§ Face-on orientation.

90

SECRET

Figure A.1 Blast line layout for Shot Cherokee, structural members and spheres.
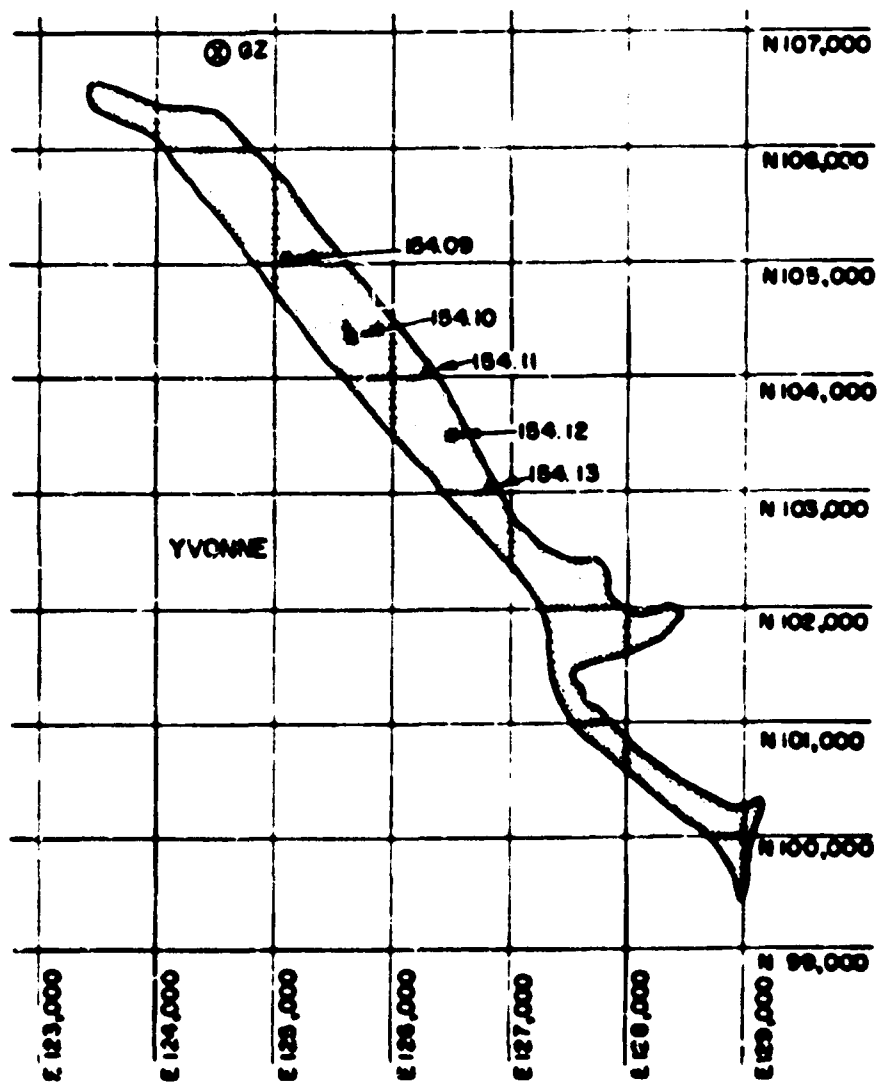

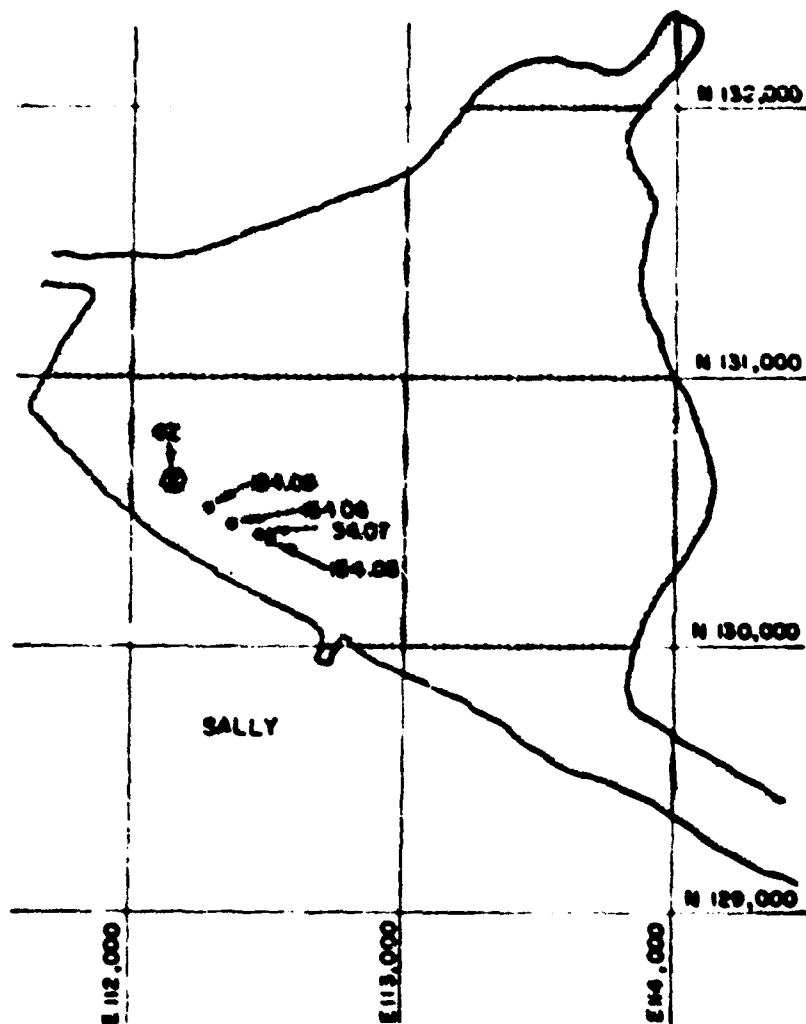Figure A.2 Blast line layout for Shot Lacrosse, military vehicles.

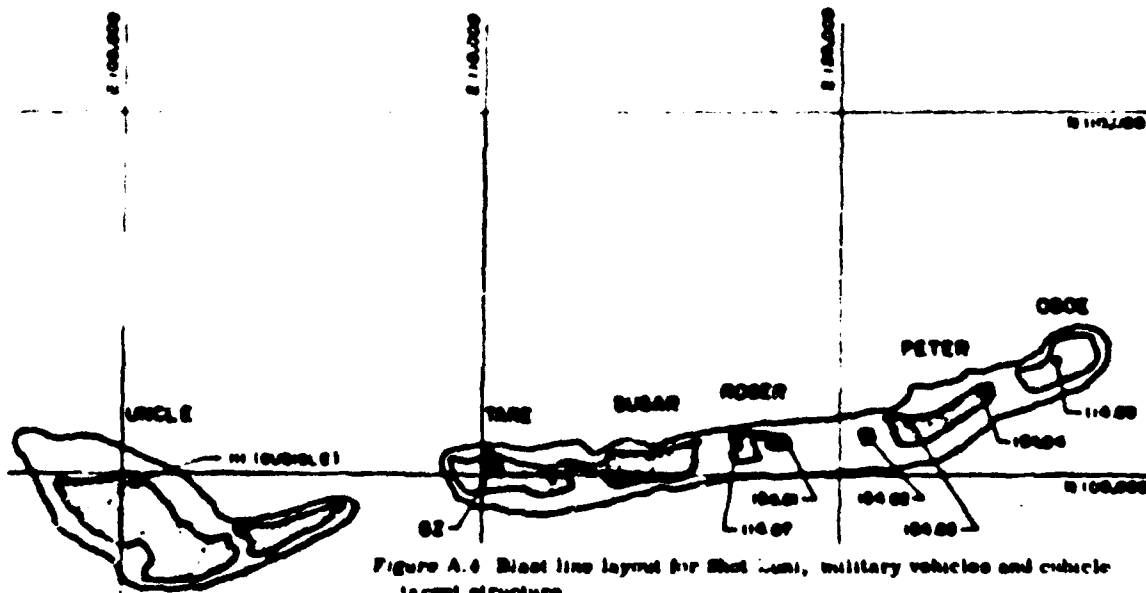Figure A.3 Blast line layout for Shot Yuma, military vehicles.

SALLY

Figure A.4 Blast line layout for Shot Yuma, military vehicles and cubicle target structure.

94

Appendix B
CATEGORIES of VEHICLE DAMAGE

The three basic categories of damage for vehicles are defined as follows (reference 20):

Severe damage is that damage which is sufficient to prevent the accomplishment of any useful military function and the repair of which is essentially impossible without removal to a major repair facility.

Moderate damage is that damage which is sufficient to prevent any military use until some repairs are effected.

Light damage is that damage which does not seriously interfere with immediate military operations but necessitates some repair to restore the item to complete military usefulness.

The numbered categories of damage (0.1, 0.2 thru 1.0) are described as follows:

Degree of Damage	Damage Description
0.1	Broken glass only.
0.2	Broken glass and bent parts, but operative.
0.3	Vehicle turned on side, operative.
0.4	Vehicle rolled, operative.
0.5	Some immediate organizational maintenance required before usable.
0.6	Field maintenance required (5 to 10 man-hours to restore to

combat use). Example: radiator repair and replacement of bent wheel required.

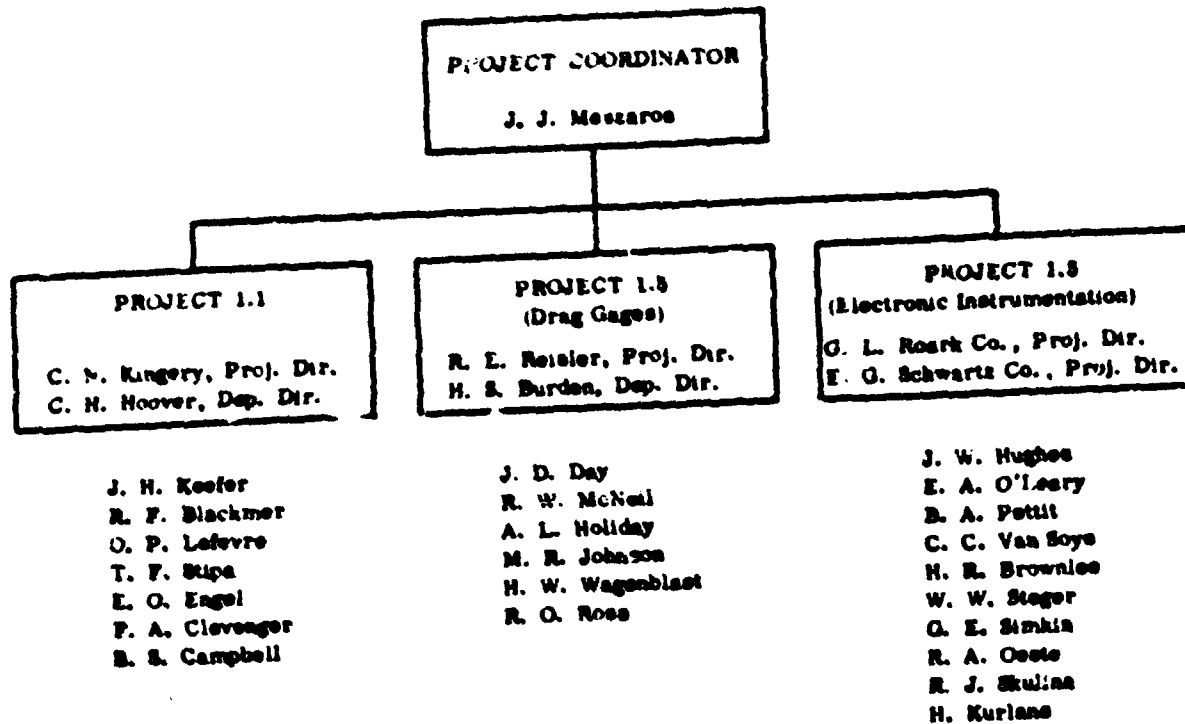|	
0.7	Field maintenance required (more than 10 man-hours). Example: severe damage to radiator and frame or steering column badly bent so as to interfere with steering.
0.8	Depot maintenance required (relatively minor). Example: entire body and instruments, steering wheel, shift levers, hood, and fuel tank crushed and badly bent.
0.9	Depot maintenance required (extensive). Example: body badly bent and twisted, grill and radiator blown back around engine, carburetor blown off, shock absorbers bent, clutch inoperative.
1.0	Vehicle completely destroyed (salvage).

Severe, moderate, and light damage were defined as the 0.8, 0.5, and 0.1 points, respectively.

Appendix C
TEST ORGANIZATION

```
┌─────────────────────────┐
│   PROJECT COORDINATOR    │
│                          │
│      J. J. Meszaros      │
└─────────────────────────┘
```

PROJECT 1.1	PROJECT 1.5 (Drag Gages)	PROJECT 1.8 (Electronic Instrumentation)
C. N. Kingery, Proj. Dir. C. H. Hoover, Dep. Dir.	R. E. Reisler, Proj. Dir. H. S. Burden, Dep. Dir.	G. L. Roark Co., Proj. Dir. E. G. Schwartz Co., Proj. Dir.
J. H. Keefer R. F. Blackmer O. P. Lefevre T. F. Stipa E. O. Engel F. A. Clevenger B. S. Campbell	J. D. Day R. W. McNeal A. L. Holliday M. R. Johnson H. W. Wagenblast R. O. Ross	J. W. Hughes E. A. O'Leary B. A. Pettit C. C. Van Soye H. R. Brownlee W. W. Steger G. E. Simkin R. A. Ooste R. J. Skulina H. Kurland

SUPPLEMENTARY

INFORMATION

Defense Nuclear Agency
6801 Telegraph Road
Alexandria, Virginia 22310-3398

ERRATA   14 September 1995

AD- 361774

MEMORANDUM TO DEFENSE TECHNICAL INFORMATION CENTER
       ATTN: OCD/Mr Bill Bush

SUBJECT: Change of Distribution Statement

     The following documents have been downgraded to Unclassified and the distribution statement changed to Statement A:

WT-1307, AD-311926	WT-1305, AD-361774
POR-2011, AD-352684	WT-1303, AD-339277
WT-1405, AD-611229	WT-1408, AD-344937
WT-1420, AD-B001855	WT-1417, AD-360872
WT-1423, AD-460283	WT-1348, AD-362108
WT-1422, AD-615737	WT-1349, AD-361977
WT-1225, AD-460282	WT-1340, AD-357964
WT-1437, AD-311158	
WT-1404, AD-491310	
WT-1421, AD-691406	
WT-1304, AD-357971	

     If you have any questions, please call MS Ardith Jarrett, at 325-1034.

FOR THE DIRECTOR:

Ardith Jarrett

for JOSEPHINE WOOD
Chief
Technical Support

ERRATA